AERODYNAMIC ANALYSIS OF LATTICE GRID FINS IN TRANSONIC FLOW

THESIS

Karl S. Orthner, Ensign, USNR

AFIT/GAE/ENY/04-J09

DEPARTMENT OF THE AIR FORCE
AIR UNIVERSITY

AIR FORCE INSTITUTE OF TECHNOLOGY

Wright-Patterson Air Force Base, Ohio

The views expressed in this thesis are those of the author and do not reflect the official policy or position of the United States Navy, United States Air Force, Department of Defense, or the United States Government.

AFIT/GAE/ENY/04-J09

AERODYNAMIC ANALYSIS OF LATTICE GRID FINS IN TRANSONIC FLOW

THESIS

Presented to the Faculty

Department of Aeronautics and Astronautics

Graduate School of Engineering and Management

Air Force Institute of Technology

Air University

Air Education and Training Command

In Partial Fulfillment of the Requirements for the

Degree of Master of Science in Aeronautical Engineering

Karl S. Orthner, BS

Ensign, USNR

June 2004

AFIT/GAE/ENY/04-J09

AERODYNAMIC ANALYSIS OF LATTICE GRID FINS IN TRANSONIC FLOW

Karl S. Orthner, BS
Ensign, USNR

Approved:

//signed//	04 June 04
Lt Col Montgomery C. Hughson (Chairman)	date
//signed//	04 June 04
Lt Col Raymond C. Maple (Member)	date
//signed//	04 June 04
Maj Richard J. McMullan (Member)	date

AFIT/GAE/ENY/04-J09

Abstract

Lattice grid fins have been studied for missile tail control for several years. A lattice grid fin can be described as an unconventional missile control surface comprised of an outer frame supported by an inner lattice grid of lifting surfaces. This unconventional fin design offers favorable lift characteristics at high angle of attack as well as almost zero hinge moments allowing the use of small and light actuators. In addition, they promise good storability for potential tube-launched and internal carriage dispenser-launched applications. The drawback for the lattice grid fins is the high drag and potentially poor radar cross section performance produced by this unconventional control surface configuration.

Current research at the United State Air Force's Aeroballistic Research Facility (ARF) at Eglin Air Force Base in Florida has indicated there is a critical transonic Mach number where normal shock waves are believed to be present within some of the grid cells. At this particular Mach number, there is a dynamic instability with severe variations of the pitch moment coefficient. A computational fluid dynamics (CFD) study was conducted to investigate these findings and elucidate the flowfield in the grid fin region. The missile model was numerically modeled in *Gridgen* and computational tests were run in *Fluent*. Finally, another fin configuration was developed that produced less drag and similar dynamic stability than the other lattice grid fin configurations tested.

To Family and Friends
Past, Present, and Future

Acknowledgments

Many people need to be recognized for their time and effort for me to complete my research. I would first like to extend my appreciation to my advisor Lt Col Hughson. He provided me guidance and support throughout this thesis process. Not only did he advise me with my research, but instructed me on the basics of computational fluid dynamics.

I would also like to recognize the director of the Department of Aeronautics and Astronautics computing facilities, Lt Col Maple. His instruction in computational modeling gave me the early techniques for grid generation and flow computation. Technical support by Lt Col Maple was vital in relieving computer issues. Maj McMullan provided significant contributions to my academic career at AFIT by guiding me through fluid computational processes. He also provided endless support in completion of this thesis. 2nd Lt John Casey aided in the flow field visualization as well as key grid generation techniques. His advice as well as knowledge aided me to completion.

Most importantly, I want to thank my family and friends who supported me throughout this process. Their endless devotion made the journey for a master's degree possible.

Karl Orthner

Table of Contents

Table of Figures

Table of Tables

Nomenclature

A	area
A^*	estimated choking area; Mach=1 condition
AOA	angle of attack
CG	center of gravity
C_{xo}	axial or drag force at zero angle of attack
$C_{m\alpha}$	pitching moment coefficient
D	diameter
Ix	x-moment of inertia
Iy	y-moment of inertia
M	Mach number
$M_{critical}$	critical freestream Mach number for choking
M_∞	freestream Mach number
S_{solid}	fin projected area
S_{total}	fin total area
c	chord
d	vane spacing
h	height
q	dynamic pressure
s	span
t	thickness of lattice web
γ	specific gas ratio; 1.4 for air
σ	solidity ratio, $\frac{S_{solid}}{S_{total}}$
μ	viscosity

Abbreviations

AMCON	U.S. Army Aviation and Missile Command
AFIT	Air Force Institute of Technology
ARF	U.S. Air Force Aeroballistics Research Facility
ARL	U.S. Army Research Laboratory
CFD	Computational Fluid Dynamics
DRDC	Defence Research and Development Canada
EDM	Electrical Discharge Machining
GTCM	Generic Tail Control Model
MOAB	Massive Ordnance Air Blast

AERODYNAMIC ANALYSIS OF LATTICE GRID FINS IN TRANSONIC FLOW

I: Introduction

Lattice Grid Fins

Lattice grid fins are a relatively new aeromechanic technology for missile tail control. A lattice grid fin is an unconventional missile control surface with an outer frame supported by an internal lattice grid of lifting surfaces. A recent example of the use of lattice grid technology is with the Massive Ordnance Air Blast (MOAB) weapon shown in Figure 1. Dynetics has been developing lattice- or grid-fin technology during the last decade. The fins were designed for a wide range of air- and surface-launched weapons and can endure speeds up to Mach 4-5. The fins could also help slow fast-moving weapons to speeds at which they can launch submunitions. (1)

Figure 1: Massive Ordnance Air Blast (MOAB) Missile

Figure 2 details multiple types of lattice grid fins. The design of these grid fins allow an effective aerodynamic control device stowed along with the body of a missile without increasing the overall dimensions. Therefore, the fin promises good storability for potential tube-launched and internal carriage dispenser-launched applications. The

internal grid structure, which forms a webbing for a tail fin, provides a high strength to weight ratio compared to planar fins that can be quite large. This, in turn, allows for the fins to have advantages of a low hinge moment and higher control effectiveness at a supersonic Mach number as well as at a low subsonic Mach number.(2) Therefore, the use of small and light actuators can be used for the lattice grid fin missile. Another major attractiveness of the lattice grid fin is that it does not stall at high angle of attacks such as a conventional fin does.

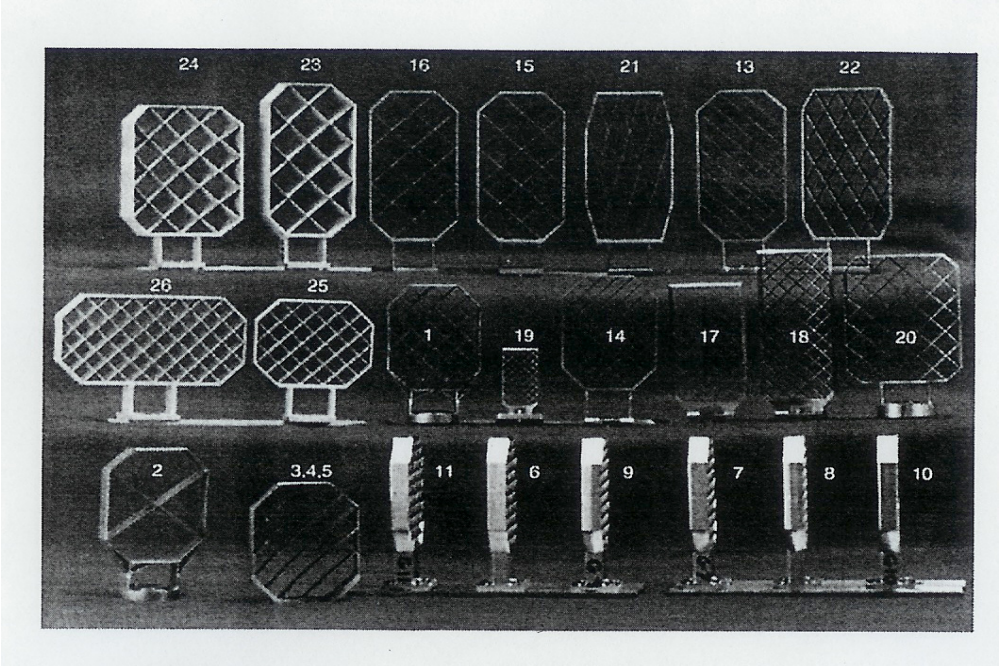

Figure 2: Example Lattice Grid Fins (3)

The major disadvantage of lattice grid fins is the increased axial force (drag) compared to conventional fins. This is a major issue that will be studied and alleviated in this paper. Another disadvantage of a lattice grid fin is its potentially high radar cross section (RCS) caused by the "resonance of a lattice dimension with the radar wavelength." (2)

Figure 3 compares the characteristics of two typical fin types (all movable surface and movable flap) with a lattice grid fin. Except for radar cross section, a lattice grid fin works very well with supersonic missiles. One can see that the lattice grid fin out-performed the two other fins in control effectiveness and hinge moment, but did worse in drag and RCS.

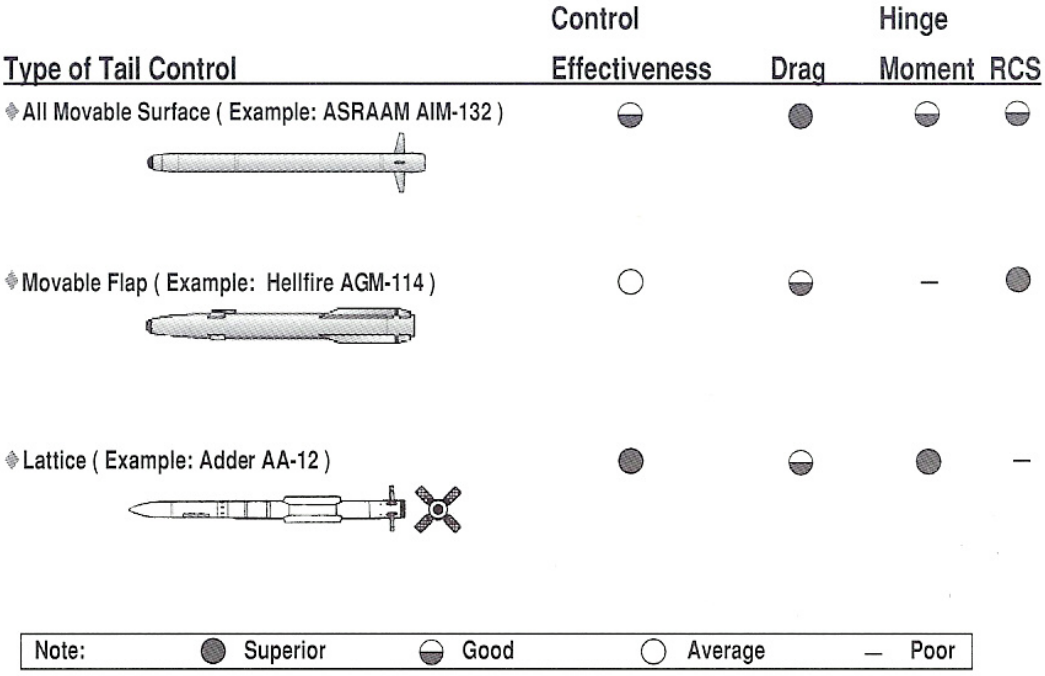

Figure 3: Characteristics of Different Missile Tail Types (2)

Previous Wind-Tunnel Research

Lattice grid fins are unconventional tail fins that have been studied over the past decade. Most of this research has been done in the fully subsonic or supersonic range, and not in the transonic realm.

Early tests (around 1993) include those done by U.S. Army Aviation and Missile Command (AMCON), formally know as the U.S. Army Missile Command, in order to

compare results to conventional planar fins at a Mach range of 0.5 to 3.5. After studying two basic lattice types, they concluded that grid fin hinge moments were extremely small, and the normal force and root-bending moments are comparable to planar fins of similar size. But, as expected, the axial forces or drag characteristics are greater than planar fins with comparable normal forces or lift characteristics. (4)

At the same facility, AMCON tested the leading edge profiles (flat, convex, and concave) with respect to the freestream direction. Their main results indicated the effects of the curvature on grid fin aerodynamic characteristics are negligible. They also tested the sweep of the grin fin with respect to the missile. They found that the grid fin sweep causes a sharp increase in drag and a decrease in lift causing static stability to decrease. (5)

AMCON next tested the effect of frame cross-sectional shape as well as web thickness on drag and other forces. Their test results yielded significant changes in drag characteristics at all Mach numbers tested, but that normal force (lift) and hinge moment characteristics showed small changes. (6)

Another group conducting wind tunnel tests was the Defence Research and Development Canada (DRDC) at Valcartier, formally known as the Defence Research Establishment Valcartier in Canada. The focus of their investigation was the comparison of lattice grid fin and conventional planar fin control surfaces. The fins were tested over a Mach range of 0.5 to 3.0. The results demonstrated an increased drag or axial force, reduced lift or normal force, and a reduction in static stability for the grid fins over the conventional planar fins. This is similar to results shown by the AMCON. (7)

Previous Computational Modeling

The U.S. Army Research Laboratory (ARL) conducted a research study using computational fluid dynamics (CFD) analysis of grid fins for maneuvering missiles. The calculations were made at a Mach number of 2.5, and performed at several angles of attack. They had three test cases: no fins, planar fins, and grid fins. When performing a viscous solution, the lift or normal force results were 11 % off the experimental test data. While, the drag was only 6.5% off from experimental test data. When the inviscid case was run, the forces were within 18% of wind tunnel data. (8)

Viscous calculations were continued by ARL to extend to aerodynamics of lattice grid fin missiles in the supersonic flow regime. This time results were obtained at Mach 2 and 3 at a range of angles of attack from -15 to 15 degrees. The results yielded good agreement among the lift or normal force and drag or axial force coefficients (around 8% error), but only reasonable results for pitching moment (16-27% error). At these Mach numbers, they experienced the same flowfield as with experimental tests. (9)

The ARL then extended their research to a CFD investigation of canard-controlled missiles with planar and lattice grid fins. CFD runs were made at Mach 1.5 and Mach 3 at various angles of attack from -15 to 15 degrees. The results were very similar to previous wind tunnel tests. They did conclude from this study that the grid tail fins improved the roll effectiveness of the canards at low supersonic speeds. (10)

Since the lattice grid fin was examined at supersonic speeds, the next test by the ARL was to examine how subsonic flow affects the canard-controlled missile with planar and lattice grid fins. Computations were done at a Mach number of 0.6 at various angles of attack from -15 to 15 degrees. These results were validated by comparison of

aerodynamic coefficients from previous wind tunnel experiments. These simulations will help ARL with further design of missile tail and control surfaces. (11)

DRDC-Valcartier in Canada also performed a comprehensive CFD investigation to see if lattice grid fins are efficient control surface devices. They studied the aerodynamic effects of a fairing ramp at the base of the grid fin as well as various thicknesses of grid fin webs of the panels. They found out that the fairing actually could increase the performance of the lattice grid fin by reducing the vertical flow at the base of the grid fin. Also, they believed that the increased thickness of the grid fin panels caused an increase of bow shocks in front of the grid fin; therefore adversely impacting performance. (12) This bow shock can be shown in the ARF shadowgraph shown below in Figure 4.

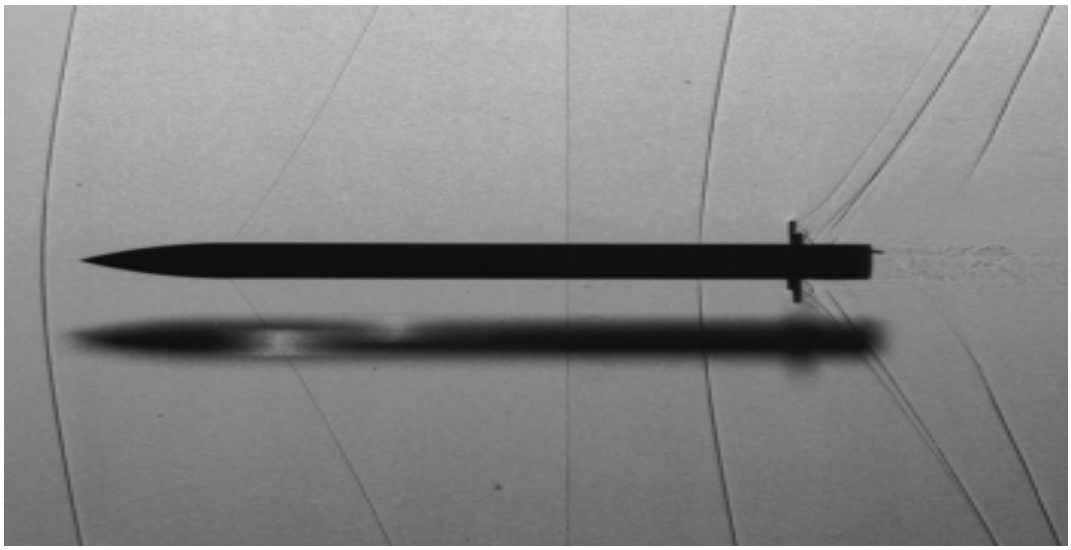

Figure 4: GTCM at Mach 1.03 at ARF (13)

Current Research Objectives

Ballistic range tests of a lattice grid fin missile have been conducted at the U.S. Air Force Aeroballistics Research Facility (ARF) located at Eglin Air Force Base in

Florida. They have documented sub-scale ballistic range flight tests of generic missile configurations with lattice grid fins at Mach numbers of 0.39 to 1.60 This data indicates that there is a critical transonic Mach number where normal shock waves occur in some or all of the grid cells with resulting choked flow. At this critical Mach number, there are dynamic instabilities with severe variations in pitching moment.

To help address the issues of instability and examine the grid fin flowfield, a numerical model was produced very similar to the model tested at the ARF and a CFD analysis was done. This investigation helped elucidate flowfield development and associated phenomena as seen in the ARF ballistic range flight tests. The CFD study was conducted at the Air Force Institute of Technology (AFIT) at Wright-Patterson Air Force Base in Ohio. Tests concentrated on the transonic regime; the location where lattice grid fin choking occurs during experimental tests. The effects of changing the angle of attack, as well as some of the static stability effects due to pitch were investigated and reported.

To further investigate lattice grid fins and attempt to alleviate drag forces, a CFD study was done on different lattice grid configurations. The overall dimensions of the fin stayed the same, but the internal webbing geometry was changed. The flowfields of these configurations were investigated with the static stability effects due to pitch as well as axial and normal forces; and are compared to the original lattice grid fin configuration tested at the ARF.

Chapter Summary

Lattice grid fins have been studied for multiple years, and this research investigated the usefulness of lattice grid fins as an effective control surface for missiles. The next chapter (Chapter 2) will discuss the experimental research done at the ARF at

Eglin Air Force Base and 1-D choking theory. Chapter 3 will discuss the numerical modeling stages of the sub-scale model used for these lattice grid fin tests. After the modeling, the discussion of the results and an elucidation of the flowfield will be done from CFD runs. Figures 5 and 6 are two shadowgraphs that illustrate the flowfield discussed in the results section. Lastly, Chapter 5 will give a brief conclusion as well as suggestions for future CFD research for lattice grid fins.

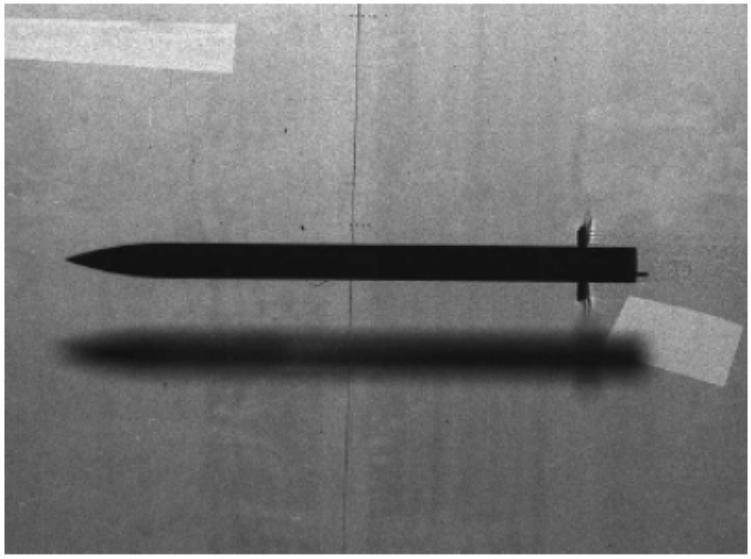

Figure 5: GTCM at Mach 0.86 at ARF (13)

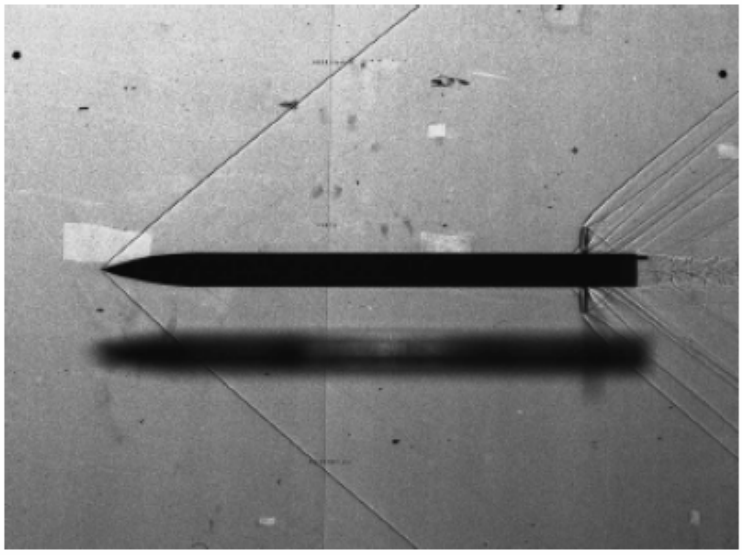

Figure 6: GTCM at Mach 1.62 at ARF (13)

II: Background and Theory

Free-Flight Testing of Missiles with Lattice Grid Fins

Previous tests with lattice grid fins (dimensions in Table 1) have been conducted at the USAF Aeroballistic Research Facility (ARF), Air Force Research Laboratory, Munitions Directorate, Eglin Air Force Base, Florida.

> "The ARF is an enclosed, concrete structure used to examine the ballistics of various free-flight projectiles. The length of the instrumented range was 207 meters with a 3.66 meter square cross section for the first 69 meters and a 4.88 meter square cross section for the remaining length. The range has 131 locations available as instrumental sites; 50 of which currently house fully instrumented orthogonal shadowgraph stations." (13)

Table 1: Model Physical Properties (13)

Configuration	Basic Research Model	GTCM Grid Fins	GTCM Planar Fins
Diameter, mm	25.4	25.4	25.4
Length, mm	254.0	406.4	406.4
Mass, g	379.4	654.3	646.0
Ix, g cm^2	324.0	504.0	501.0
Iy, g cm^2	20,396.0	91,264.0	89,246.0
CG, mm from Nose	133.5	193.6	191.8

Besides the shadowgraph stations, the facility contains one direct shadowgraph station for the flow field visualization.

> "This station is located up-range of the instrumented section. The range has the temperature controlled to 22 $\pm$ degree C as well as the relative humidity to less than 55%. A chronograph system provides the times for the projectile at each station. Taking together the time, spatial position, and orientation of the model taken from the orthogonal photographs provide the basic trajectory data from which their aerodynamic coefficients are extracted." (13)

The first tests done by ARF using three geometries: US Air Force Basic Research Model with grid fins (Figure 7), Generic Tail Control Model (GTCM) with grid fins (Figure 8), and GTCM Model with planar fins (Figure 9). Table 1 gives the physical properties for the model configurations.

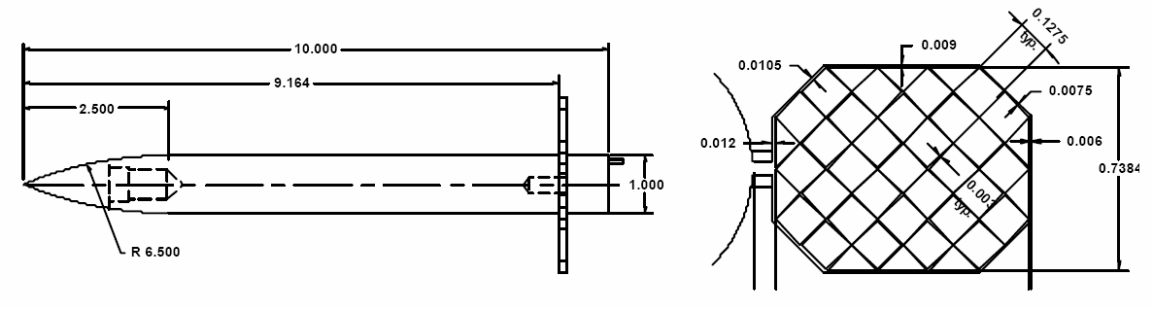

Figure 7: USAF Basic Research Model (13)

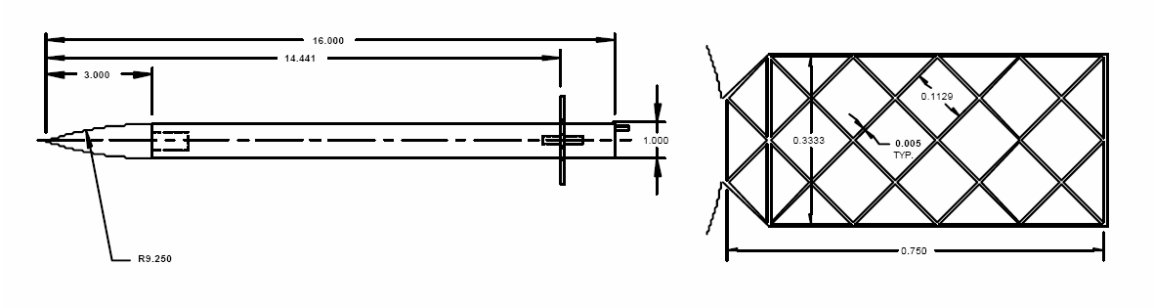

Figure 8: GTCM Model with Grid Fins (13)

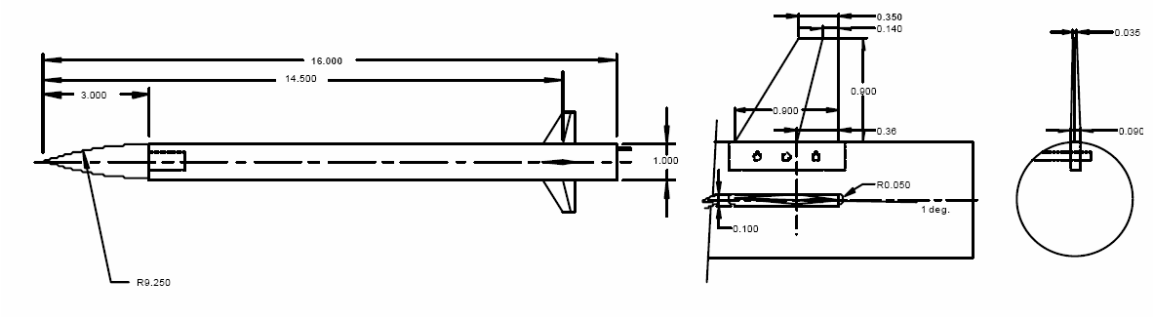

Figure 9: GTCM Model with Planar Fins (13)

The US Air Force Research Model was used because of previous research with this type of fin. The GTCM model with grid fin was used "in an effort to bring together different research activities on grid fins." (13) Lastly, the GTCM Model with planar fins was tested to compare with the lattice grid fin models. The lattice grid fin models were made using an electrical discharge machining (EDM) process. For the grid fin webs, the required thickness was 0.125 mm. However, the thickness of the webbing varied from 0.125 mm to 0.175 mm. (14)

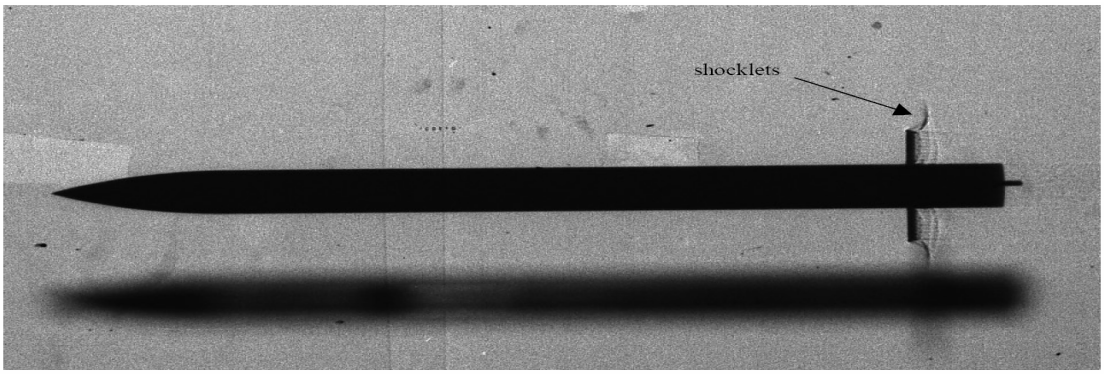

Figure 10: GTCM Shadowgraph-Mach 0.879 (14)

In observing only the GTCM model with grid fins, the highly complicated flow can be observed in various shadowgraphs. The shadowgraph in Figure 10 demonstrates the shocklets produced at Mach numbers below Mach 1. However, the flow structure for speeds above Mach 1 can be seen in Figure 11. (14) Shock 1 is the stand-off shock and attaches to the nose at Mach 1.17. Shock 2 is a very weak shock that occurs from the transition from nose to body. Shock 3 is formed in the front of the lattice grid fin. Shock 4 (a,b, and c) are formed by the flow through and around the fins at different Mach numbers. Lastly, shock 5 is a shock from the recompression of the flow behind the missile's base.

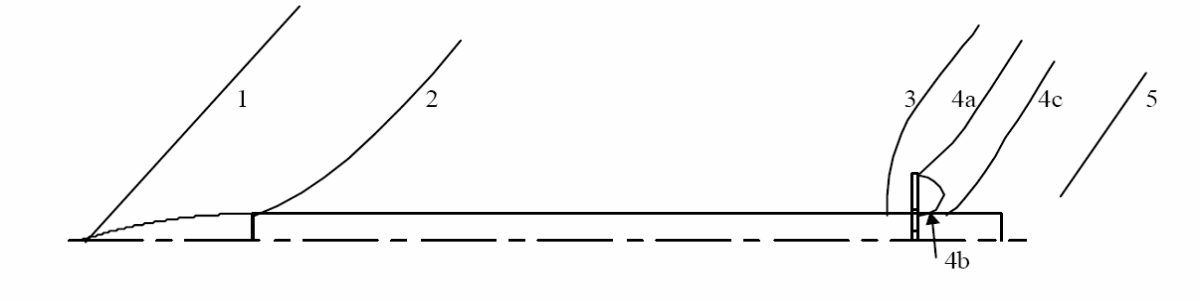

Figure 11: Flow around Missile with Mach Number Greater than 1 (13)

For the aerodynamic coefficients, all coefficients and derivatives have a reference length of the model diameter (d) and the reference area is the cross sectional area of the model ($A=\pi/4*d^2$). The following figures will show the difference between the planar and lattice grid fins. The planar fin data is mostly shown with a trend-line determined via the PRODAS (15) program, an aerodynamic prediction code. Because the planar data fit on the trend line, fewer shots were needed for comparison purposes.

The zero yaw axial force coefficient (C_{X_o}) versus Mach number can be seen in Figure 12. The filled in symbols represent multiple shots at a given mach number. A trend-line was set for the lattice grid fin model, and the PRODAS trend line was used in the planar case. As expected, there is an increase of drag for the lattice grid models versus the planar model. The estimates came to a 100% increase in the subsonic regime as well as a 67% increase in the supersonic regime.

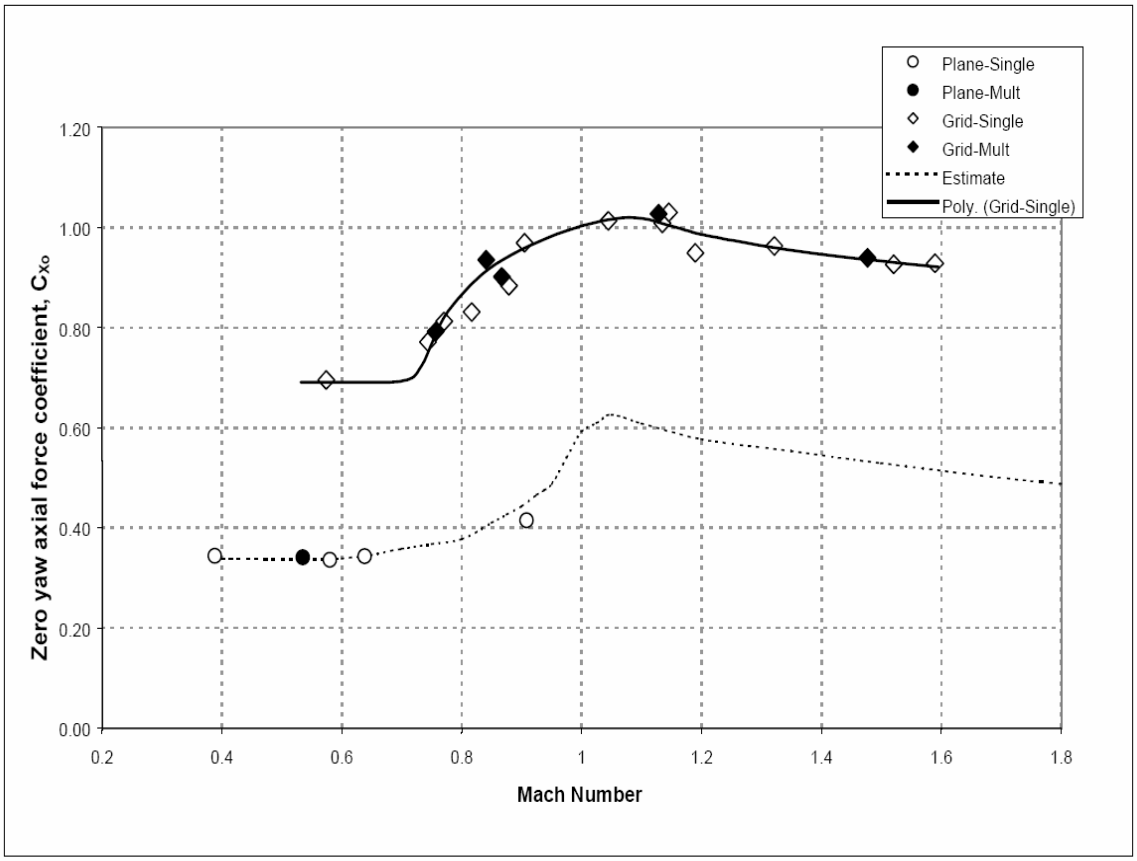

Figure 12: Axial Force Coefficient: Planar vs. Grid Fin (14)

The pitching moment coefficient ($C_{m\alpha}$) versus Mach number can be seen in Figure 13. The trend of the grid fin data is very similar to that of the planar fin data. But, there was a constant decrease of stability for this type of configuration. It is interesting to note the discontinuity that occurs at Mach 0.77. This Mach number was tested many times and the discontinuity is not attributed to measurement error. There is also a loss of static stability margin at Mach numbers from 1.2 to 1.6.

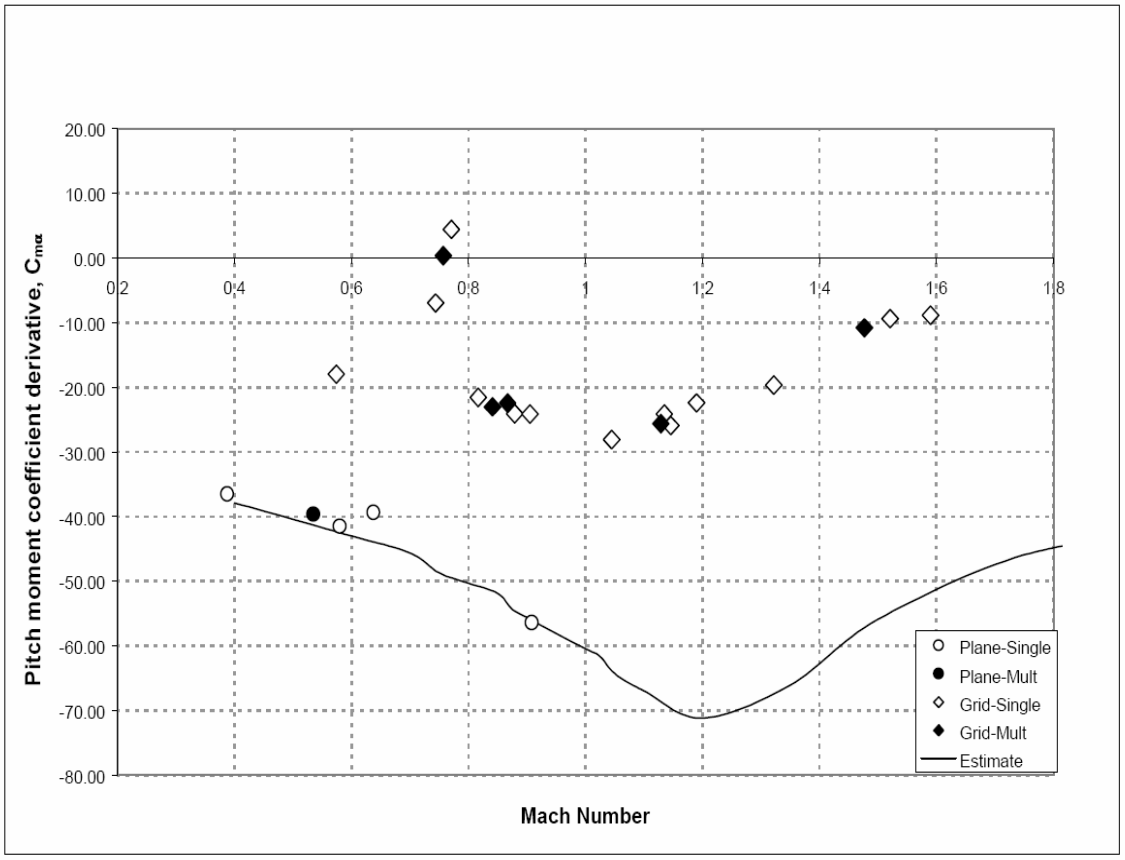

Figure 13: Pitching Moment Coefficient: Planar vs. Grid Fin(14)

The next sets of tests that were taken at the ARF involved different lattice grid fin geometries. They first used the baseline fin model used in previous tests. Next, they had a 'thin' fin model which had a web thickness at 0.004d compared to 0.007d for the baseline model. Finally, a 'coarse' fin model was produced with an elimination of some of the webbing. Figure 14 shows the comparison among the three types of lattice grid fins tested.

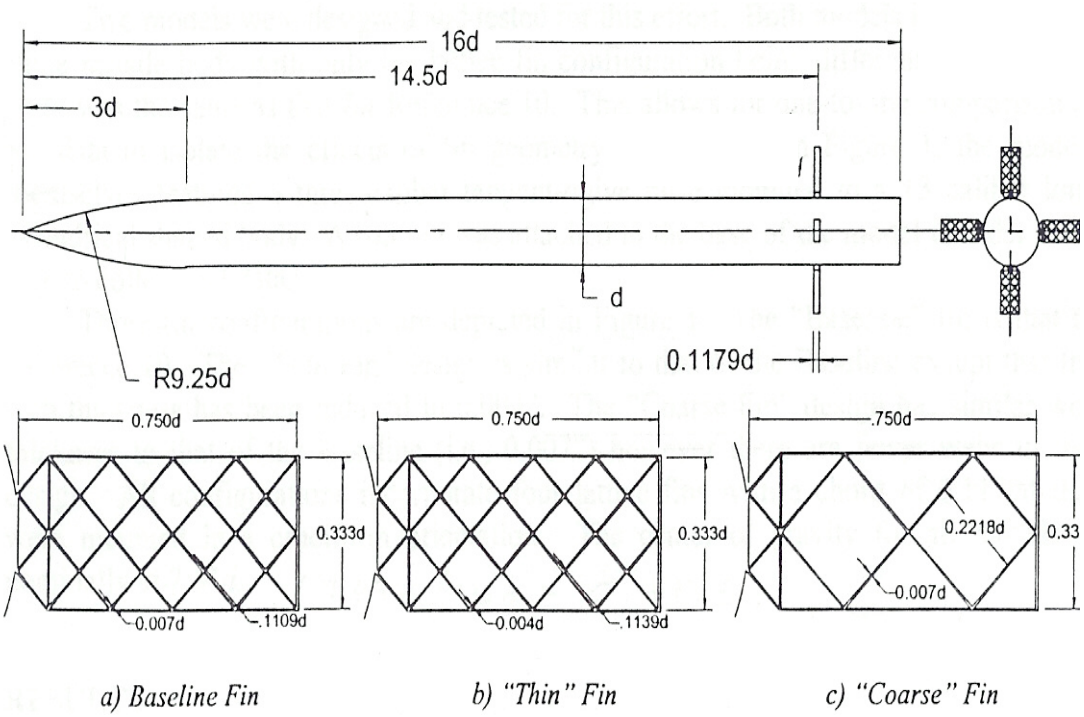

Figure 14: Lattice Grid Fins Tested at ARF (16)

When calculating the results, the reference length is from the model diameter (d) and the reference area is the cross section area of the model ($A= \pi/4*d^2$). The zero yaw drag coefficient (C_{X_o}) versus Mach number flight data can be seen for all the aerodynamic coefficients and derivatives in Figure 15. The drag data indicates a reduction in drag of 16% for the 'thin' fin lattice grid and a 22% reduction for the 'coarse' fin lattice grid. The authors believed this to be true because drag is 'directly related to the thickness of the webs and the number of webs present." (16)

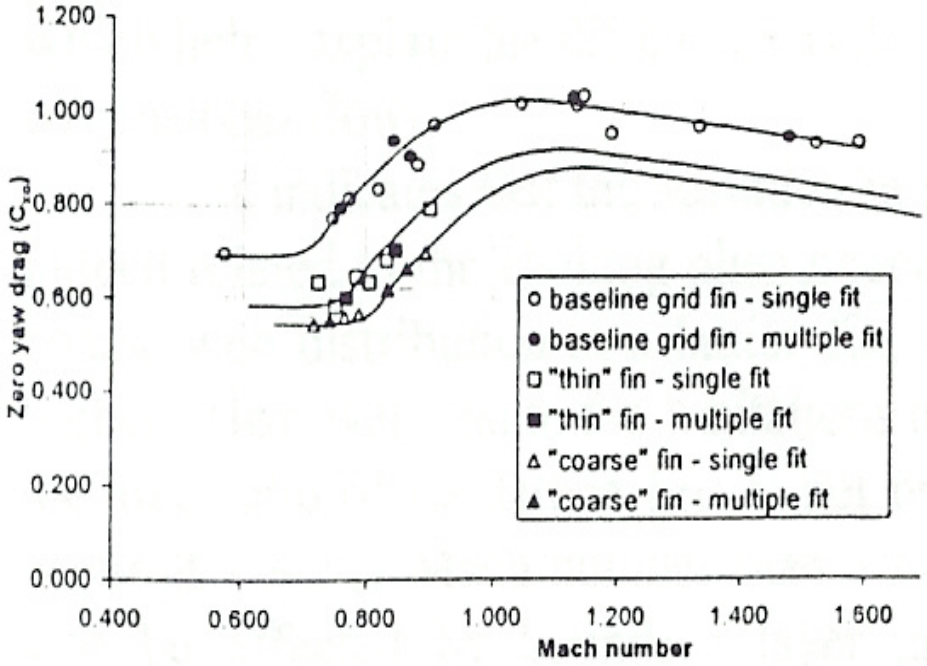

Figure 15: ARF Lattice Grid Fin Axial Force Coefficients(16)

Figure 16 contains the pitching coefficient derivative ($C_{m\alpha}$) ARF data as a function of Mach number. As seen before, there is a discontinuity at a certain transonic Mach number. But, this time it occurred near Mach 0.8, not 0.77 as before with the baseline model.

From these experiments, the authors concluded that choking occurs in the lattice grid fins at a critical transonic Mach number for any of the grid fin configurations. This choking causes some temporary instability of the missile flight dynamics, even though the Mach range of this instability seems to be quite small.

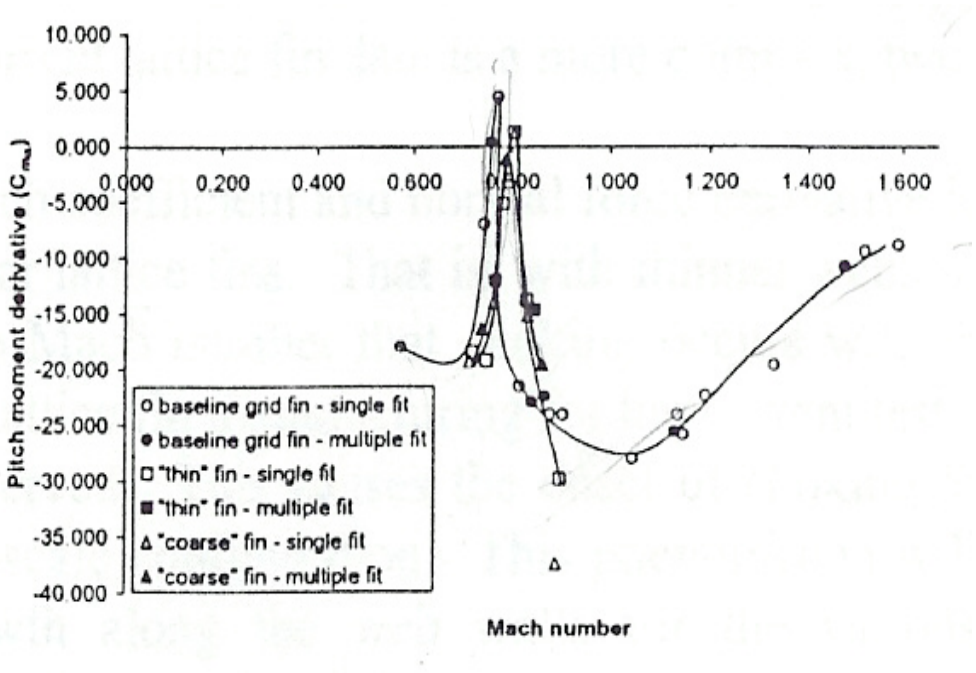

Figure 16: ARF Lattice Grid Fin Pitching Moment Coefficient Derivative (16)

Choking Theory

When determining the choking qualities that are seen with the lattice grid fin configurations, one can see similarities with subsonic inlets. Subsonic inlets have been studied for many years and have documented occurrences of choking phenomenon for them. Figure 17 shows a typical streamline pattern for a subsonic inlet. Because the capture area difference is so large, some of the flow is deflected and accelerated as it flows over the inlet lip; this phenomenon is called 'spill over'. (17) This high velocity and accompanying low pressure effects the boundary layer in two ways: boundary separation or partially supersonic flow could occur. (18) These local supersonic regions usually develop shocks, and the shock-wall interaction causes boundary layer separation. This boundary layer separation needs to be avoided because the presence of the separation causes excessive external drag on the body.

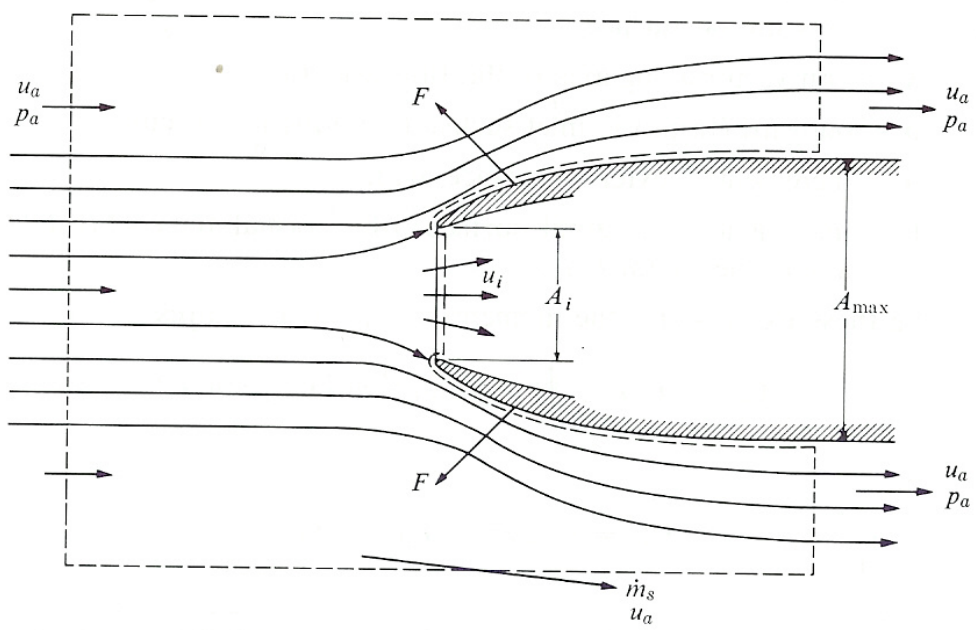

Figure 17: Subsonic Inlet Streamline Pattern(18)

This can be related to a lattice grid fin with a relatively short chord length when compared to an inlet. Similarly to a subsonic inlet, the lattice grids in the fin act like capture areas where each cell is like an inlet and the flow is spilled over the exterior of the lattice grid fin. Figure 18 shows the transition the flow field experiences when going transonic and then supersonic. It can be noted numerous reflection of the slightly greater than normal oblique shocks in a grid cell occurs at low supersonic Mach numbers which significantly increases drag. But, the oblique shock angle increases and pressure jumps decreases in strength as the Mach number is increased and this shock does not reflect in a grid cell. This led Fleeman to conclude that "lattice [grid] fins have their best application at low subsonic and high supersonic Mach number, where they have low drag and high control effectiveness." (2)

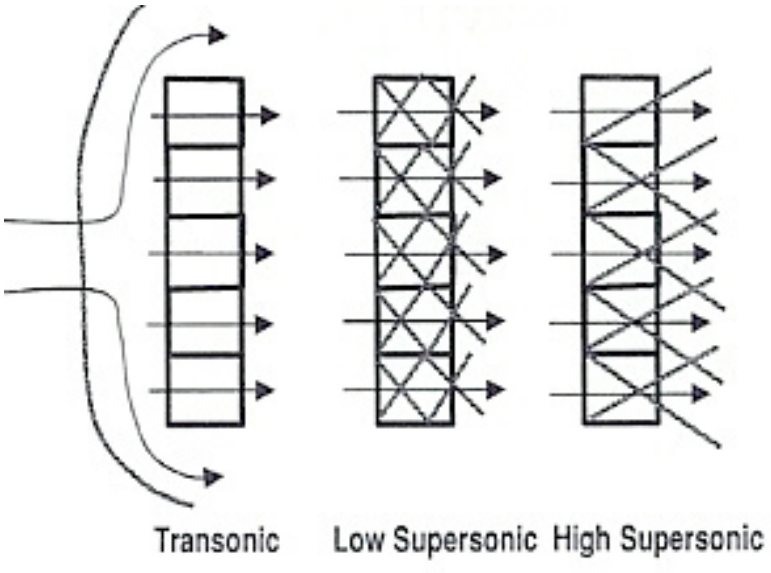

Figure 18: Transonic and Supersonic Lattice Grid Fin Flowfield Streamline and Shock Pattern (2)

Numerical Theory

The theory for inlets and internal flow can be extended to the lattice grid fins because of the similar flow qualities that are occurring. For analytical calculations, it is easy to use the quasi-one-dimensional nozzle theory with choked flow to predict a critical transonic Mach number where choked flow may occur. This compressible flow theory relationship is as follows (19):

$$\left(\frac{A}{A^*}\right)^2 = \frac{1}{M_\infty^2}\left[\frac{2}{\gamma+1}\left(1+\frac{\gamma-1}{2}M_\infty^2\right)\right]^{\frac{\gamma+1}{\gamma-1}}$$

This equation can be easily applied to a lattice grid fin geometry by considering the area ratio to be the ratio between the nominal area in the control volume upstream of a cell of the lattice grid fin and the open area around the cell. Once this area ratio is determined, the critical Mach number for each lattice grid fin geometry can be evaluated.

A correlation then can be made with the observed critical Mach numbers in the ballistic tests.

The nominal area for the control volume was assumed to be the width of the open area of the square lattice grid cell plus one span of the thickness of the webbing as shown in Figure 19. Note that in 1-D 'area' is essentially a single dimension and that the area is always assumed to be a squared term for unit depth.

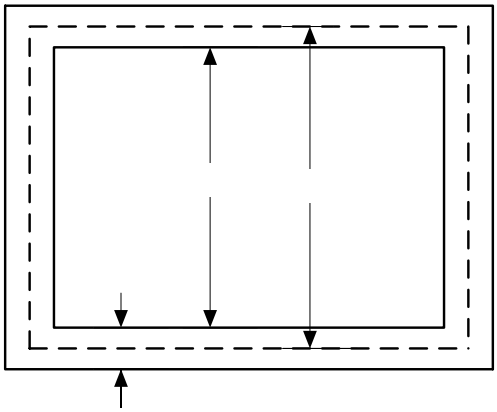

Figure 19: Cell Area Dimensions for 1-D Theory

The open area is simply the open area in the square lattice grid fin cell. In terms of the equation given for the lattice grid control parameter above, the area ratio is defined as follows:

$$\left(\frac{A}{A^*}\right)^2 = \left(\frac{d+t}{d}\right)^2$$

The following table (Table 2) shows the analytical estimates and experimentally observed data for critical transonic Mach numbers and choked flow. As one can see, the difference between the analytical and experimental data was less than 3%. This should

d

t

give confidence in making predictions of critical transonic Mach number for other lattice grid fin geometries.

Table 2: Critical Transonic Mach Numbers for Lattice Grid Fin Cell Choking

Configuration	d	t	A/A^*	$M_{Critical}$	$M_{Critical}$ *(Test)*	% Off
Baseline	0.1109	0.007	1.13	0.7487	0.77	-2.8
Thin	0.1139	0.004	1.071	0.8077	0.8	1.0
Coarse	0.2288	0.007	1.062	0.8196	0.8	2.45

Chapter Summary

Extensive experimental research has been done at the USAF ARF on lattice grid fins by analyzing the stability conditions as well as the drag data with different lattice grid fin geometries. The issue of choking has been observed at certain critical transonic Mach numbers. This can also be estimated by using 1-D compressible flow theory with the area ratio determining a critical transonic Mach number. A computational fluid dynamics (CFD) model has been made in order to investigate the location of this critical transonic Mach number and the lattice grid fin flowfield as well predicting drag, static stability, and choking for other lattice grid fin configurations.

III: Numerical Modeling

Gridgen

In order to produce the meshes for computational modeling, the software program called *Gridgen* was used. Figure 20 shows an example of a numerical mesh done commercially using *Gridgen.*

> *"Gridgen* is a complete meshing toolkit used to generate three-dimensional (3D) grids for complex geometries in a production environment, often where CFD is mission critical. The software's origins are in the demanding U.S. aerospace industry, where *Gridgen* continues to earn its reputation for usability and high quality grids, both of which are vital for reliable simulations. Today *Gridgen* is used worldwide in aerospace, automotive, power generation, chemical process and other industries for which CFD is an integral part of the design process. The meshes that are generated by *Gridgen* are of highest quality that leads to more accurate and faster solutions." (20)

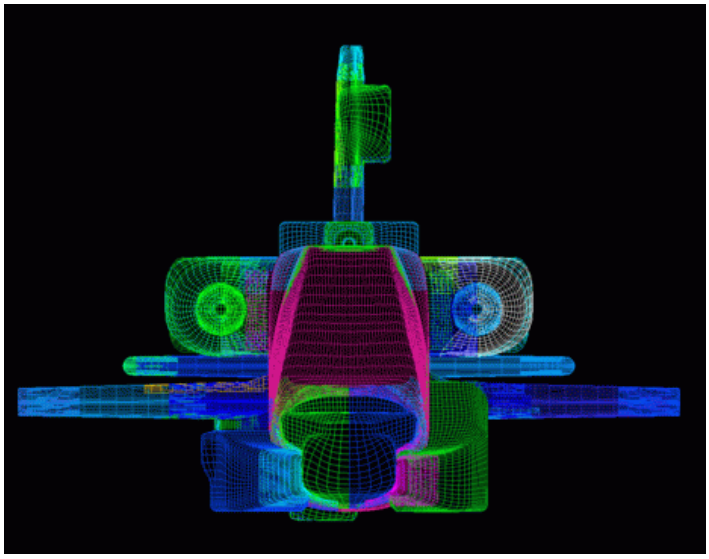

Figure 20: Apache Model Using *Gridgen* (20)

Missile Modeling

When producing a numerical model for comparison to the experimental tests done at Eglin AFB, the missile body had to be replicated as close as possible. The dimensions were given by the ARF for the missile geometry in inches. With the help of Lt Col Montgomery Hughson at the Air Force Institute of Technology, this model was duplicated in *Gridgen* with the same dimensions. Figures 21 and 22 compare the two models. Note that the roll pin of the ARF model was not duplicated in the numerical model.

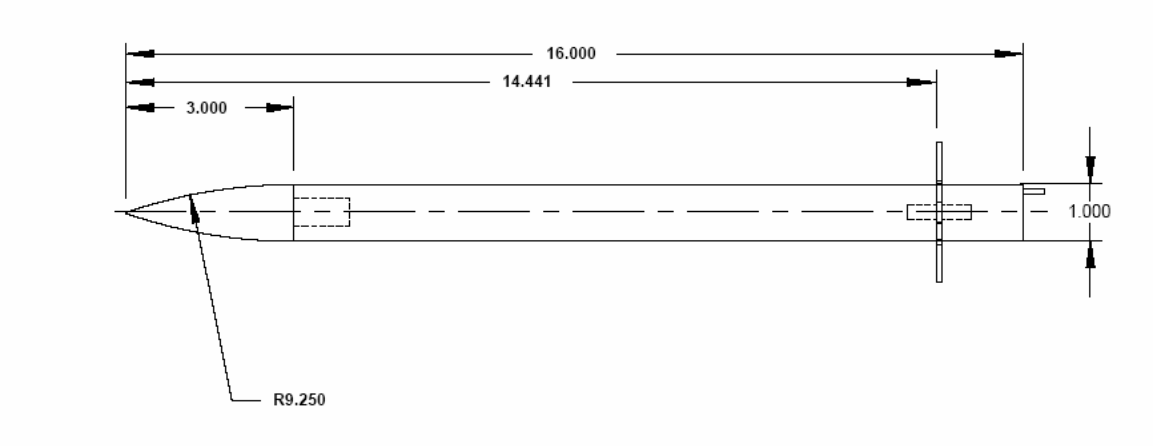

Figure 21: Missile Dimensions at ARF (14)

Figure 22: Missile Generated in *Gridgen*

After building the numerical model of the missile tested at the ARF, the next step is to produce a mesh on the missile body. The mesh chosen for this study was unstructured because the initial computational study was going to be in the inviscid realm. The body then was split up into three sections: nose, body, and tail. An independent mesh was generated for each section because of their geometric differences and to allow for the ease of extracting aerodynamic coefficient data for each entity. The number of mesh cells was chosen that produced the best results and had a fast run time. After doing a grid convergence study (in Appendix A), the number of cells for each section (as well as the fins) fit both of the characteristics listed above.

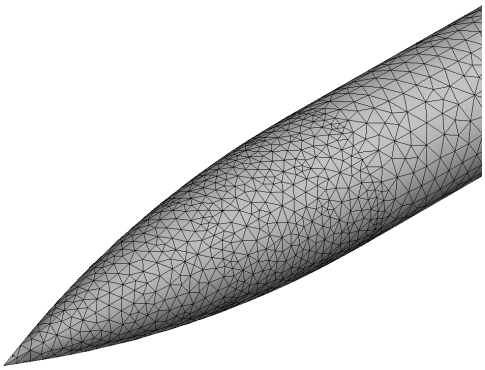

Figure 23: Grid Generated on the Nose of the Missile

The nose section contained the most amount of axial curvature compared to the other two sections. Also, it was known that a shock will be located at the tip as well as at the transition to the body of the missile for supersonic freestream Mach numbers. With this in mind, a total of 30 points were allocated for this 3 inch section. Therefore, this gave a nominal grid spacing of 0.1 inches. The cross section area of the nose located at the base contained 60 points. This gave a nominal grid spacing of 0.05 inches. Figure 23 shows the unstructured grid on the nose of the missile.

The missile body section was modeled next with the same cross-section spacing of 60 points. The body extended to the 13 inch mark from the nose. The rest of the body was contained in the tail section. Axially, the missile body contained 60 points with a spacing of 0.2. This spacing is increased from the nose spacing because the flowfield changes smoothly along the body of the missile. Figure 24 below shows the unstructured grid located on the body.

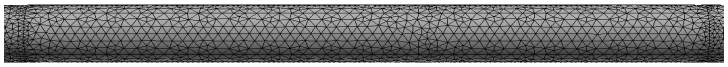

Figure 24: Grid Generated on the Body of the Missile

The tail section required different modeling techniques and more points than the body and the nose because of the importance of the aerodynamic data needed at this section of the missile. The last 4.5 inches contained 30 points axially giving a spacing of 0.15. This spacing is greater than the nose, but only occurs at the greatest distance from the fins. At the location of the fin and missile connection, there is a distance of 0.1179 inches. Here, 15 points were allocated for this very short distance for a spacing ratio of 0.00786. This is necessary in order to obtain data for the fin and body interaction. Figure 25 of the tail section shows how the cells from the fin increase in size as one travels away from the fin.

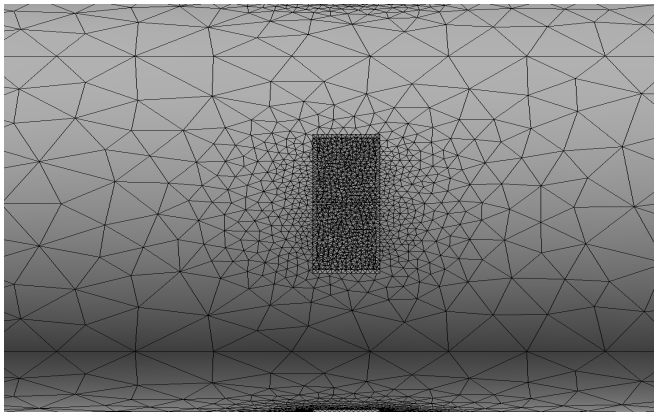

Figure 25: Grid Generated on the Tail of the Missile

Baseline Lattice Grid Fin

The baseline lattice grid fin was the first type of fin tested by ARF. Therefore, it was the first type of lattice fin modeled for computational fluid dynamic solution. Once again, the dimensions (shown in Figure 26) came from ARF and were replicated in *Gridgen* which is shown in Figure 27.

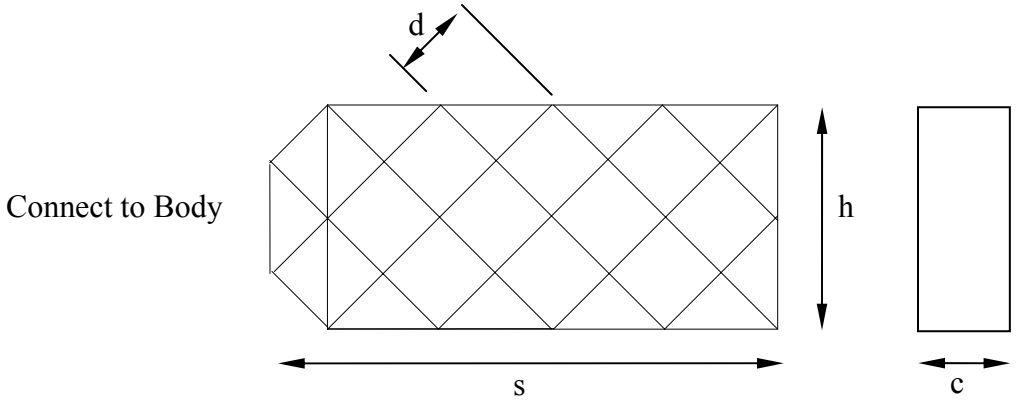

h (height)	0.333D
s (span)	0.75D
c (chord)	0.1179D
d (vane spacing)	0.1109D (open area = d^2)
t (thickness)	0.005D

(D=1 inch)

Figure 26: Baseline Geometry

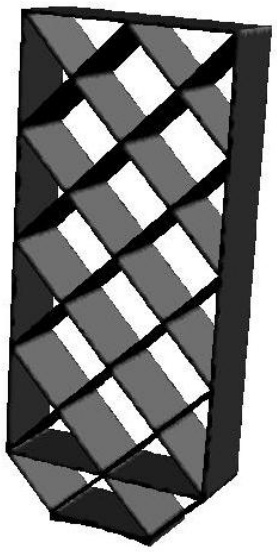

Figure 27: Baseline Lattice Grid Fin

The original baseline model used in testing had a range of thicknesses for the webbing (0.0047D to 0.0069D) compared to the desired value of 0.007D. Therefore, it was convenient for numerical modeling to use 0.005D as the thickness of the webbing. Even with this decrease of thickness, there was a slight issue with the production of the numerical model; the webbing would not fit exactly in the outer shell. This was caused by the inconsistent production of the sub-scale model for the ARF. With this in mind, the numerical model was produced to best accuracy possible. Except for the thickness of the webbing, all the other dimensions were kept the same.

The next step was to produce a mesh for the baseline lattice grid fin. Because this study requires extensive information of the flowfield in and around the lattice grid fin, an extremely small mesh was made. A total of 15 points were placed along the chord

of each webbing plate which made a spacing of 0.0222 inches. The faces of the lattice grid fins had 60 points which produced a spacing of 0.0125 inches.

Coarse Lattice Grid Fin

The coarse lattice grid fin was the first type of fin investigated by ARF as a solution to the choking problem. This was the next numerical model made for CFD analysis. Just like before, the dimensions came from ARF as shown in Figure 28 and were replicated in *Gridgen as* shown in Figure 29.

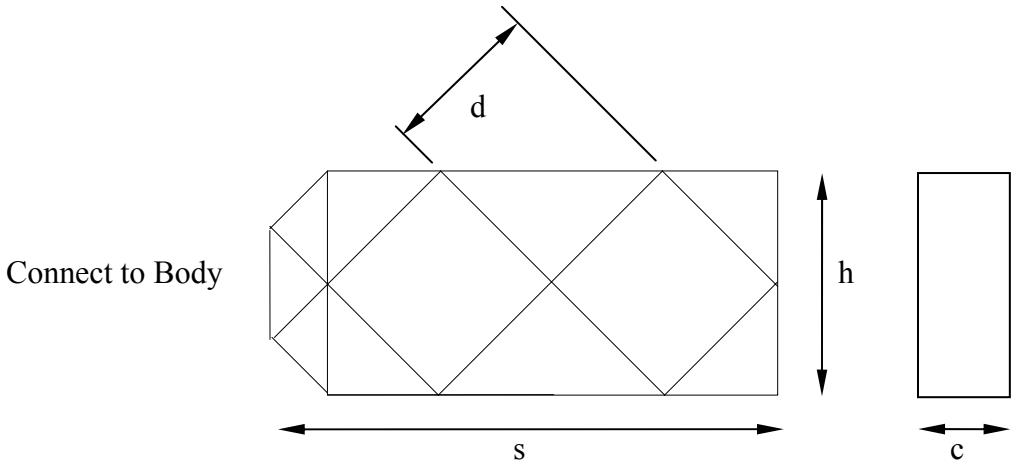

h (height)	0.333D
s (span)	0.75D
c (chord)	0.1179D
d (vane spacing)	0.2288D (open area = d^2)
t (thickness)	0.005D

(D=1 inch)

Figure 28: Coarse Lattice Grid Fin Geometry

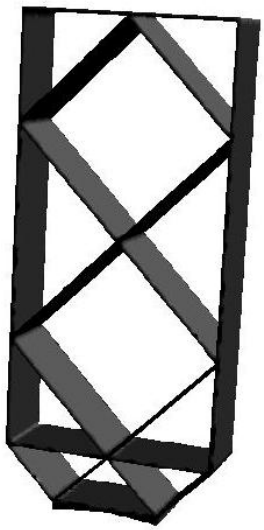

Figure 29: Coarse Lattice Grid Fin

The coarse model, just like the baseline model, used in the experimental tests had a range of thicknesses for the webbing (0.0047D to 0.0069D) compared to the desired value of 0.007D. This was caused by the inconsistent production of the sub-scale model for the ARF. Therefore, it was once again convenient to use 0.005D as the thickness of the webbing. With this in mind, this numerical model was also produced to best accuracy possible. Except for the thickness of the webbing, all the outer dimensions were kept the same.

The next step was to produce a mesh for the coarse lattice grid fin. Just as with the baseline model, there was a requirement to have extensive information of the flow field in and around the lattice grid fin and an extremely small mesh was made. A total of 15 points were placed along the chord of each webbing plate which made a spacing of 0.0222 inches. The faces of the lattice grid fins had 60 points which produced a spacing of 0.0125 inches. This is the same spacing as in the baseline model.

AFIT Lattice Grid Fin

The Department of Aeronautics and Astronautics and this author have proposed lattice grid tail fin geometry called the AFIT Coarse Lattice Grid geometry with dimensions shown in Figure 30 to alleviate the choking problem. It was tested and compared to numerical tests of the other two types of lattice grid fins tested at ARF.

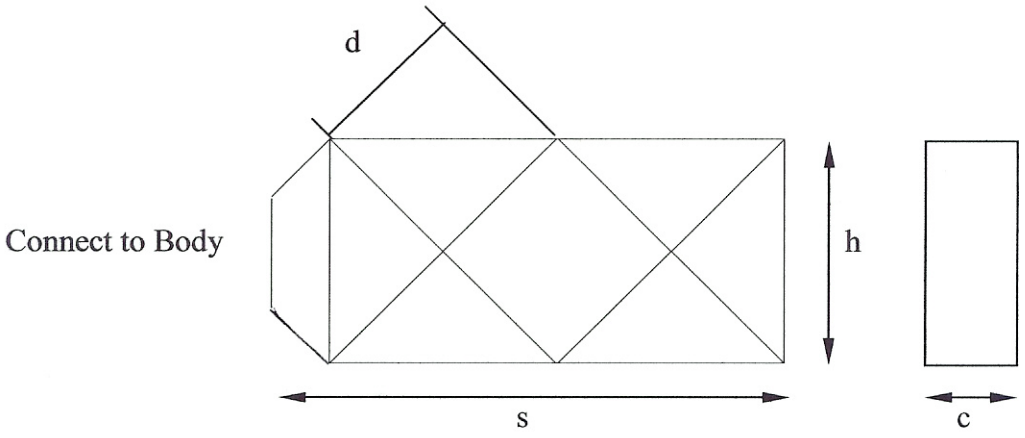

h (height)	0.333D
s (span)	0.75D
c (chord)	0.1179D
d (vane spacing)	0.2288D (open area = d^2)
t (thickness)	0.005D

(D=1 inch)

Figure 30: AFIT Coarse Lattice Grid Fin Geometry

It is believed that the AFIT design would be better than the previous lattice grid fins because this layout doubles the area of the cells in the main body of the fin while retaining a similar shape. This in turn would provide a smaller 'solidity' ratio. As described by Hoerner (21), the solidity ratio (σ) is defined as the 'ratio of the projected area, S_{solid}, to the total area, S_{total}' and that the loss of flow momentum 'through a

pervious or porous material is a function of shape and solidity ratio of the elements or ribs.' This theory can be used directly with the analysis of drag characteristics for grid-like devices. The solidity ratio for the tested sub-scale models as well as the AFIT coarse design are shown in Table 3.

Table 3: Solidity Ratios for Sub-Scale Lattice Grid Fins

Configuration	$\sigma = S_{Solid} / S_{Total}$
Baseline	$0.1722 \simeq 0.2$
Thin	$0.0984 \simeq 0.1$
Coarse	$0.0999 \simeq 0.1$
AFIT Coarse	0.0901

It is interesting to note that the solidity ratio for the thin and coarse configurations have the same solidity ratio; this could explain why the critical transonic Mach number was the same for those cases in the ARF tests. (16) Because of the decrease in the solidity ratio for the AFIT coarse design by nearly 40% from the baseline model, it is reasonable to conclude that the critical transonic Mach number will be increased. Table 4 shows the calculation made from the area ratio Mach relation stated earlier. It shows that the critical transonic Mach number would be increased from previously tested lattice grid fins. The estimated error was made based on trends from earlier results with the baseline and coarse fins.

Table 4: Critical Transonic Mach Number for AFIT Coarse Fin

Configuration	d	t	A/A^*	$M_{Critical}$	$M_{Critical}$ *(Test)*	% Off
AFIT Coarse	0.2288	0.005	1.044	0.846	~0.82	~3

The AFIT coarse model shown in Figure 31 will be modeled the same as the other two lattice grid fins. Therefore, it was convenient to use 0.005D as the thickness of the webbing for this model just like before. The major difference will be the different webbing configuration as well as the elimination of the webbing near the base of the fin.

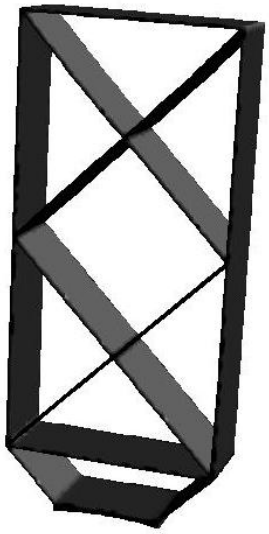

Figure 31: AFIT Coarse Lattice Grid Fin

The next step was to produce a mesh for the AFIT coarse lattice grid fin. An extremely small mesh was made in order to capture the important flow information needed on and around the fin. Just like the other two fins modeled, 15 points were placed along the chord of each webbing plate which made a spacing of 0.0222 inches. The faces of the lattice grid fins had 60 points which produced a spacing of 0.0125 inches. This is the same spacing as in the baseline model.

Farfield

The last stage of numerical modeling was to produce an outer boundary (Farfield condition) for the extent of the numerical domain which would contain the aerodynamic

flow. It must be located far enough away to completely contain all shocks and other discontinuities or the solution would not be as accurate. When completing the grid convergence study, another finding was an appropriate boundary of the domain. The chosen distance ahead of the missile was 11D with the height above and below the missile being 11D as well. This allowed for the containment of the shock at the nose as well as the shock at the transition to the body. At the rear of the missile, 20D was decided upon in order to capture the flow from the lattice grid fin and the rear of the missile. The outer boundary was modeled with a smaller amount of points because it was not crucial to have detailed information at the uniform flow boundary. A 2D cross section can be seen in Figure 32. The total amount of cells of missile, tail, and farfield came to around 140,000 cells.

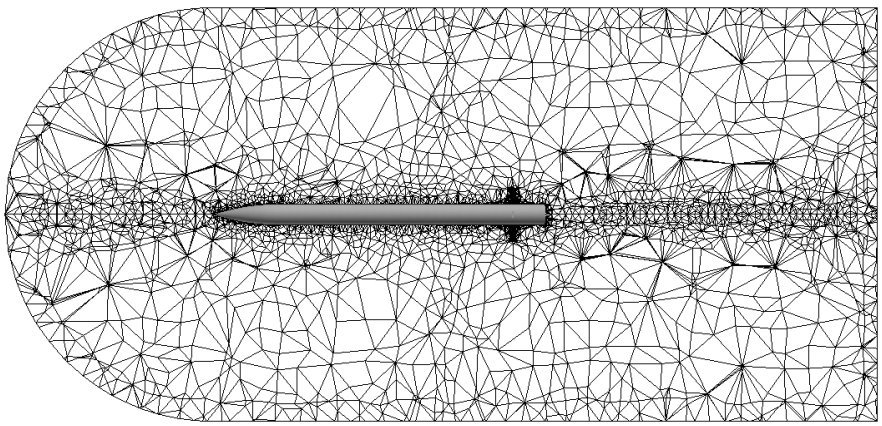

Figure 32: Complete Numerical Model

Chapter Summary

Gridgen was the computer software used to generate the meshes for the sub-scale missile numerical model. The missile body was modeled first to exact specifications with the mesh being sectioned into nose, body, and tail. Next, the baseline fin was modeled as close to possible with the experimental model used at ARF. An extremely tight mesh was generated in order to obtain important information from this section of the CFD analysis. The coarse fin designed at ARF was modeled next and the same type of mesh was made as the baseline model. Lastly, the AFIT coarse fin was designed, modeled, and meshed in the AFIT ENY department.

IV: Numerical Results and Analysis

Fluent

In order to produce solutions for the numerical models, *Fluent* was the software program of choice.

> "*Fluent* is the world leading CFD code for a wide range of flow modeling applications. With its long-standing reputation of being user-friendly, *Fluent* makes it easy for new users to come up to productive speed. Its unique capabilities in an unstructured, finite volume based solver are near-ideal in parallel performance. To ensure that *Fluent* is ready to deploy right out-of-the-box, they put the program through a comprehensive program of industrial-strength testing." (22)

Because of the availability of *Fluent* at AFIT and the relatively small amount of time to complete this thesis for naval students, this commercial program was used instead of generating a unique CFD code for this situation. The Department of Aeronautics and Astronautics has a 16-node, 32-processor Beowulf cluster for high performance computing and this platform was used along with *Fluent* run in parallel for the CFD study. Complete details of *Fluent* can be found at their website in Reference 22.

A basic setup was used for all cases. *Fluent* was set to use a coupled and implicit solver as well as ignoring viscous calculations for these initial design runs. The ARF temperature was maintained at a steady level during the experimental tests (71 ^{o}F) and therefore was duplicated in the numerical runs. The density during the numerical runs was set from the density provided in the baseline runs at ARF at nominally 1.2 kg/m^3. These initial data allowed for a matching between the experimental tests and numerical runs as initial and boundary conditions.

Baseline Drag

As stated earlier, it is very important to obtain the axial or drag force produced by the lattice grid fin. Even though the model was run with no viscous effects, correction factors were used to account for viscous drag and trends can be seen in the results of the inviscid numerical runs.

In order to account for viscous effects on the missile body, Fleeman developed a formula for the skin friction drag: (2)

$$(C_{D_o})_{Body,Friction} = 0.053\left(\frac{l}{d}\right)\left[\frac{M}{ql}\right]^{0.2}$$

In this equation, l is the length of the missile, d is the diameter of the missile, M is the Mach number, and q is the dynamic pressure. The assumptions made when producing this equation was the body area can be approximated by the wetted area of a cylinder, the variation in the freestream speed of sound and viscosity with altitude is very small, and that there is a turbulent boundary layer.

Another approximation that was used to approximate the drag produced by the lattice grid fin was the laminar flat-plate boundary layer theory as stated in White (23):

$$(C_{D_o})_{Fin} = \frac{0.664(\rho\mu L)^{1/2}U^{3/2}a}{(1/2)\rho U^2}$$

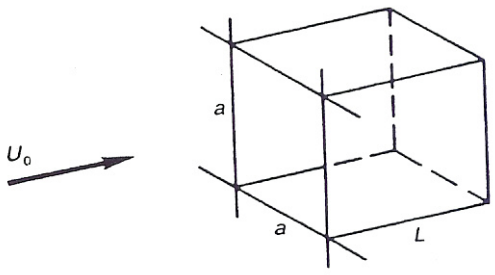

Figure 33: Laminar Flat-plate Boundary-layer Theory Cell (23)

In this equation, ρ is density, μ is viscosity, U is the freestream velocity, L and a are the dimensions for the box shown in Figure 33. For the grid cell L equals c, chord length, and a equals the width of the cell. Each square cell has four surfaces and each triangular cell has three surfaces which experience a shear force that can be approximated using laminar boundary-layer theory. These cells are very similar to the lattice grid fin cells, therefore this would be a good approximation to viscous drag on the fin. The lattice grid fin laminar boundary-layer equation for C_D was applied to every interior cell as well as to the outer surfaces of the fin. These viscous drag corrections were applied to the inviscid drag results. Appendices B, C, and D contain the raw data from the runs done in *Fluent* for the baseline, coarse, and AFIT lattice grid fins and contain the drag coefficient data.

Figure 34 shows the axial force of the numerical runs with the baseline lattice grid fin connected to the missile. Compare this to the experimental data from ARF shown in Figure 35.

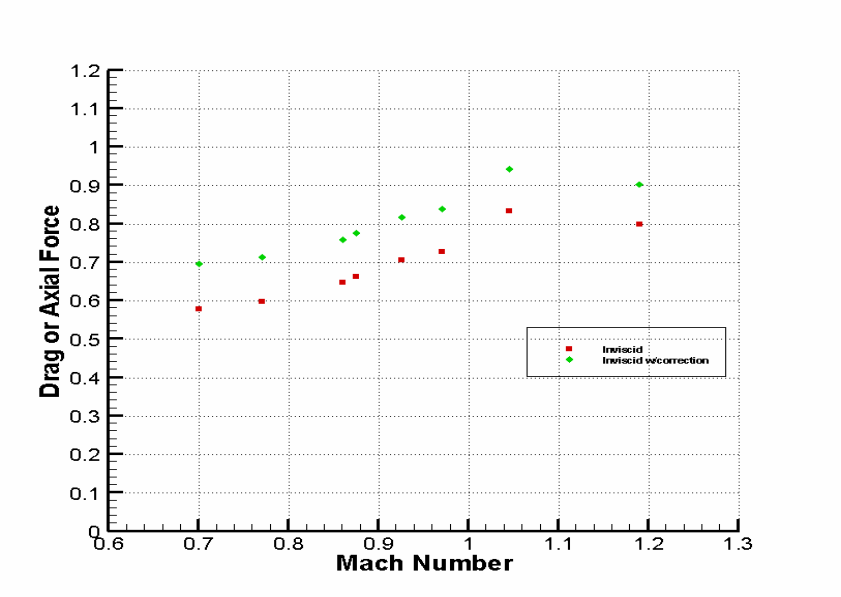

Figure 34: Numerical Drag

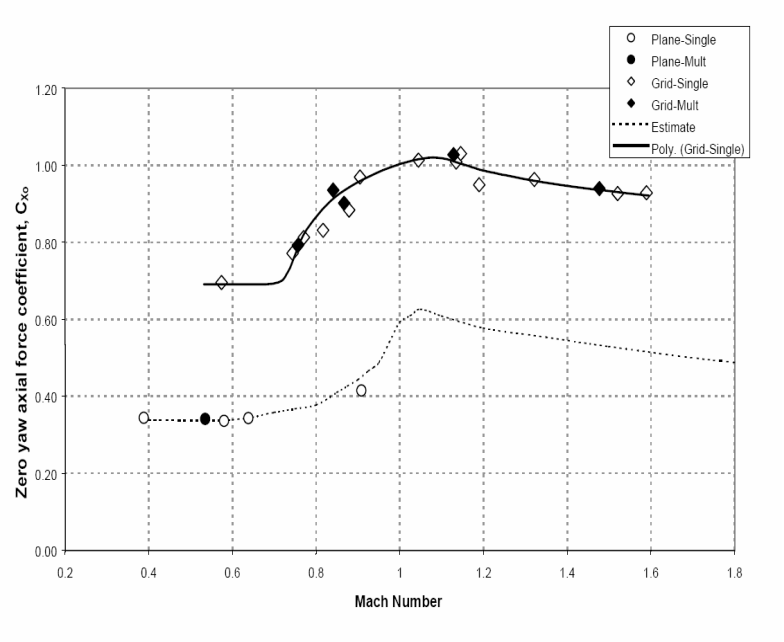

Figure 35: ARF Experimental Drag (13)

Figure 34 of the viscous corrected numerical drag calculations from the inviscid runs are very comparable to the data produced for the experimental tests done at ARF shown in Figure 35. It is very important to point out the impact that the skin friction calculation and cell fin correction had on the axial force. For example, at Mach=0.7, the numerical run yielded a coefficient of drag of 0.5783, the body skin friction approximation came to 0.1139, and the cell correction produced a coefficient of drag of 0.0067. The total coefficient of drag came to 0.6987. From the ARF experimental drag in Figure 35, one can see the drag coefficient is around 0.7. This numerical test point, as well as the others, produced results that were well within 10% of the experimental findings.

The trend lines for both the numerical calculations and the experimental tests showed good agreement. Even though the numerical results were inviscid, this is not

unexpected because pressure drag is a higher percentage of the total drag than friction drag, especially when you transition into the supersonic flow regime. The difference with the results occurs in that the numerical data is much more of a linear increase with the Mach number than the experimental cases. This could be due to the fact that more test data points were concentrated around this transonic Mach range during the experiment at ARF and the numerical results miss the transonic drag rise.

Baseline Moment Coefficient

In order to produce a pitching moment vs. Mach number comparison with experimental results, numerical runs were made at an individual Mach number and angle of attack. This was done multiple times to produce adequate results. Figure 36 shows the Mach moment lines for multiple cases.

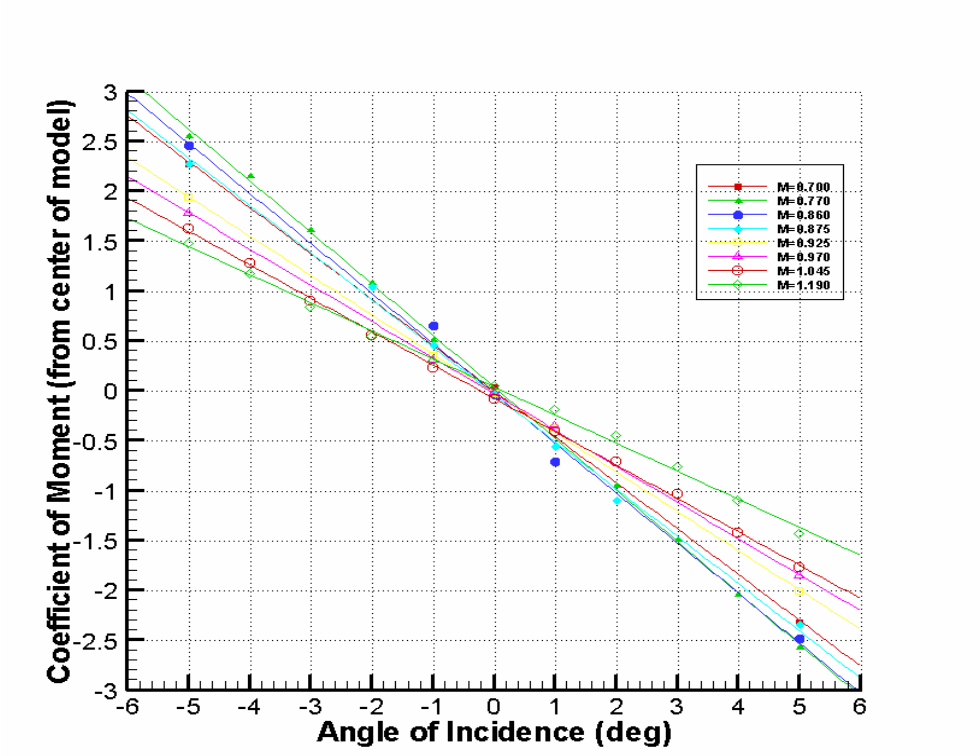

Figure 36: Numerical Moment Coefficients-ARF Geometry

Figure 37 is not the Mach moment lines for the missile at ARF, but another lattice grid fin missile with a different size missile and lattice grid fin configuration produced by the DRDC-Valcartier in Canada. This figure provides an example of trend lines seen in missiles with lattice grid fins at transonic Mach numbers.

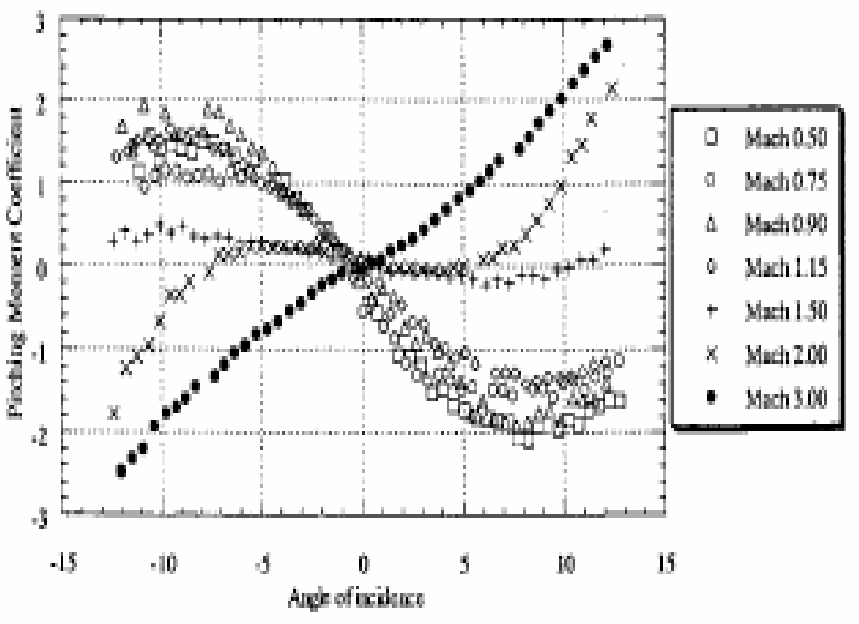

Figure 37: Experimental Moment Coefficients- DRDC Missile (7)

As the Mach number is increased, the slope of the pitching moment coefficient decreased as shown Figure 37. This also occurred in the numerical results in Figure 36. The only exception is at low Mach numbers, where the normal force starts decreasing as well. This describes the Mach 0.70 numerical case and the Mach 0.50 for the experimental case. With this in mind, the trends of both curves are the same at angles of attack between -5 and 5 degrees. This allowed for continuation for plotting of the slope of the pitching moment vs. Mach number.

Baseline Pitching Moment Derivative

When calculating the pitching moment derivative for each case, a linear approximation between -5 and 5 degrees was used. This was appropriate in that the data is somewhat linear in this range. Upon approaching 8 degrees, the pitching moment coefficient levels off and is no longer linear. Figure 38 shows the numerical pitching moment derivative and Figure 39 shows the ARF experimental results.

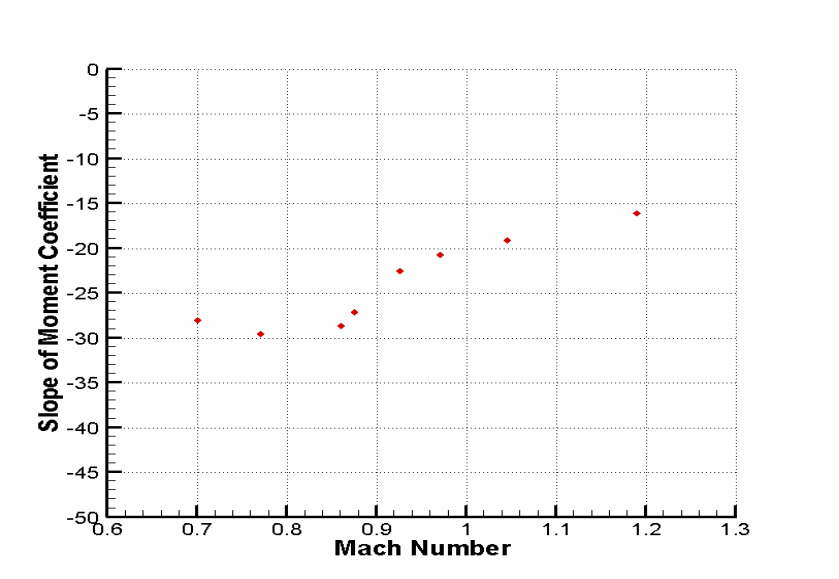

Figure 38: Numerical Pitching Moment Derivatives

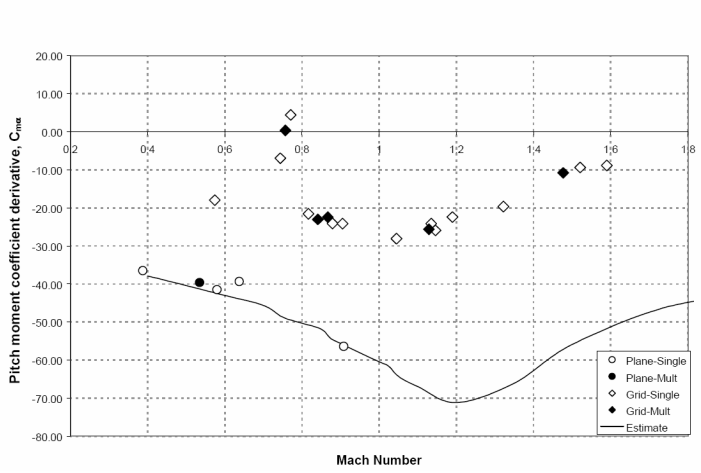

Figure 39: ARF Experimental Pitching Moment Derivatives (13)

Unlike the axial force calculations and the moment coefficient, the trend for the pitching moment derivative is not as accurate for the given Mach number. The reason for this could be due to the inviscid calculations used for the numerical model. A correction factor had to be used in order for the axial force or drag calculations to be comparatively accurate with the experimental results. There was no correction factor for the pitching moment derivative. It seems though that there is an offset of the numerical data collected from experimental results. If the numerical data is offset by a Mach number 0.2, then the data is much more accurate than before. Therefore, the Mach range tested numerically in the invicsid flow regime appears to be above the experimentally observed critical transonic Mach number for choked flow.

Baseline Flowfield

An important investigation that was made at ARF was the complex flowfield which the lattice grid fins made during the experimental tests. The numerical runs in *Fluent* were also made to support the grid fin flowfieds produced. Figure 40 shows Mach contours and streamlines for one of the tests.

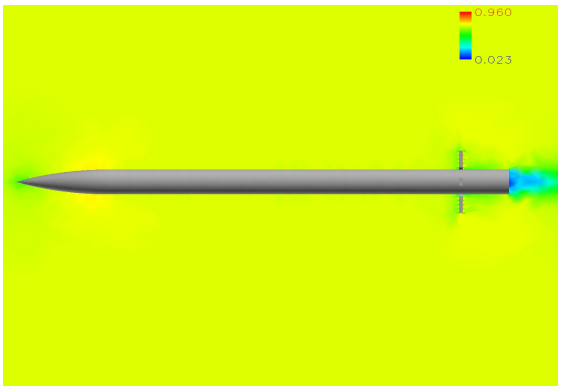

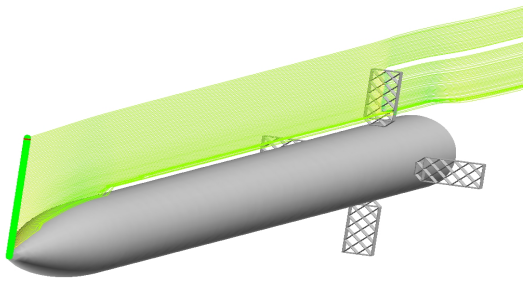

Mach Contour Streamlines

Figure 40: Numerical Mach Contours/Streamlines M=0.7

This missile flowfield shown in Figure 40 is typical for flows at or below Mach 1. There is little happening on the body of the missile and there is an expected disturbance or impeded flow around the fin area. The conductors of the experimental tests described this disturbance as locally transonic flow occurring in the fin region due to the narrowing within the grid cell flow area. The numerical runs support this theory based on the similarity between drag data for the experimental and numerical tests. Figure 41 demonstrates the flowfield located in the fins at Mach 0.7. It is interesting to point out that the streamlines in Figure 40 show that the flow coming off the front of the missile bypasses the bottom section of the fin creating a stagnated flow region. This can be seen better in Figure 41 with the top fin Mach contours.

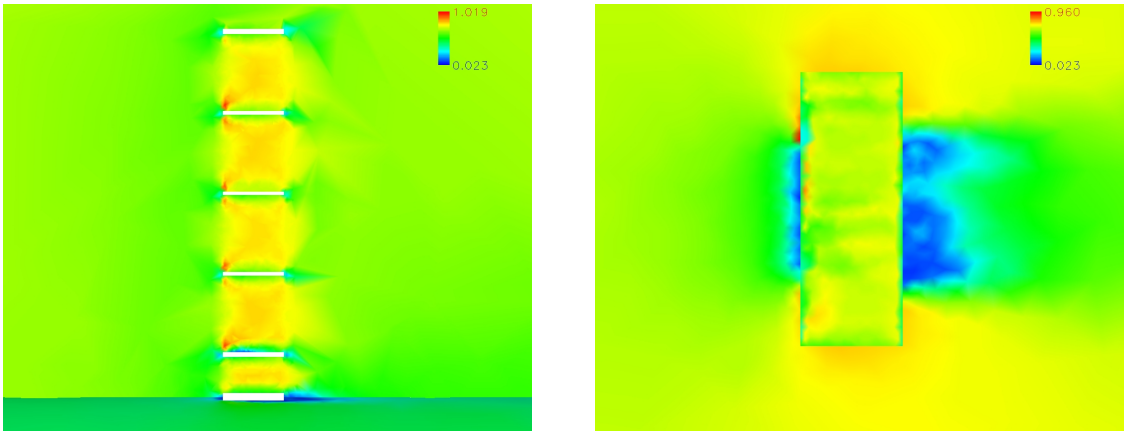

Top Fin-Side View Top Fin-Top View

Figure 41: Mach Contours of Baseline Fin M=0.7 AOA=0 deg

As is seen in Figure 41, the top fin has somewhat of a uniform flowfield through most cells of the fin. One can see introduction of oblique shocklets at the leading edge of the cells even at this low Mach number of 0.7. Once again, this is expected since the fin is acting like a subsonic inlet nozzle as stated before. The bottom cell section, however,

does not experience these oblique shocks based up on the flow moving higher on the lattice grid fin. At the base of the fin, there is a stagnation region which increases drag.

At an angle of attack of -5 degrees, the lattice grid fin flowfield changes. Figures 42 describe the flowfield mach contours that occur. The streamlines in Figure 43 demonstrates that the flow travels around the top of the missile. This causes the obliques shocklets to be more symmetrical on the top and even stronger on the top lattice for the bottom fin. This is shown in Figure 44.

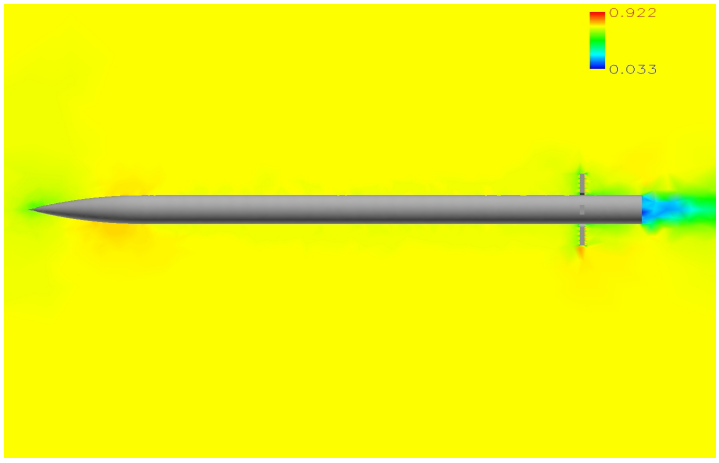

Figure 42: Numerical Mach Contours M=0.7 AOA=-5 deg

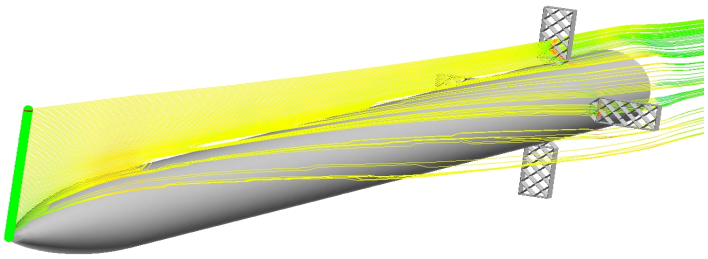

Figure 43: Numerical Streamlines M=0.7 AOA=-5 deg

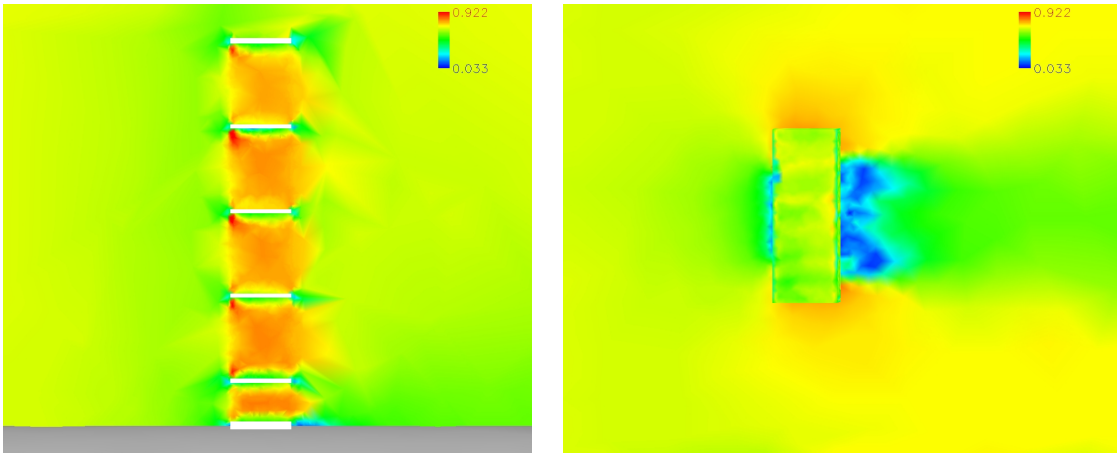

Top Fin

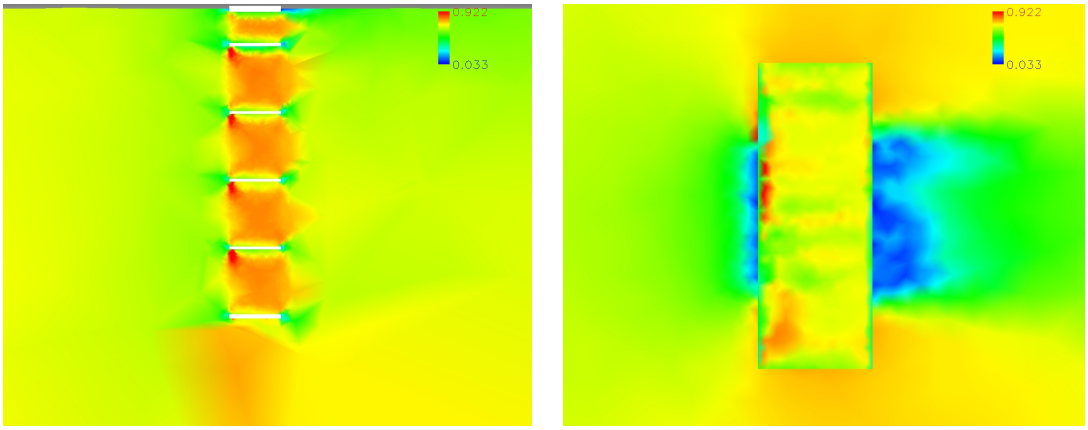

Bottom Fin

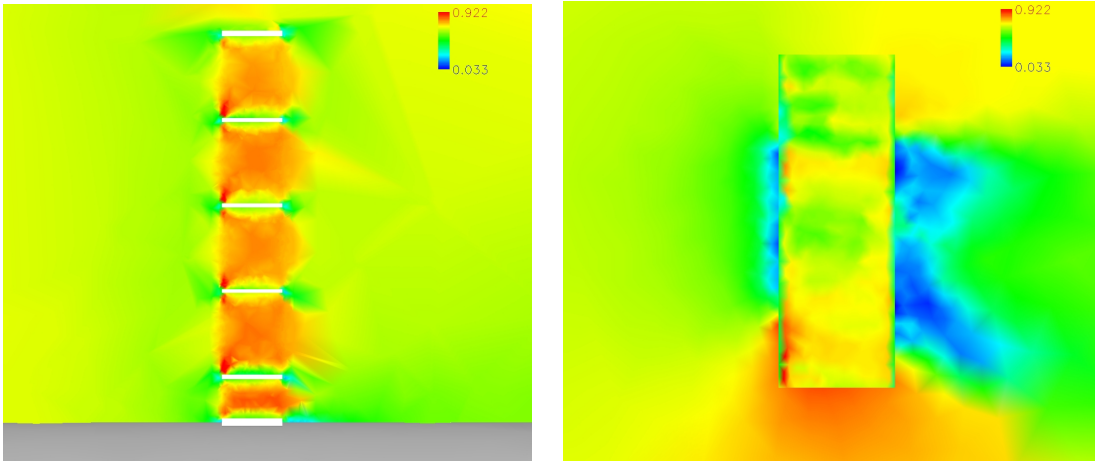

Side Fin

Figure 44: Mach Contours of Baseline Fin M=0.7 AOA=-5 deg

The interior cells at -5 deg have a very similar flow field to that at 0 deg. The major difference is the formation of the shock at the farthest extend of the bottom fin. This is typical based on an expansion wave forming based on the change of angle of attack of the missile with accelerate the flow and then requires a shock to slow it down. As seen in the streamlines of Figure 43 and the side fin Mach contours, the flow is traveling over the top of the bottom fin. This again causes the disturbance at the bottom of the missile.

A totally different type of flowfield occurs when the Mach number increases over one. Figure 45 is a shadowgraph from the ARF experiment which shows the complex shock system at this Mach number. The Mach contours and streamlines from the numerical runs is seen in Figure 46.

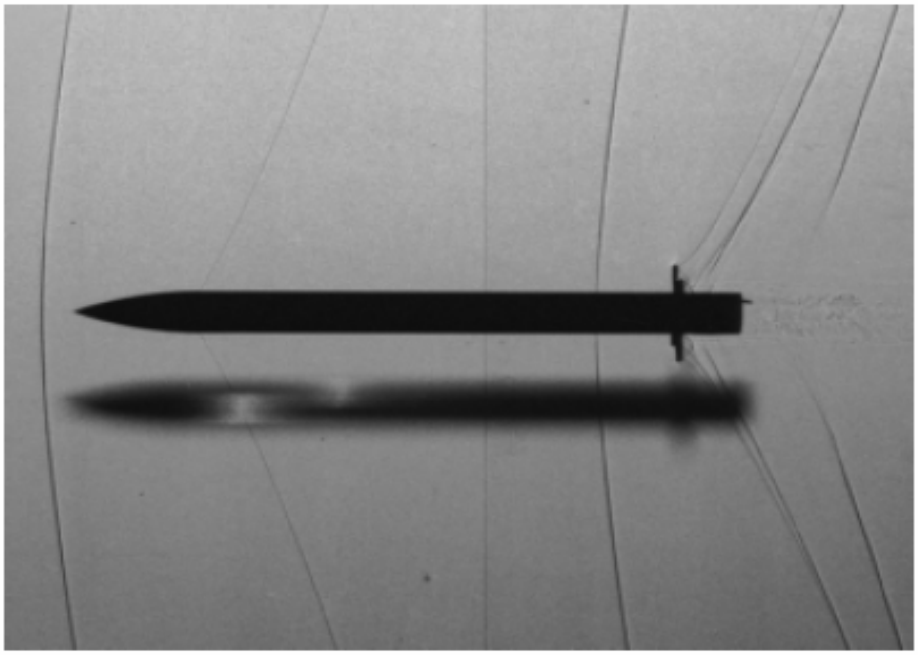

Figure 45: ARF Experimental Test M=1.17

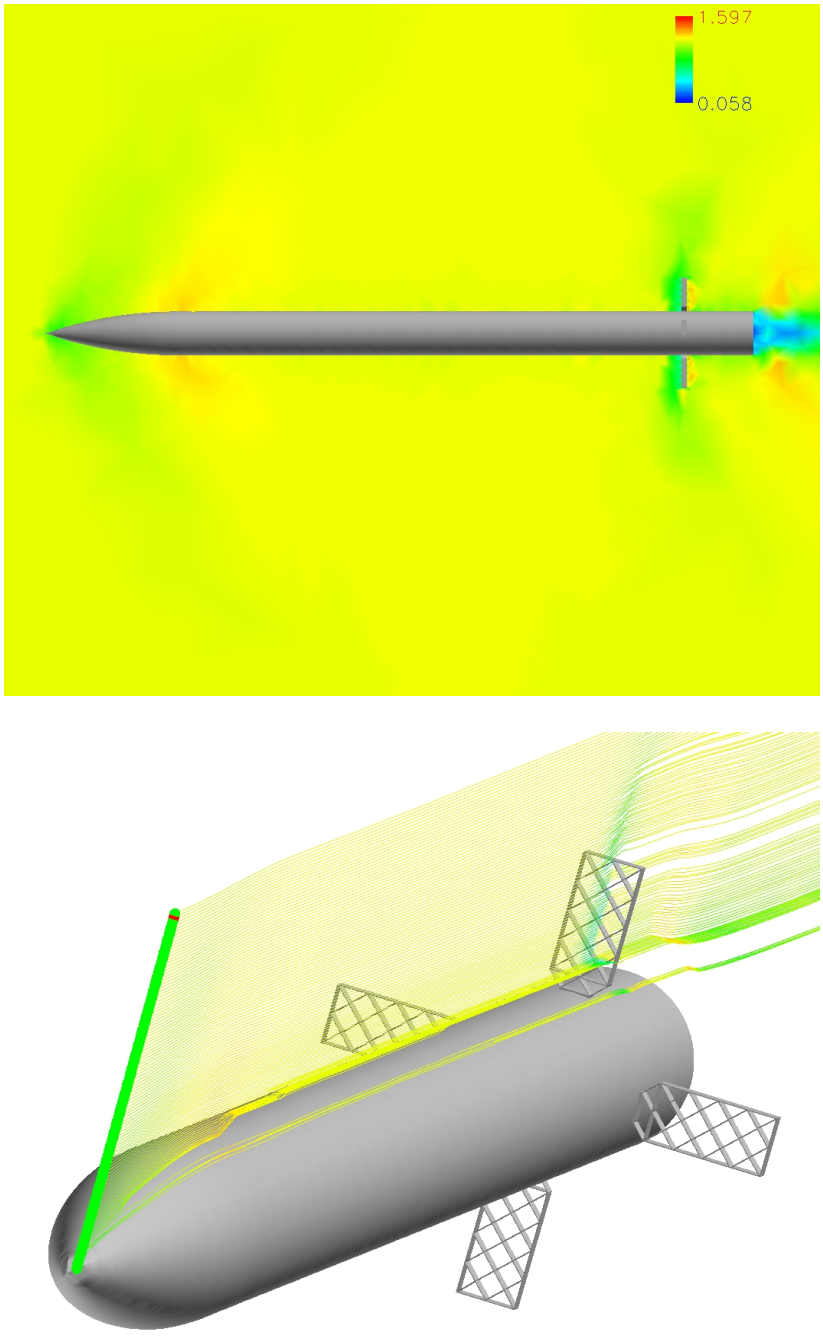

Figure 46: Baseline Mach Contours/Streamlines M=1.19

As documented in the ARF experimental tests results and the numerical runs, there are 5 types of shocks that occur when Mach number is greater than 1. Both the experimental and numerical tests produce the same types of shock waves. The first shock is the stand-off shock located at the nose of the missile. The next shock is weaker and occurs at the transition of the nose and body of the missile. Another shock occurs in front of the fins, the shock moves toward the fins as the Mach number is increased. A shock also forms from the interaction of the flow traveling through the lattice grid fins and is shown in the following Figure 47. The last shock occurs at the rear of the missile by the recompression of the flow behind the model's base. The details of the shock dealing with the fin are seen in Figure 47. The formation of the bubble (shock 4c) forms at a Mach number greater than one. Also, the formations of shocks at the front of the lattices become even more defined. The flow with the 5 shocks determined by the numerical runs are very similar to those documented at ARF in Figure 11.

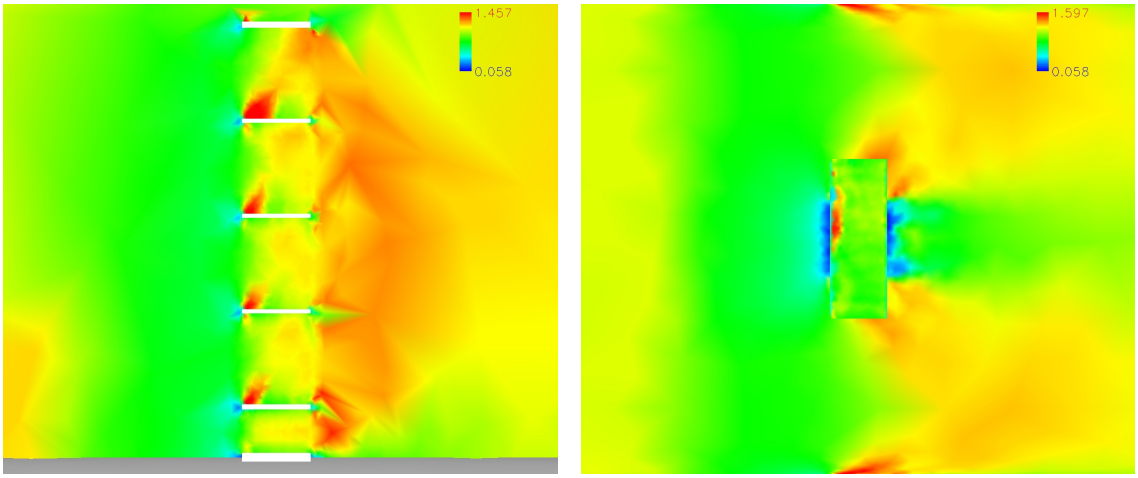

Top Fin-Side View Top Fin-Top View

Figure 47: Mach Contours of Baseline Fin M=1.19 AOA=0 deg

The Mach contours of the top fin in Figure 47 depict the bubble shock 4c as seen earlier in ARF experiments in Figure 45. One can also notice that the oblique shocks in the cells are stronger with the increase of Mach number. But, the bottom cell region of the top fin does not show the presence of oblique shocks. Once again, this occurs with the flow traveling over the nose and bypassing the bottom cell of the fin as seen in the streamlines of Figure 46. Note also the oblique shocks generated by the outer frame of the fins interacting between the four fins shown in Figure 47. It seems at higher Mach numbers that they intersect, causing a stronger shock.

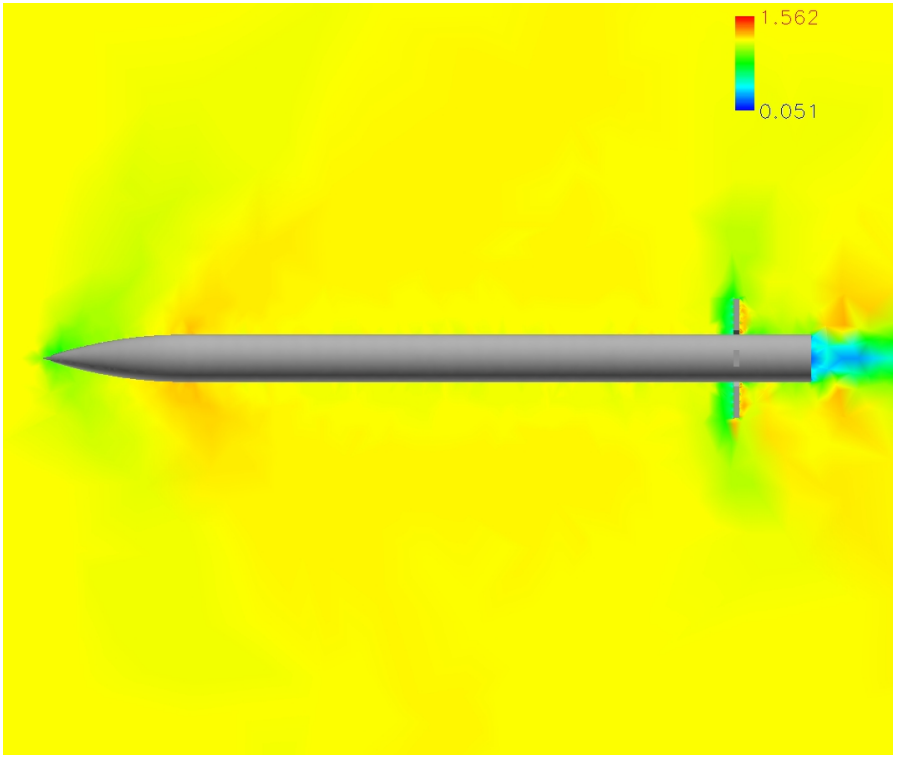

Figure 48: Baseline Mach Contours M-1.19 AOA=-5 deg

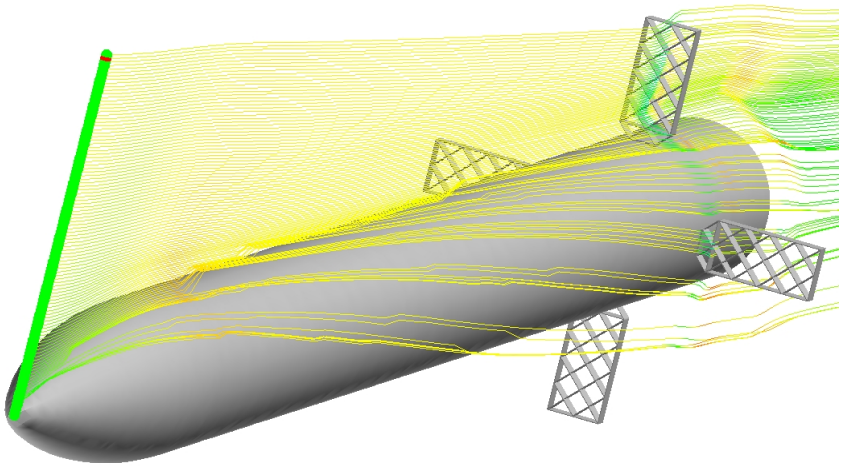

Figure 49: Baseline Streamlines M=1.19 AOA=-5 deg

When looking at the Mach contours of the missile in Figure 48 with an angle of attack of -5 degrees, it seems that there is little difference in the flow compared to the 0 degree angle of attack. But the streamlines in Figure 49 shows the movement of particles over and around the top of the missile. Figure 50 depicts a formation of a shock caused by the compression of the flow at the furthest extent of the bottom fin. Because of the increase of the Mach number, it is a stronger shock. It is interesting however that the shocks formed on the front lattices seem to be symmetrical on the top and bottom of the top fin (side view). This is not seen in the cell of the fin with the zero angle of attack. This might be caused by the flow traveling over the body and not into the bottom section of the fin. It seems this would cause the middle cells to choke before the bottom cell.

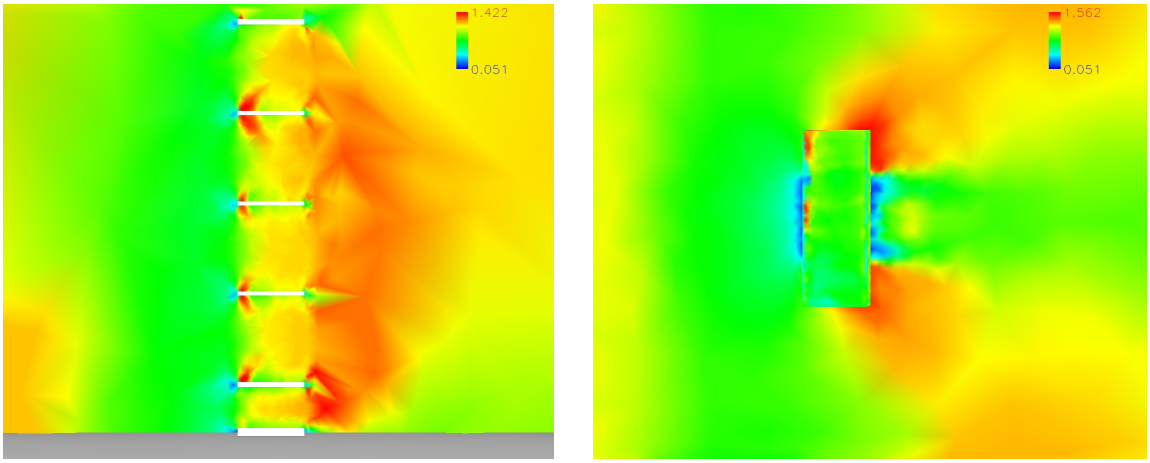

Top Fin

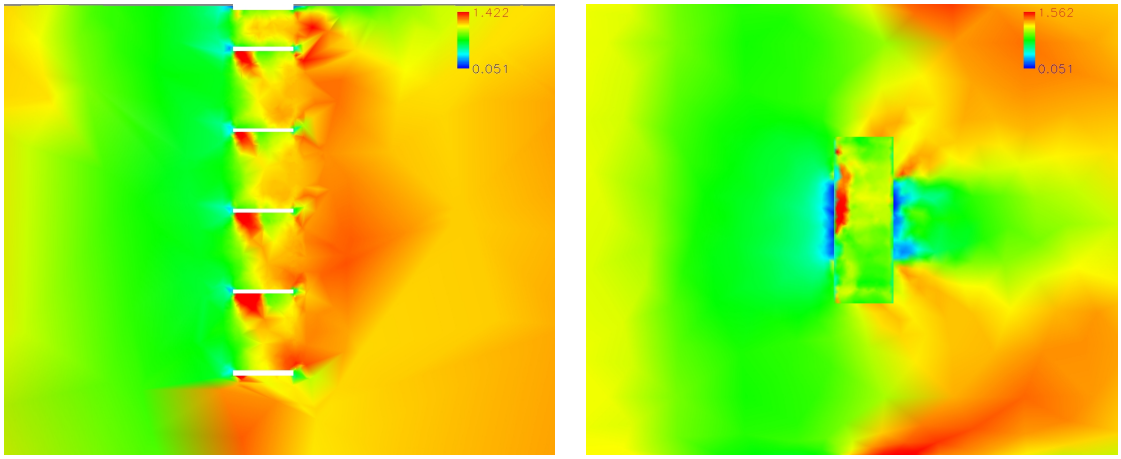

Bottom Fin

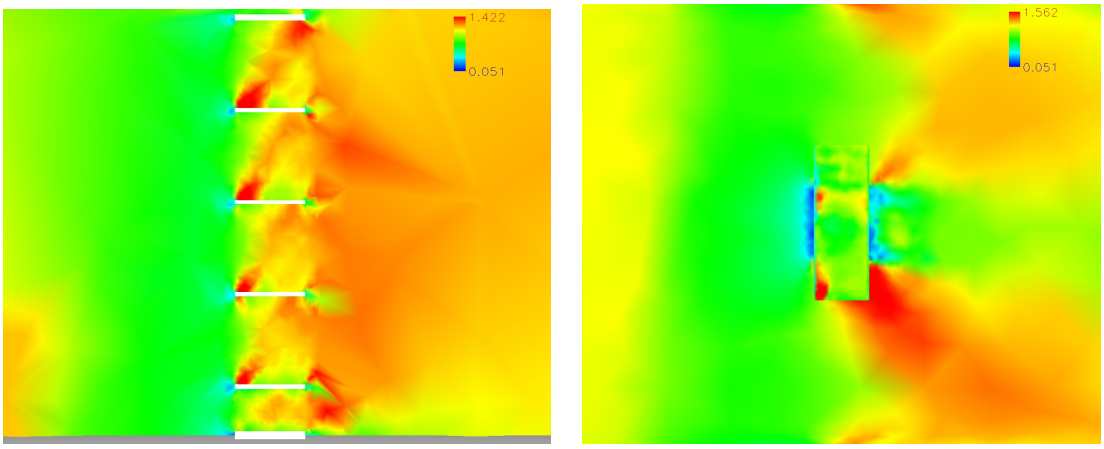

Side Fin

Figure 50: Mach Contours of Baseline Fin M=1.190 AOA=-5 deg

Coarse Drag

Figure 51 shows the axial or drag force of the numerical runs with the baseline lattice grid fin connected to the missile and Figure 52 shows the experimental data from ARF.

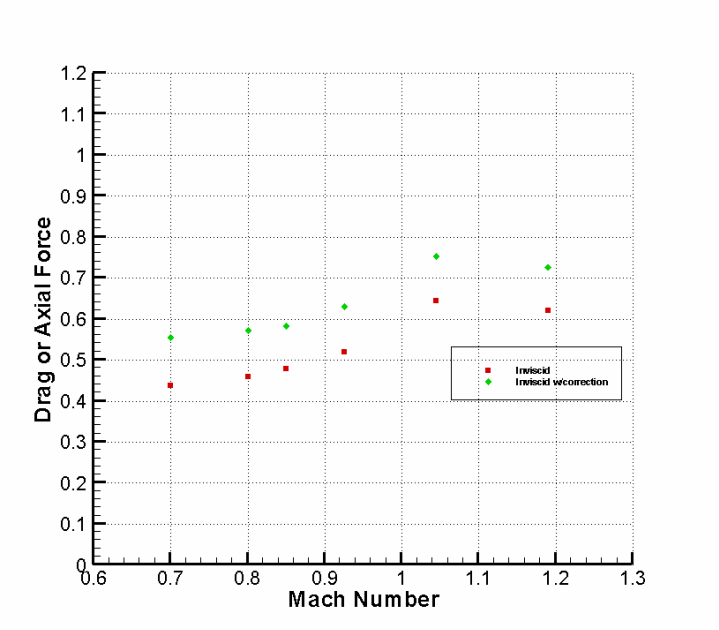

Figure 51: Numerical Coarse Drag

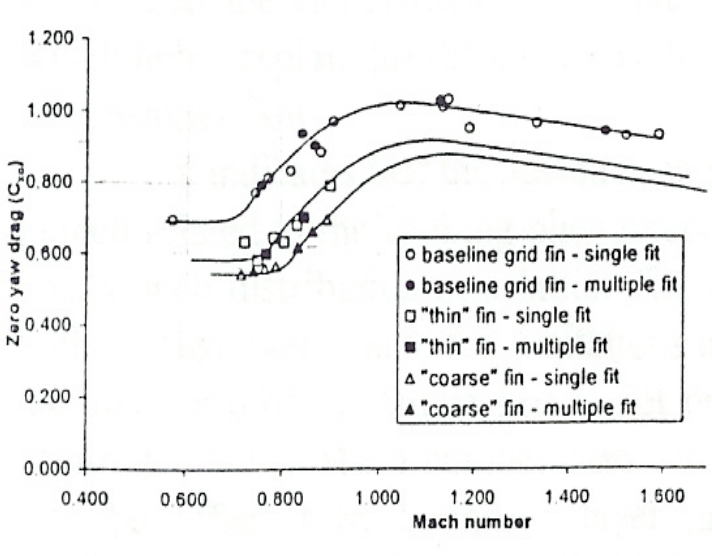

Figure 52: Experimental Coarse Drag (16)

The data in Figure 51 of the corrected numerical drag calculations are, once again, quite comparable to the data produced for the experimental tests done at ARF shown in Figure 52. The skin friction force approximation was added to the coarse grid fin data. This produced results that compared to within 10% of the experimental findings. Just like the baseline lattice grid fin geometry, the trend lines for both the numerical calculations and the experimental tests were nearly the same for the coarse fin geometry.

Coarse Moment Lines

In order to produce a pitching moment vs. Mach number plot from the computational tests for comparison with experimental results, numerical runs had to be made at an individual Mach number and angle. Once again, this was done multiple times to produce adequate results. Figure 53 shows the Mach moment lines for multiple cases which is similar to what was done in the baseline geometry case.

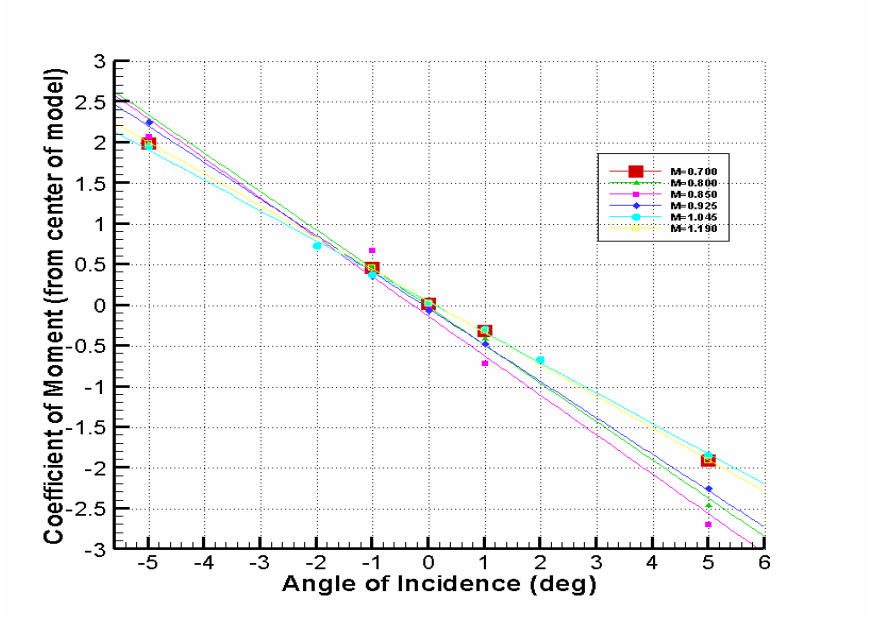

Figure 53: Numerical Coarse Moment Coefficients

It is shown again that as the Mach number is increased, the slope of the pitching moment coefficient decreased. This also occurred in the numerical results very similar to the baseline lattice grid fin. At low Mach numbers, the pitching moment decreased. This describes why the Mach 0.7 numerical case and the Mach 1.045 almost falls on top of each other. The trends of the curves between -5 and 5 degrees appear linear and therefore, were used in the approximation of the slopes.

Coarse Pitching Moment Derivative

Once again, when calculating the pitching moment derivative for each case, a linear approximation between -5 and 5 degrees was used. This was appropriate in that the data is somewhat linear in this range and was the basis for the pitching moment coefficients in previous research of lattice grid fins. Figure 54 shows the numerical pitching moment coefficients and Figure 55 shows the ARF experimental results.

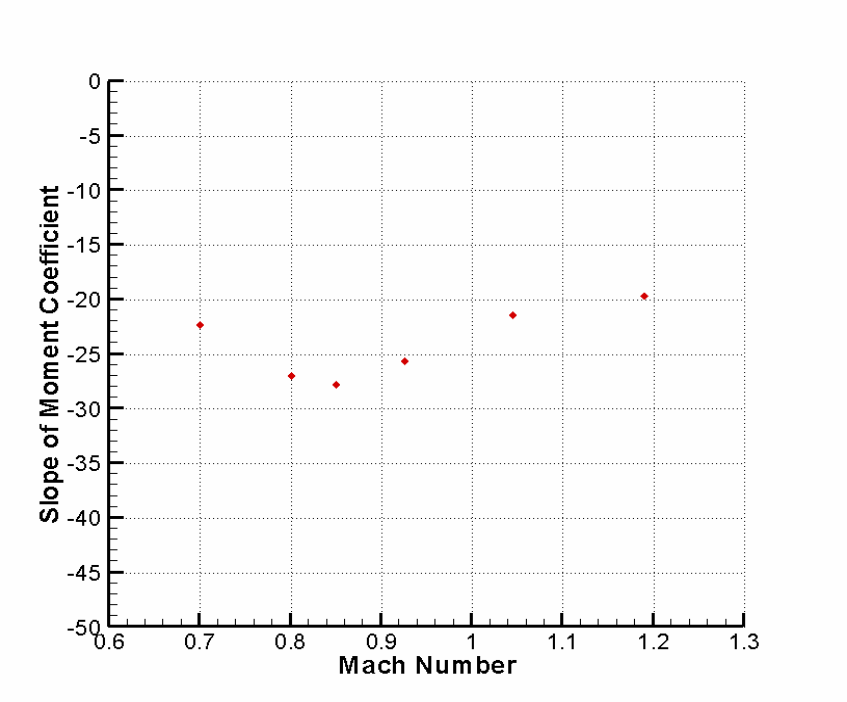

Figure 54: Numerical Coarse Pitching Moment Derivatives

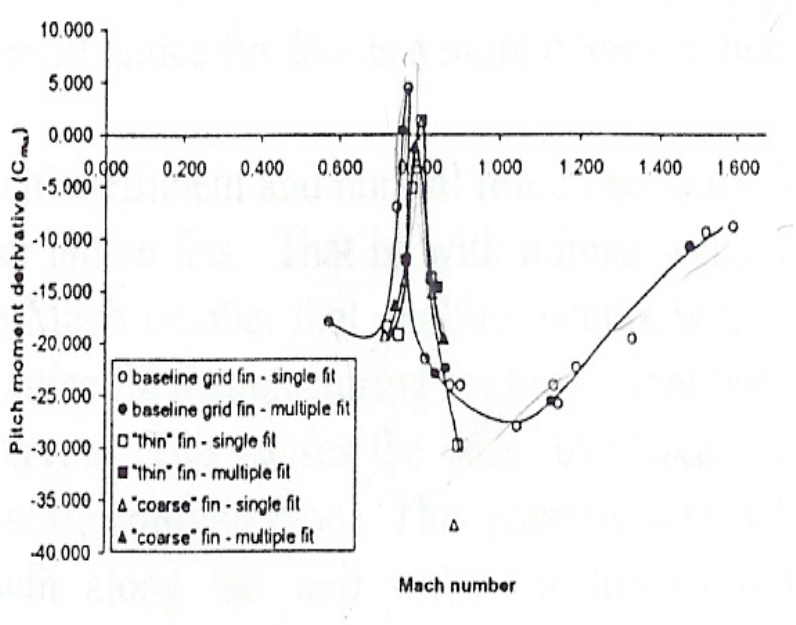

Figure 55: ARF Experimental Comparison of Pitching Moment Derivatives (16)

Unlike the axial force calculations and the moment coefficient, the trend for the pitching moment derivative is not as accurate for the given Mach number which is expected based on what was seen with the baseline grid fin comparisons. Once again, the reason for this may be due to the inviscid calculation used for the numerical model with no correction factor. There was no viscous correction factor for the pitching moment derivative. It seems though that there is an offset of the numerical data collected from experimental results just like before. If the numerical data is offset by a Mach number 0.2, then the data is much more accurate than before. Therefore, the Mach range tested numerically appears to be above the experimentally observed critical transonic Mach number for choked flow. Both the baseline and coarse numerical data support the theory that there is a shift in the inviscid results from the viscous experimental data.

Coarse Flowfield

There were no documented flowfield pictures involving the coarse lattice grid fin configuration. Therefore, Figures 56 and 57 are from numerical run calculations.

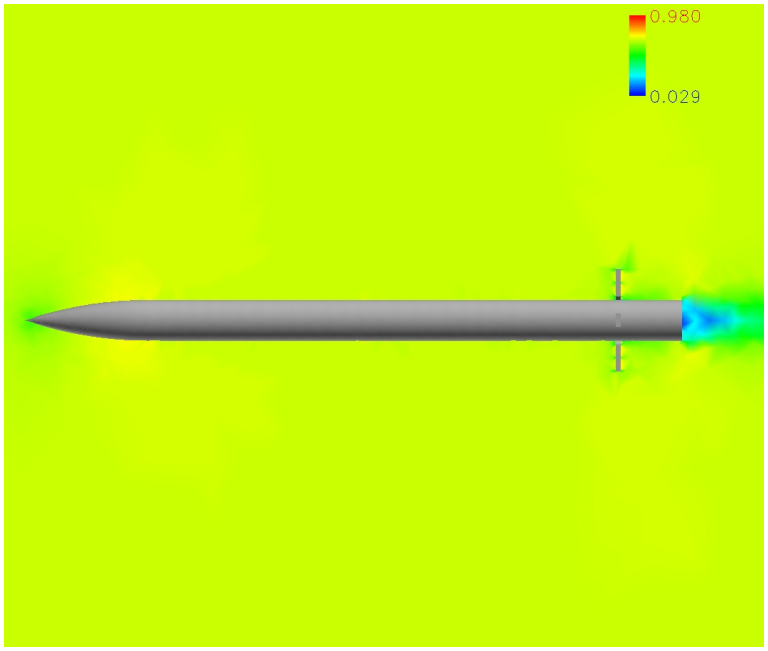

Figure 56: Coarse Fin Mach Contours M=0.7 AOA=0 deg

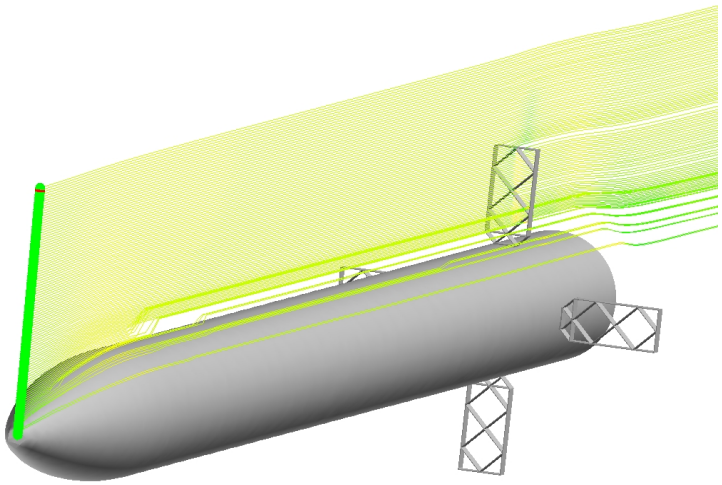

Figure 57: Coarse Fin Streamlines M=0.7 AOA=0 deg

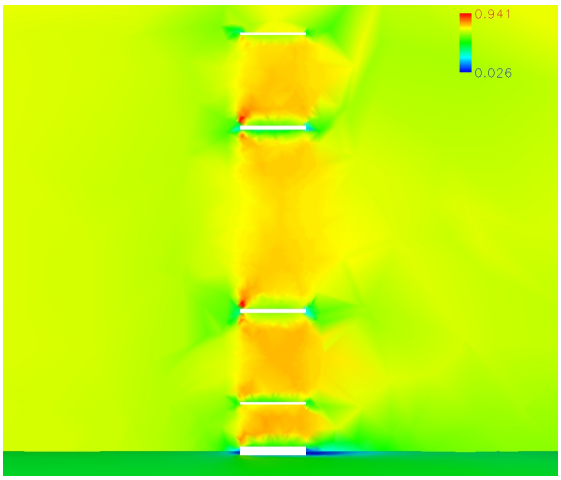

Top Fin-Side View

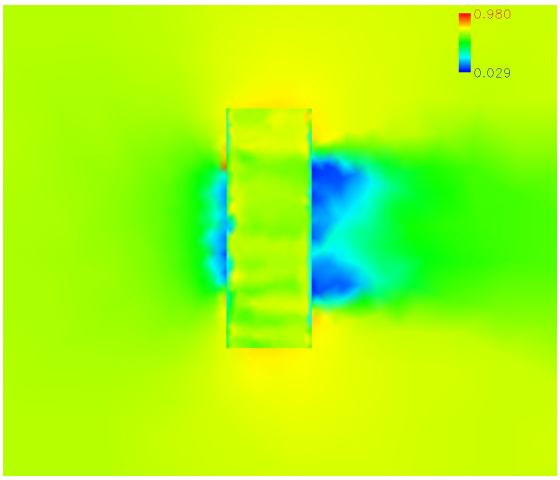

Top Fin-Top View

Figure 58: Coarse Model Top Fin M=0.7 AOA=0 deg

As expected, the overall flowfield from the coarse lattice grid fin configuration is similar to that of the baseline model. At Mach 0.7 (shown in Figure 58), there is the beginning of the formations of shocks at the front or leading edge of the lattices which was expected since they occurred in the experimental and numerical tests for the baseline model. The bottom cell of the top fin still had weaker oblique shocks than in the cells above. The streamlines in Figure 60 shows a similar flow to that of the baseline model in that flow from the nose travels above the bottom cell of each fin. When dealing at an angle of attack of -5 degrees, the Mach contours of the flowfield (Figure 59) is also similar to that of the baseline model at that angle of attack. The Mach contours of the fin described in Figure 61 show the movement of the flow as well as the equal oblique shocks on top and bottom of the lattices. The major difference however, is the formation of the shock at the farthest extent of the bottom fin.

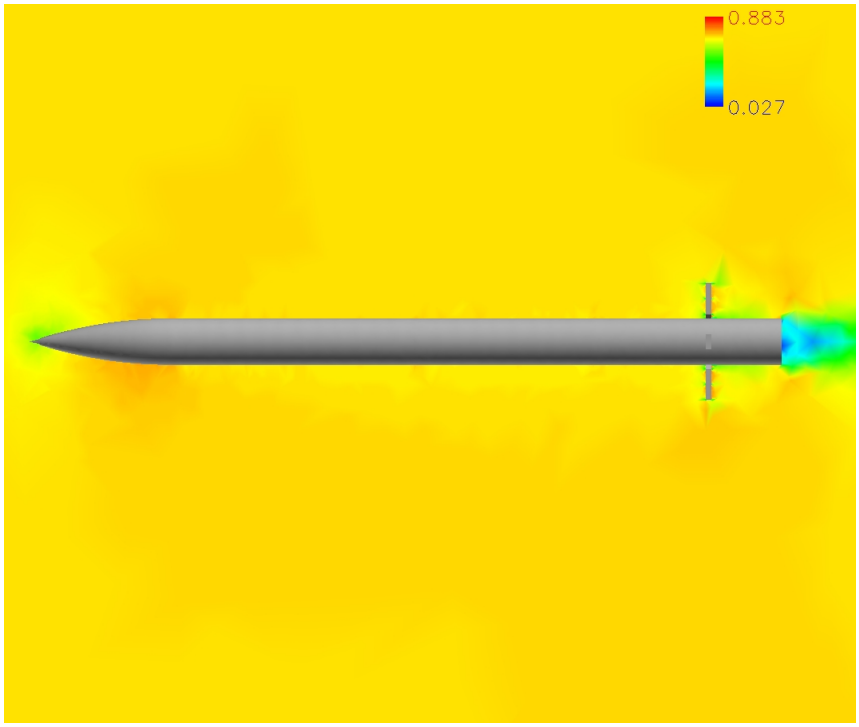

Figure 59: Coarse Fin Mach Contours M=0.7 AOA=-5 deg

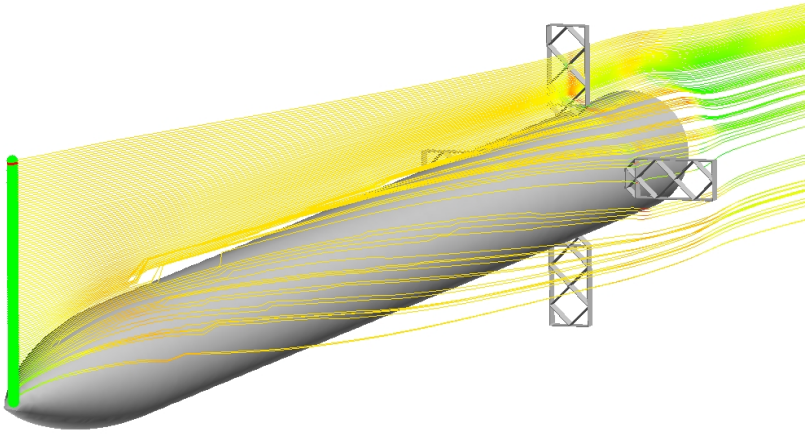

Figure 60: Coarse Fin Streamlines M=0.7 AOA=-5 deg

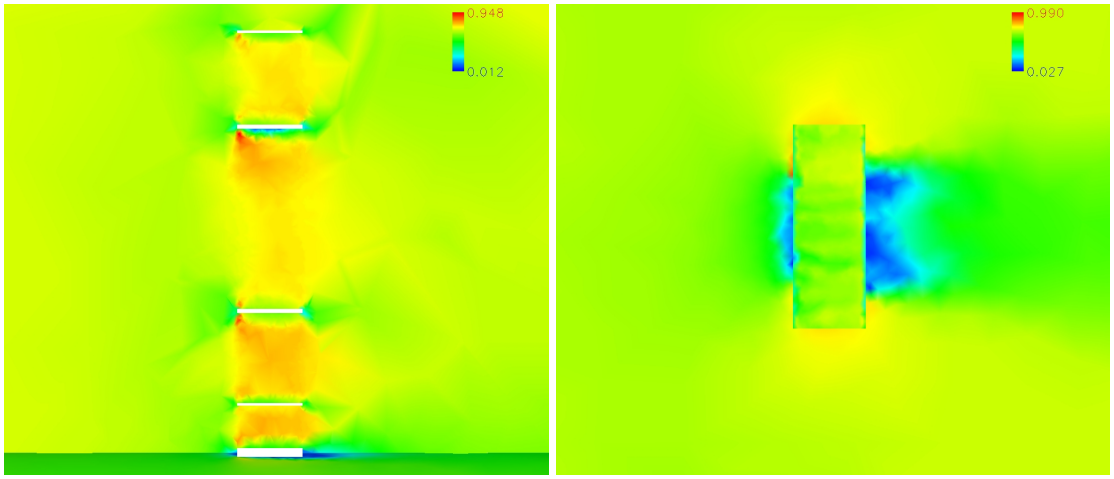

Top Fin

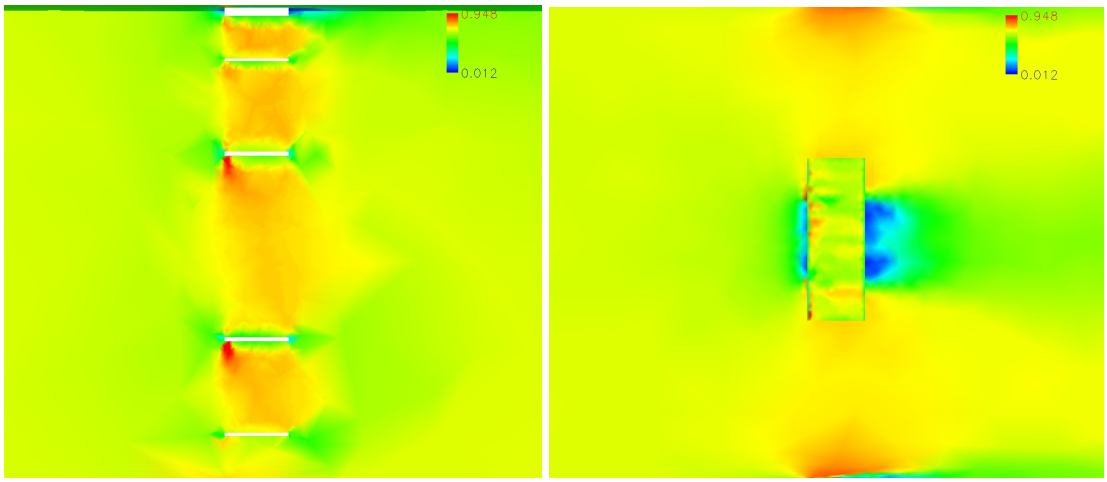

Bottom Fin

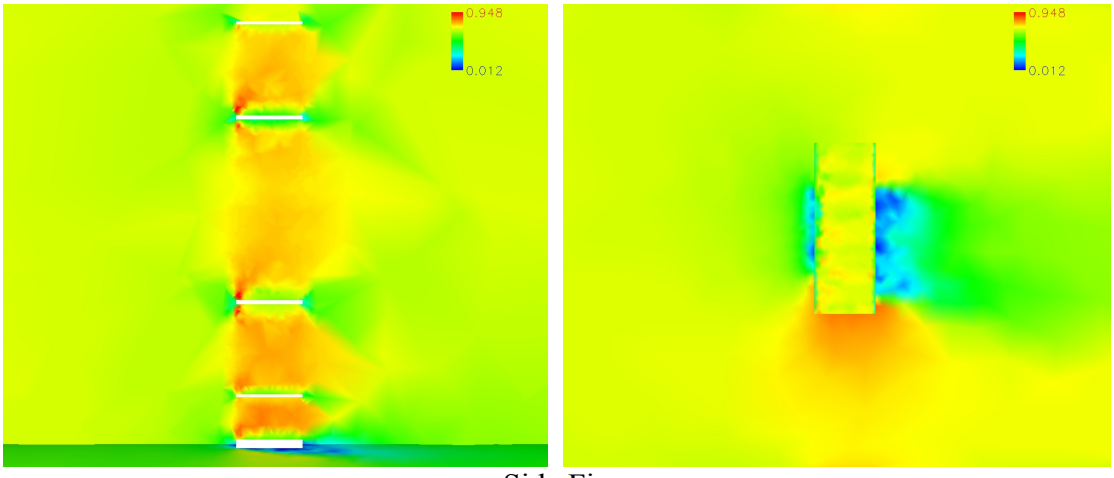

Side Fin

Figure 61: Coarse Fin Contours M=0.7 AOA=-5 deg

At higher Mach numbers (such as M=1.190), the shocks are much stronger and affect more of the flow within the cells. The same types and number of shocks occur as in the higher Mach baseline model results as shown in Figure 62. The streamlines in Figure 63 describe the same flowfield with the particles traveling in and around the fin as well as flow not traveling in the bottom cell of the fin. This causes the absence of the shocks located in the bottom cells, as well as stronger shocks in the upper cells. Figure 64 shows this phenomena and the interaction of the shocks from the fins.

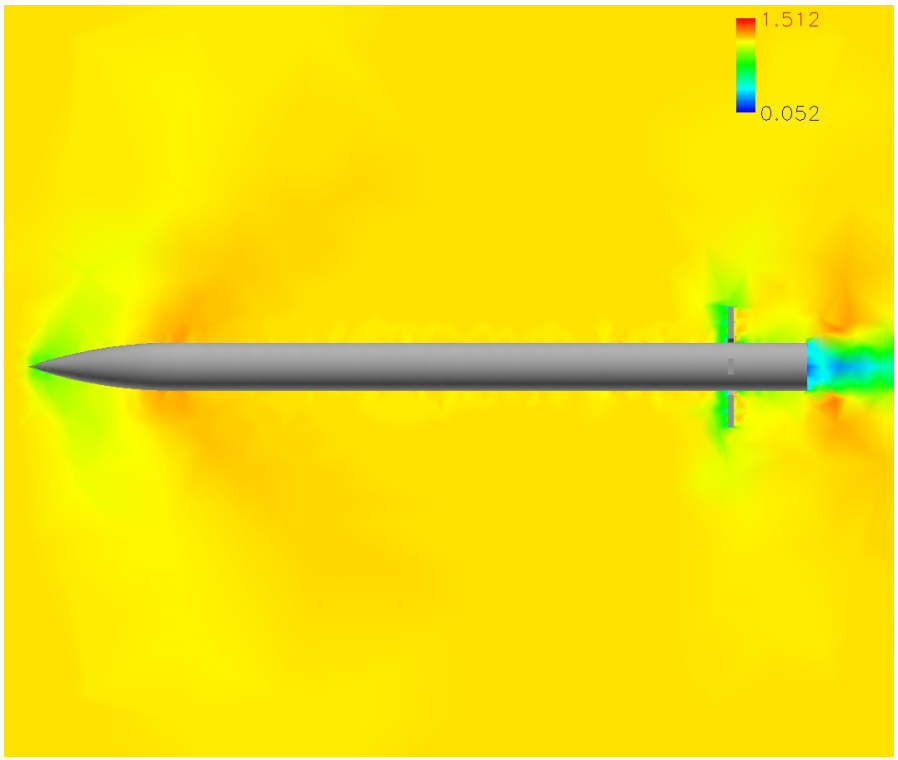

Figure 62: Coarse Fin Mach Contours M=1.190 AOA=0 deg

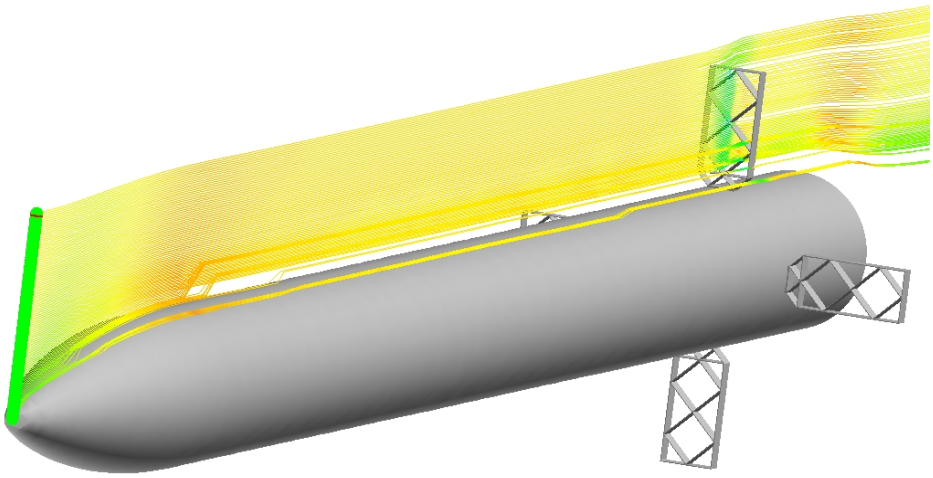

Figure 63: Coarse Fin Streamlines M=1.190 AOA=0 deg

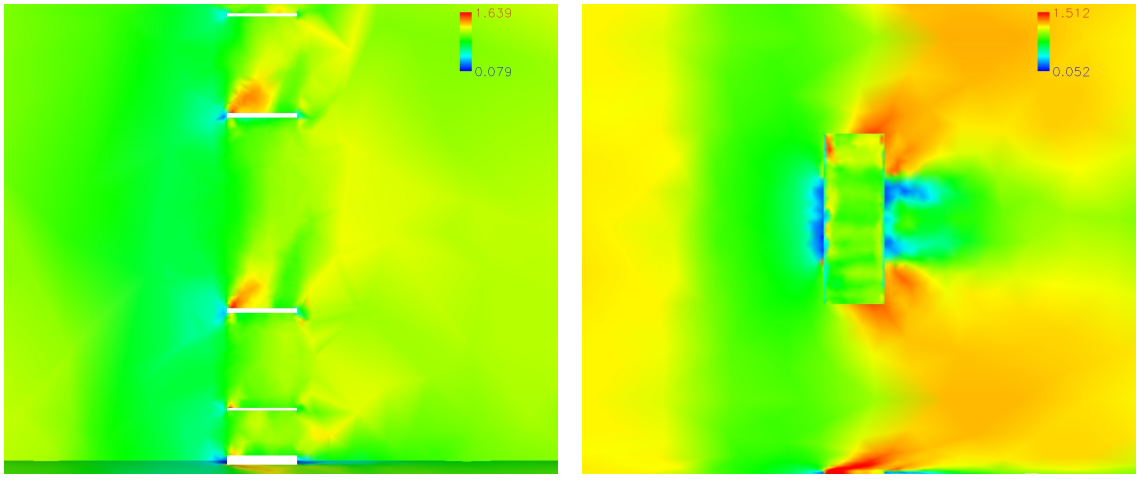

Top Fin Side Fin

Figure 64: Coarse Model Top Fin Mach Contours M=1.190 AOA=0 deg

In agreement with the baseline model, the coarse model flowfield was different at a different angle of attack as shown with the Mach contours in Figure 65 and streamlines in Figure 66. The bottom fin had stronger shocks than that of the top fin as well as the presence of shock after the expansion at the lattice furthest from the missile shown in Figure 67.

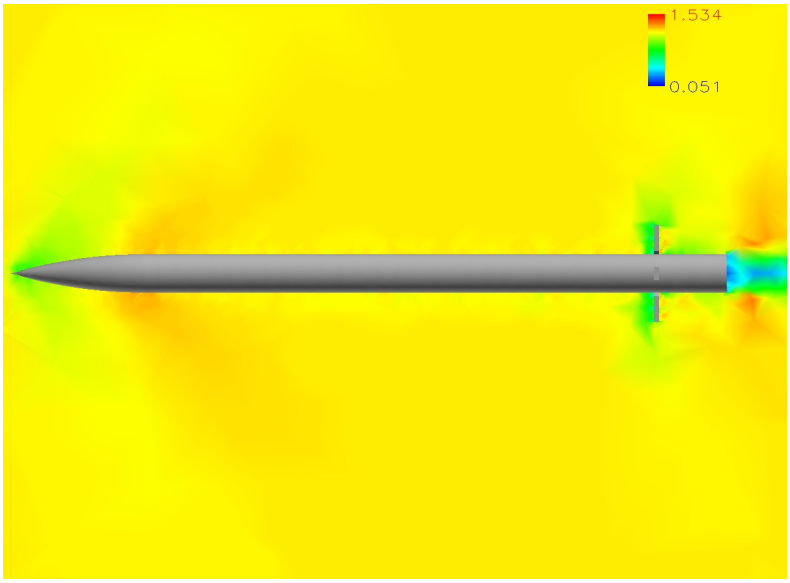

Figure 65: Coarse Fin Mach Contours M=1.190 AOA=-5 deg

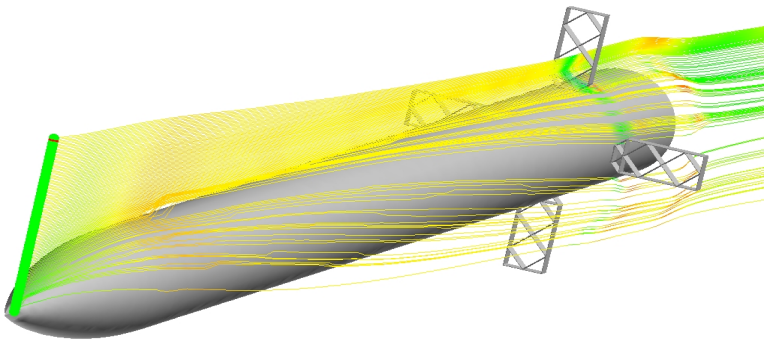

Figure 66: Coarse Fin Streamlines M=1.190 AOA=-5 deg

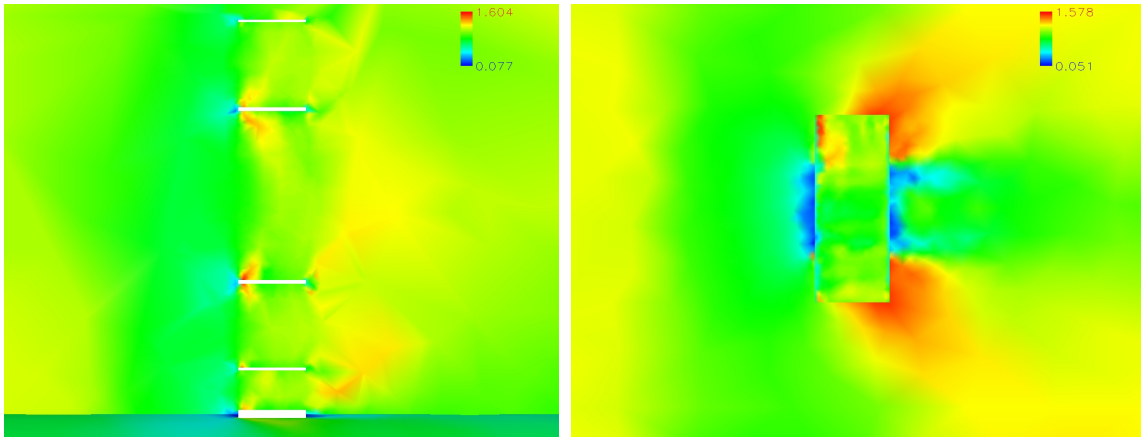

Top Fin

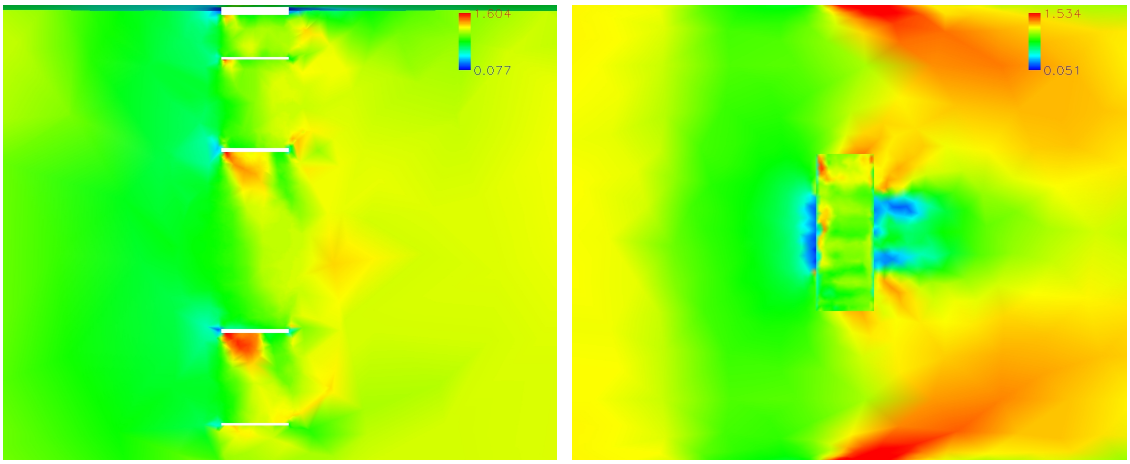

Bottom Fin

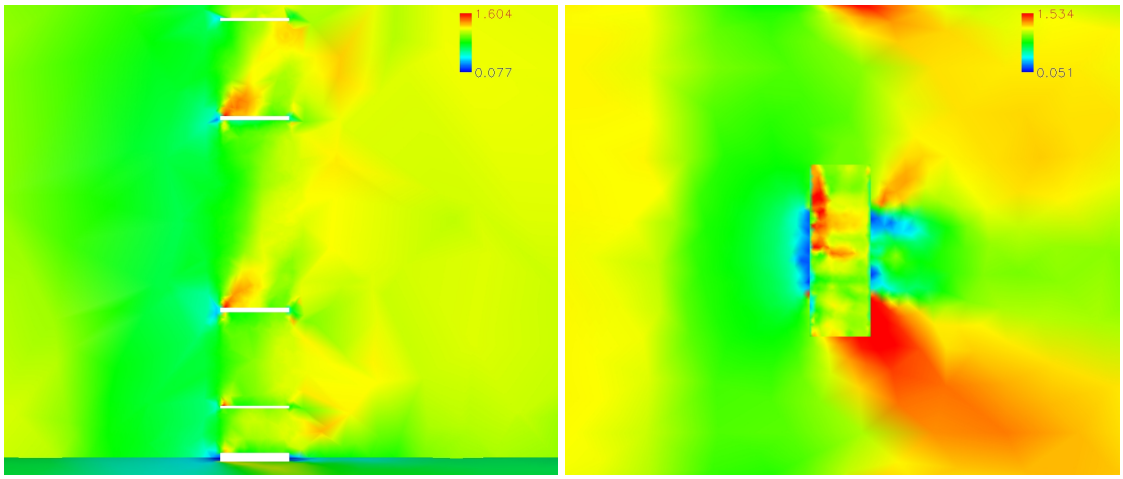

Side Fin

Figure 67: Coarse Model Mach Contours M=1.190 AOA=-5 deg

AFIT Drag

Because the design of the AFIT lattice grid fin is an original idea, there has been no experimental data for this configuration. Therefore, it is convenient to compare the results with that of the baseline model and the coarse model. The baseline, coarse, and AFIT drag calculations include the skin friction correction as explained before. This will help guide experimental results to be compared to which is shown in Figure 68.

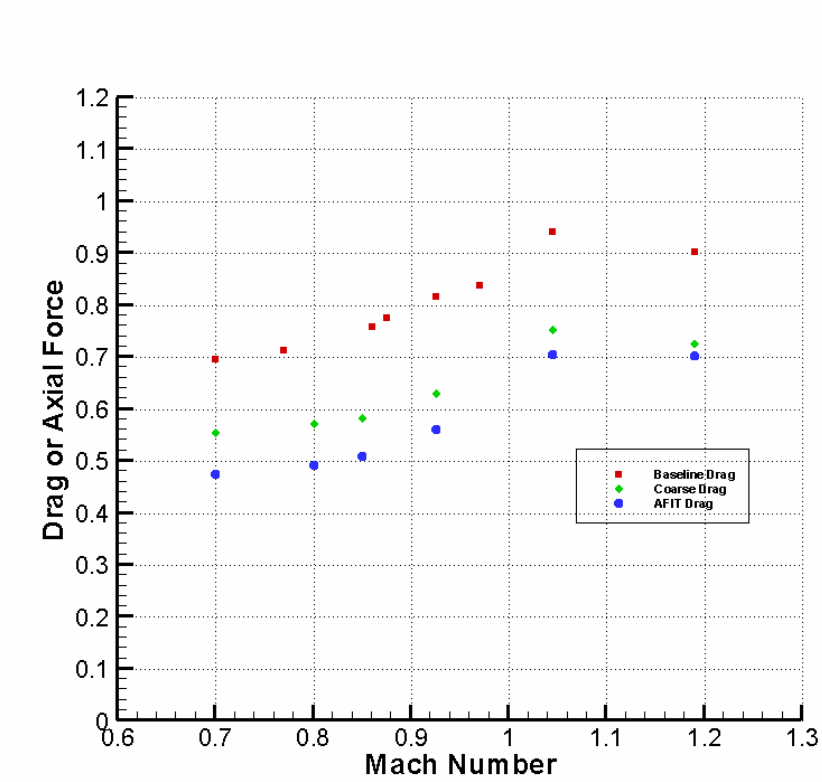

Figure 68: Numerical AFIT Drag

When examining the results from the numerical lattice grid fin models, the AFIT lattice grid fin approximation produced less drag than the other two configurations. The trend line for the AFIT configuration had the same characteristics as the others tested. It

is also shown that the baseline lattice grid fin configuration had the highest coefficient of drag based on the increased amount of webbing than the coarse and AFIT configurations. This was supported by the solidity ratio calculation by Hoerner which theorized that the drag would be greatest with the baseline configuration and least with the AFIT fin configuration. Therefore, it is optimal to use the AFIT lattice grid fin to limit the drag on the missile.

AFIT Moment Lines

Numerical runs had to be made at an individual Mach number and angle to produce the pitching moment vs. Mach data. Figure 69 shows the Mach moment coefficient lines for multiple cases.

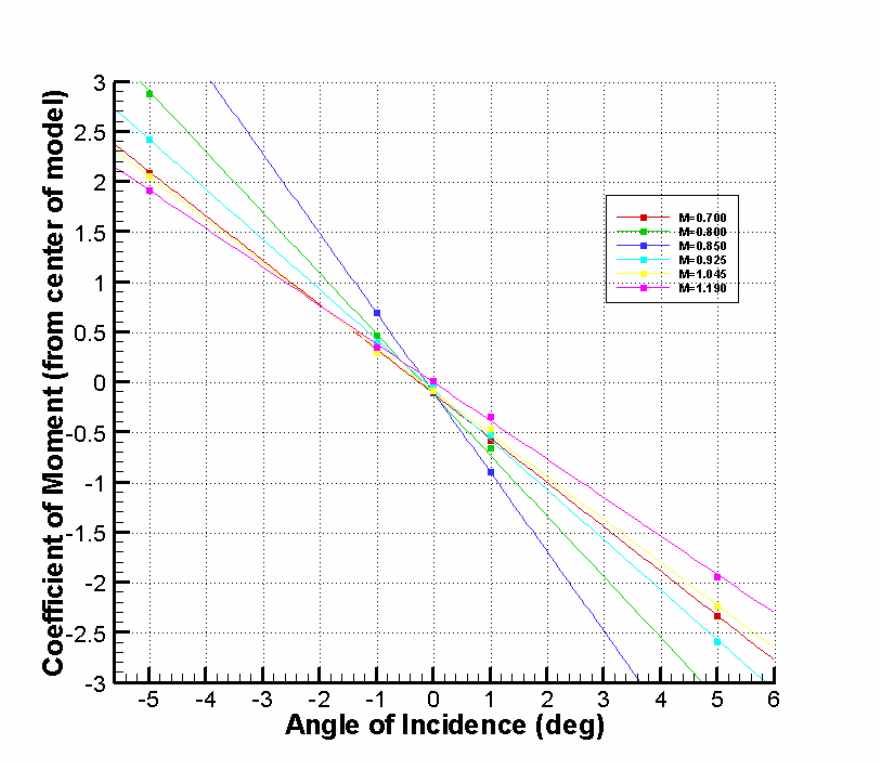

Figure 69: Numerical AFIT Moment Coefficients

The numerical AFIT moment derivatives were calculated by the slope of the numerical AFIT moment coefficients. The trends of the curves between -5 and 5 degrees appear linear and therefore, were used in the approximation of the slopes. It is shown again that as the Mach number is increased, the slope of the pitching moment coefficient decreased. This also occurred in the numerical results for the baseline and coarse lattice grid fins.

AFIT Pitching Moment Derivative

Figure 70 shows the numerical pitching moment derivatives of the AFIT, coarse, and baseline lattice grid fin configurations.

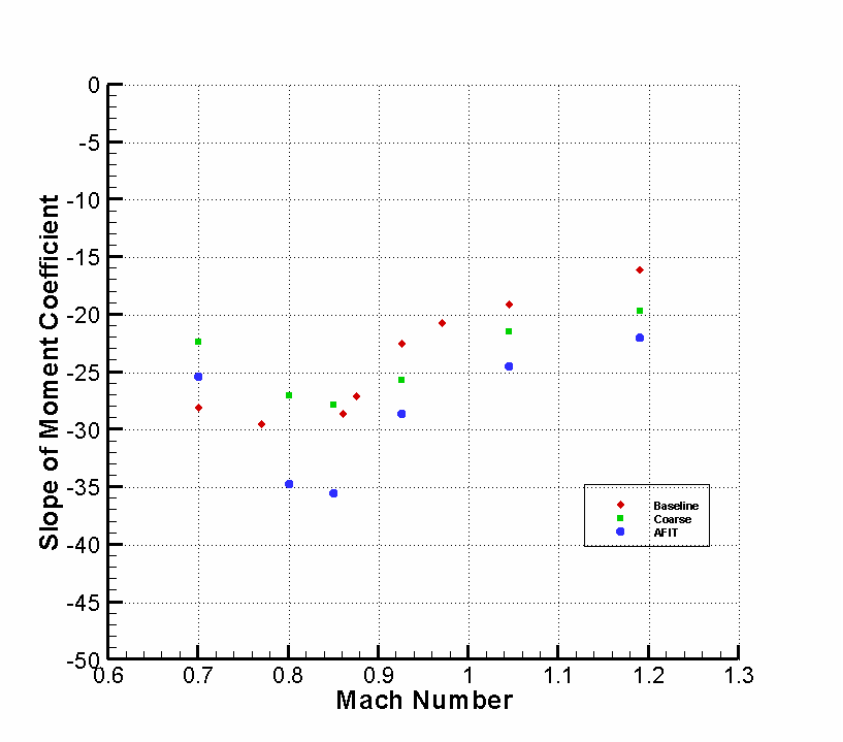

Figure 70: Numerical AFIT Moment Derivatives

The numerical results of the AFIT lattice grid fin seem to be consistent to hypothesis in that the static stability should be similar to that of the baseline and coarse

models. For this Mach number range, the AFIT trend line has the same temporary increase of moment derivative. This occurs close to that of the coarse grid fin configuration; this is expected in that the AFIT model configuration is closer to that of the ARF coarse fin than to the ARF baseline fin.

The trend for the pitching moment derivative is probably not as accurate for the given Mach number because of the numerical model being run inviscid for all calculations with no correction factor. Previous numerical results demonstrated an offset of the numerical data collected from experimental results. If the numerical data is offset by a Mach number 0.2, then the data is much more accurate than before. Both the baseline and coarse numerical data support the theory that there is a shift in the inviscid results from the viscous experimental data and this should continue with the AFIT lattice grid fin geometry.

AFIT Flowfield

The flowfield that occurs with the AFIT lattice grid geometry is consistent with the other two models tested experimentally and numerically. The same type of shocks that are formed by the nose, transition, fin, and base are found when the Mach number increases over one (Figures 77,78, and 79), but are not shown when the Mach number is below one (Figures 71, 72, and 73).

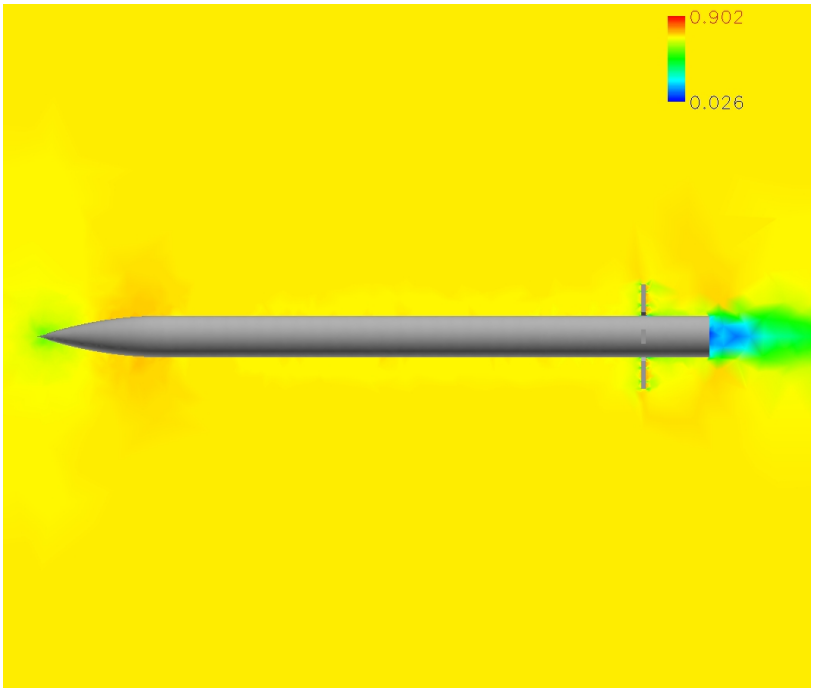

Figure 71: AFIT Mach Contours M=0.7 AOA=0 deg

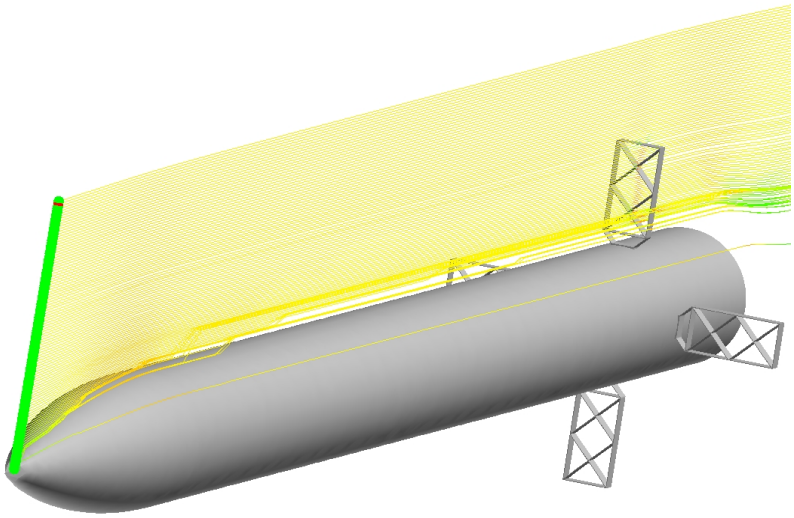

Figure 72: AFIT Streamlines M=0.7 AOA=0 deg

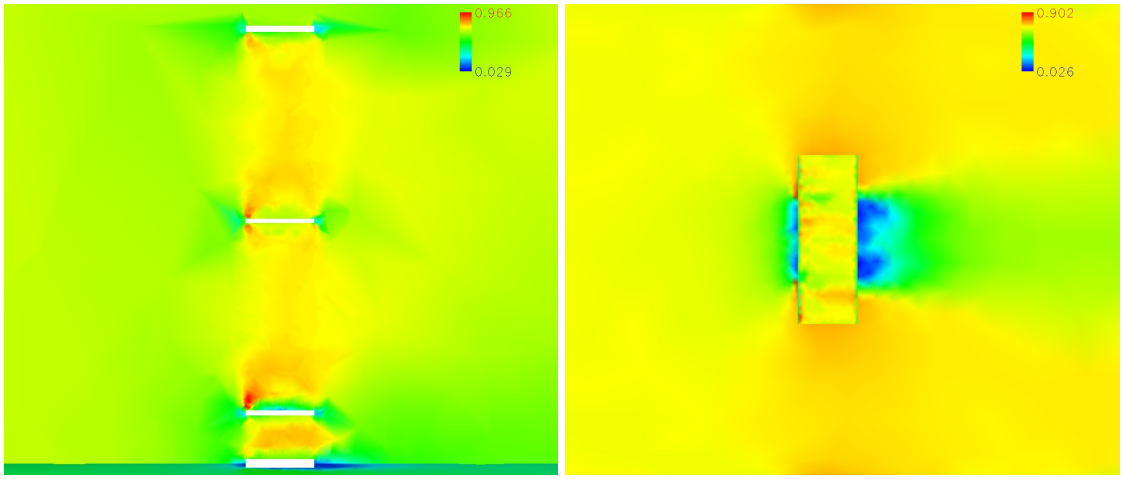

Top Fin-Side View Top Fin-Top View

Figure 73: AFIT Top Fin Mach Contours M=0.7

As expected, the flowfield from the AFIT lattice grid fin configuration is similar to that of the baseline and coarse models. At Mach 0.7, there is the beginning of the formation of shocks at the front leading edges of the lattices as well as a stagnation pressure region at the rear of the fin. The flow shown in the streamlines of Figure 75 and the Mach contours of Figure 74 are similar to that of the baseline and the coarse model in that flow travels over the nose and body and does not enter the bottom cell lattice of the grid fin when the angle is decreased to -5 deg. Figure 76 shows that at the decrease of angle of attack, the top fin experiences oblique shocklets that are symmetrical at the lattice fin face. However, the bottom fin experiences stronger shocklets at the top face of the lattice grid fins.

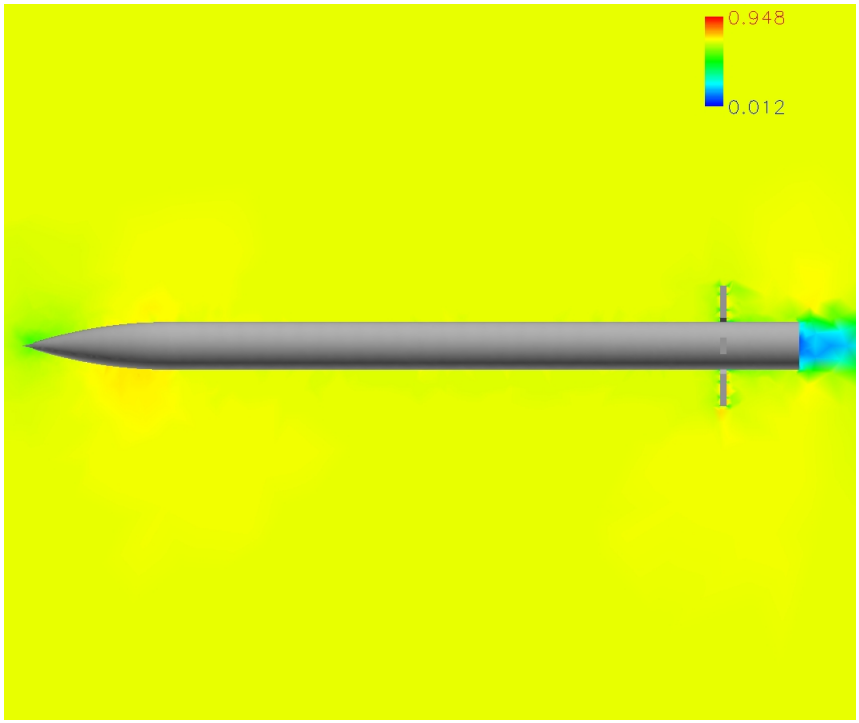

Figure 74: AFIT Mach Contours M=0.7 AOA=-5 deg

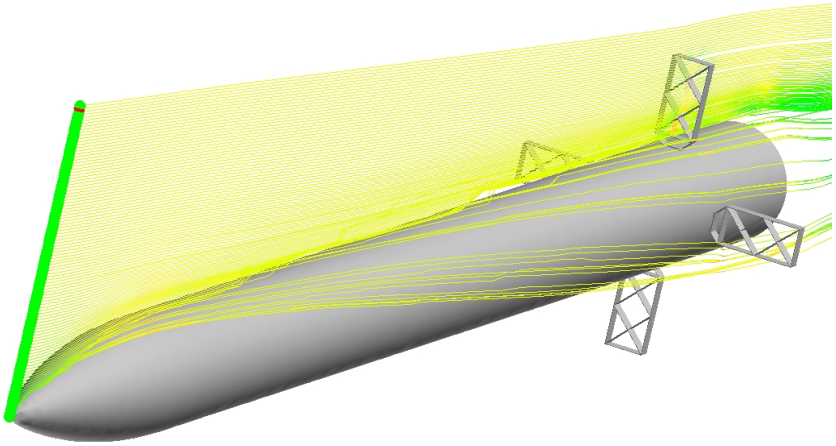

Figure 75: AFIT Streamlines M=0.7 AOA=-5 deg

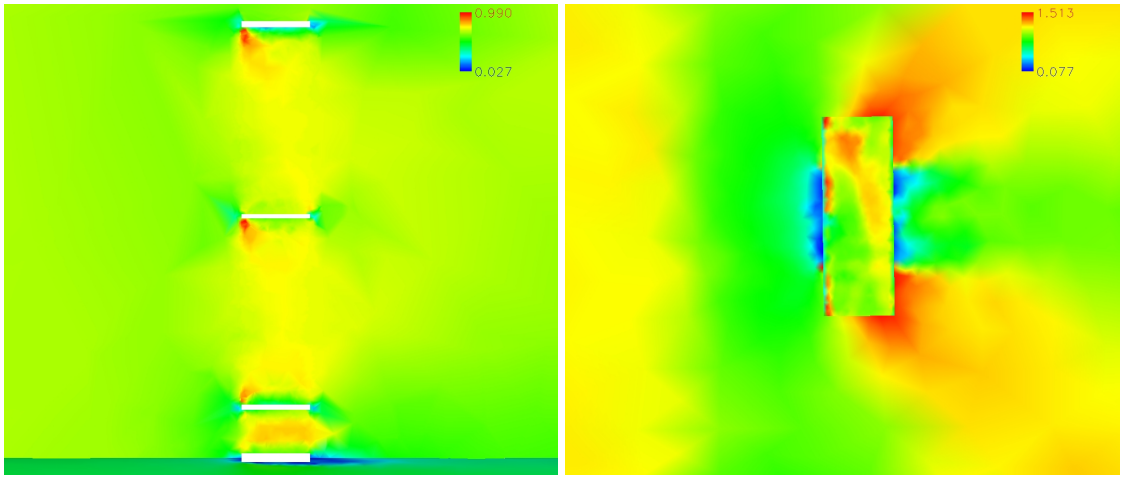

Top Fin

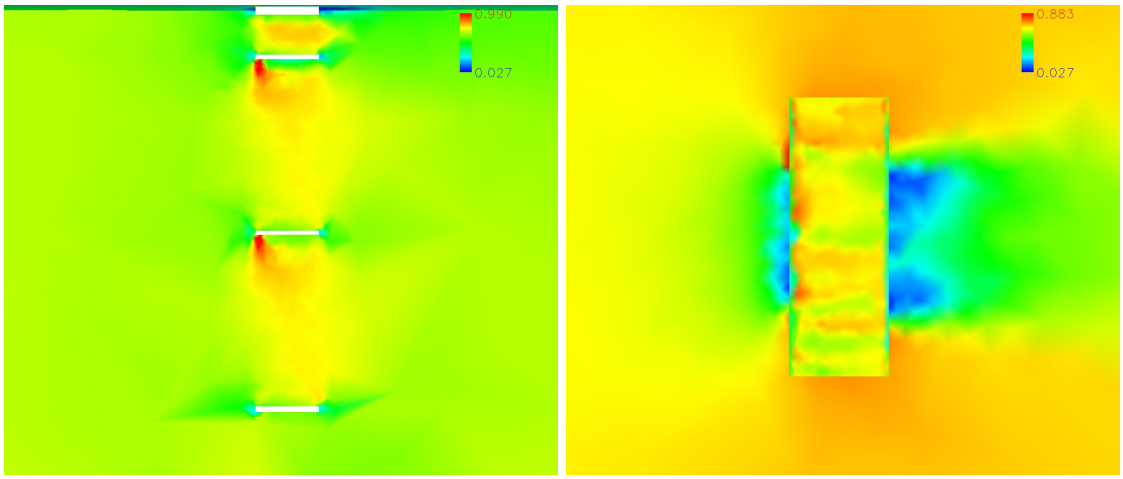

Bottom Fin

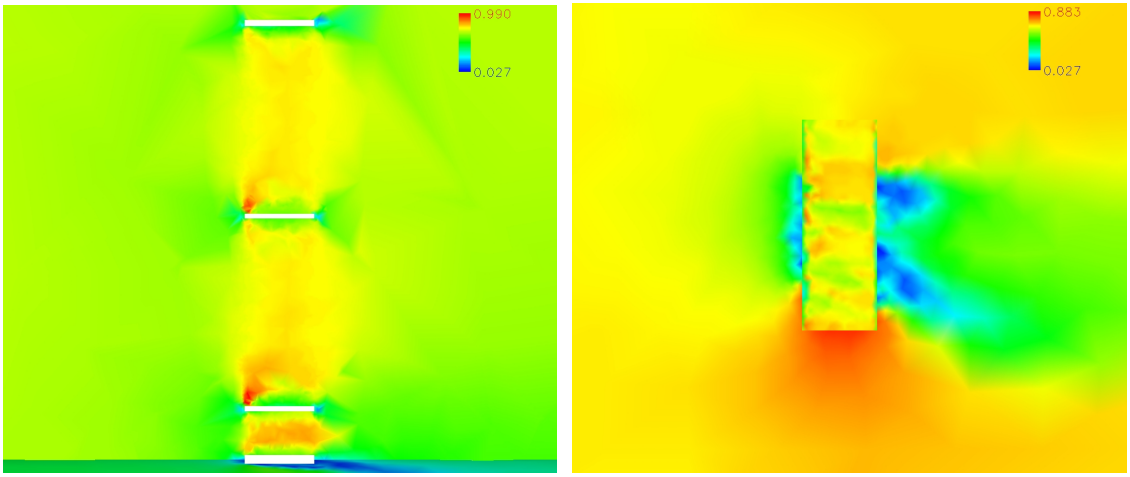

Side Fin

Figure 76: AFIT Mach Contours M=0.7 AOA=-5 deg

At higher Mach numbers (such as M=1.19), the shocks are much stronger and affects more of the flow within the cells as shown in Figures 77-81. In agreement with the other two models, the AFIT model flowfields were different at different angles of attack. There is a formation of the shocks at the back of the fin that was documented in the ARF experiments as a bubble shock 4c. The bottom fin had stronger shocks than that of the top fin as well as the presence of a shock after the expansion at the lattice furthest from the missile.

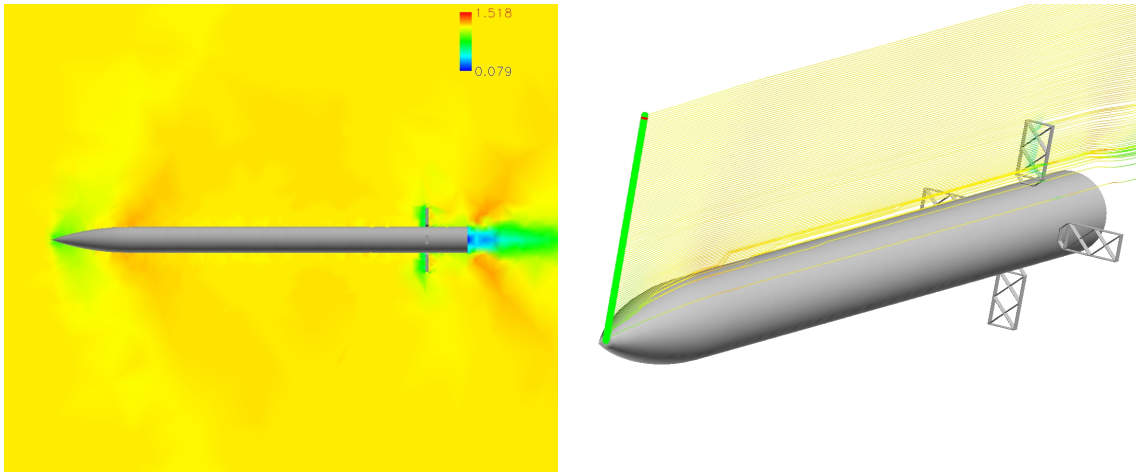

Figure 77: AFIT Model Mach Contours/Streamlines M=1.19 AOA=0 deg

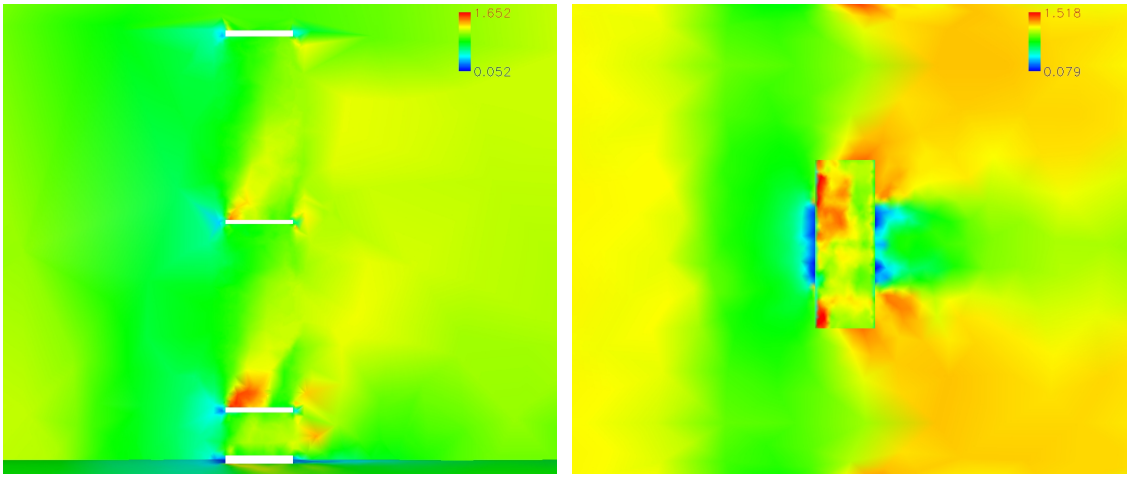

Top Fin-Side View Top Fin-Top View

Figure 78: AFIT Model Top Fin Mach Contours M=1.19 AOA=0 deg

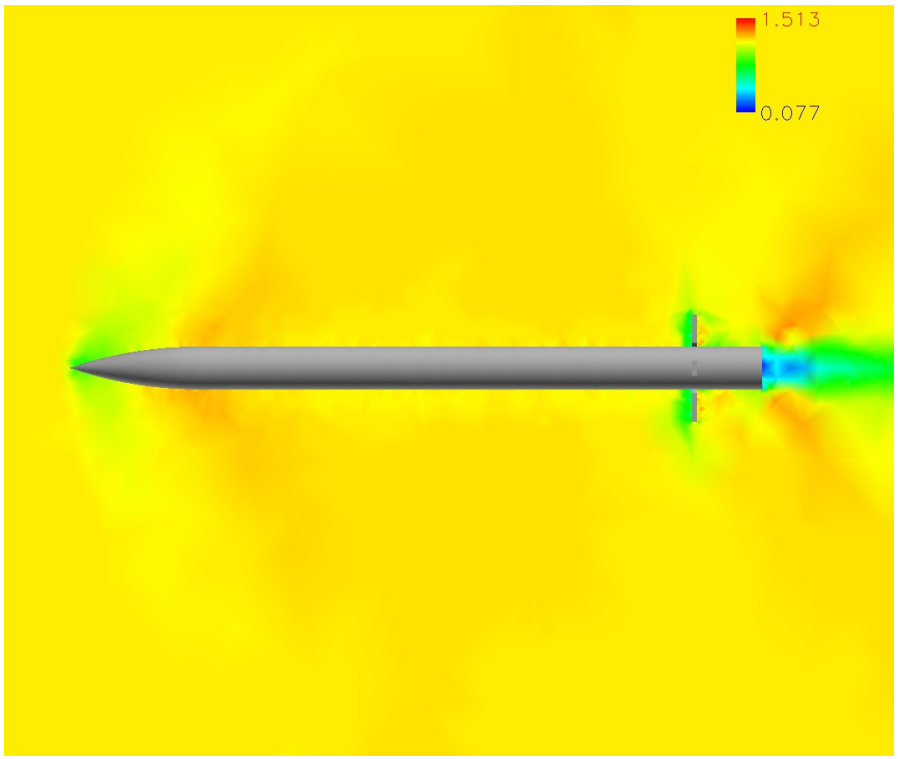

Figure 79: AFIT Model Mach Contours M=1.19 AOA=-5 deg

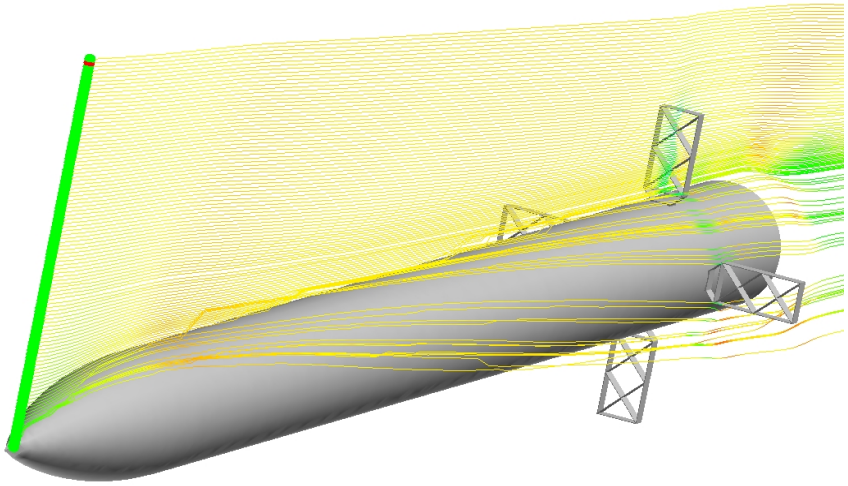

Figure 80: AFIT Model Streamlines M=1.19 AOA=-5 deg

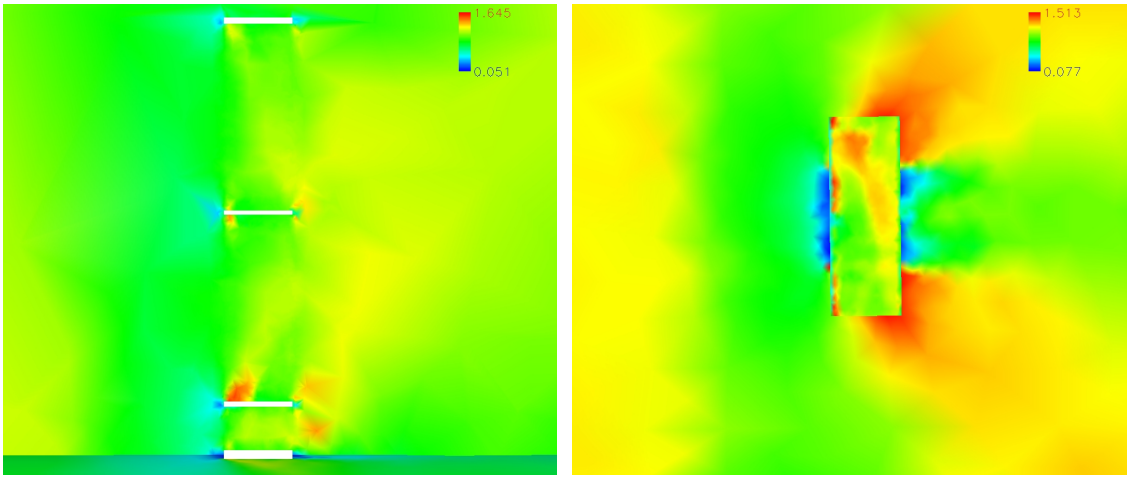

Top Fin

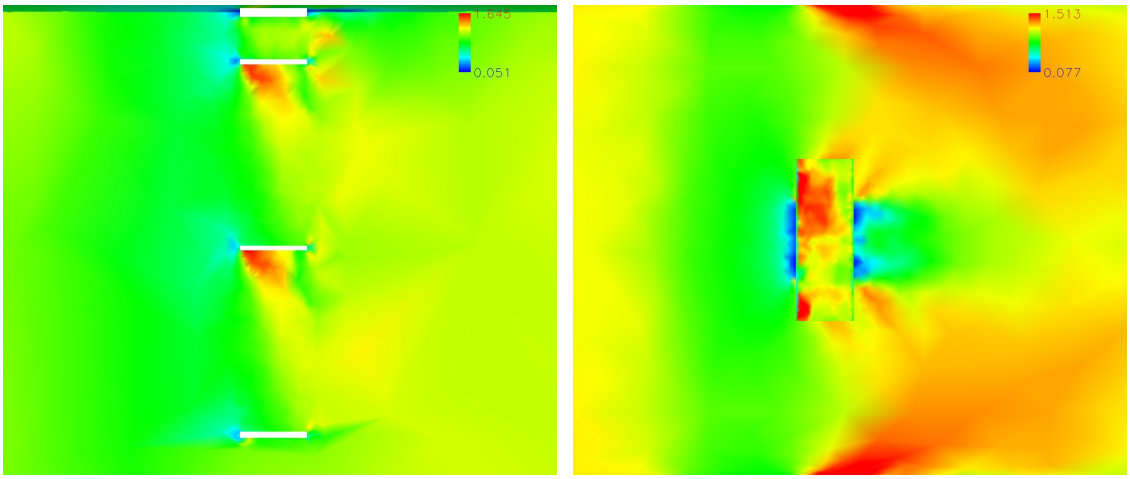

Bottom Fin

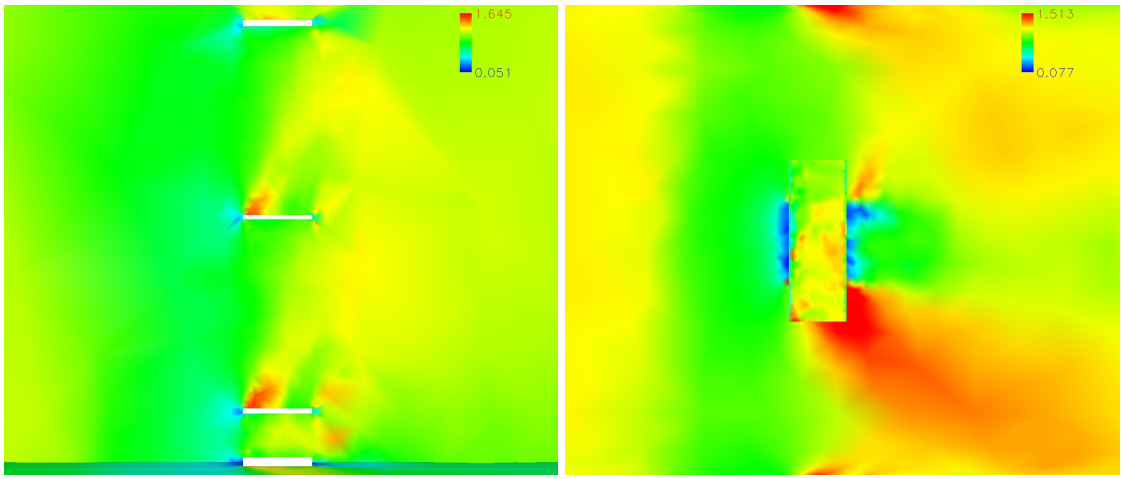

Side Fin

Figure 81: AFIT Model Mach Contours M=1.19 AOA=-5 deg

Lattice Grid Fin Lift Comparisons

An important comparison that has to be made is that the normal force coefficient or lifting force remains somewhat constant when changing the lattice grid fin geometry. This can be done by graphing the normal force coefficient with angle of attack. Figure 82 shows the lifting force comparisons between the different lattice geometries at Mach 0.7 and 1.19, respectively.

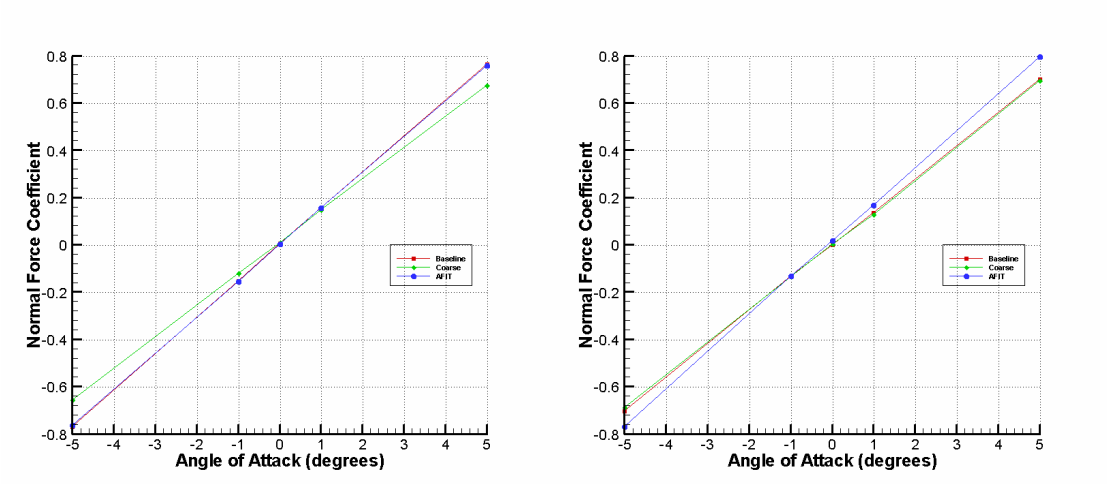

M=0.7 M=1.19

Figure 82: Normal Force Coefficient Comparisons

At a lower Mach number, the baseline and AFIT normal force coefficients are nearly the same. But as the Mach number increases, the coarse and baseline models are slightly different. However, the discrepancies between the three lattice grid fin configurations are negligible. This is desired so that each configuration will achieve the same amount of lift, while allowing for drag reduction based on changing the interior lattice geometry and surface area.

V. Conclusions and Recommendations

Research conducted at the United States Air Force Aeroballistic Research Facility (ARF) at Eglin AFB indicated that there is a critical transonic Mach number where normal shock waves and choked flow are believed to be present within some of the grid cells. At this particular Mach number, there is a severe dynamic instability with severe variations of the pitch moment coefficient. A computational fluid dynamics (CFD) study was made to investigate these findings and examine the lattice grid fin flowfield. The missile model was numerically modeled in *Gridgen* and computational tests were run inviscidly in *Fluent*. A viscous correction factor was applied to the drag coefficients in order to develop results closer to that of the experimental data and validate the numerical model.

The results of the drag calculation found that the baseline lattice grid fin configuration had the most drag at different Mach numbers. The AFIT lattice grid fin configuration was designed in order to decrease the drag without sacrificing lift. The numerical results proved that the AFIT lattice grid fin design did decrease the overall drag of the missile, appears to be a promising geometry to mitigate the choked flow phenomena at transonic Mach numbers.

No correction factor was found for the pitching moment coefficients, but the trend line results showed the same characteristics of the experimental data. There seemed to be an offset of the data by a Mach number of 0.2. This may have caused the absence of the moment coefficient spike seen in the ARF experimental data. More numerical test points need to be performed at lower Mach numbers to see if the shock spike does occur

inviscidly at low Mach numbers. The AFIT lattice grid fin configuration had some difference in static stability than the other configurations, but not nearly enough to discredit it as being unstable when compared to the baseline and coarse models based on the numerical runs completed.

Further research can be done in the development of lattice grid fins. By applying a viscous grid to the numerical models, the offset of the data might not have occurred. This should be done and compared to the experimental tests as well as the invicsid numerical runs completed. This would also confirm the skin friction correction factor used for the drag analysis. Additionally, unsteady computational tests should be conducted to determine if the spike in the moment data observed in the experiments is a transient, dynamic phenomenon. Experimental tests should also be continued with the AFIT lattice grid fin configuration; this would be compared to the numerical tests for accuracy of the predicted flowfield.

Bibliography

1. Fulghum, David A. "It's the Big One (MOAB actuall fits in a B-2)," *Aviation Week & Space Technology* (March 16, 2003)

2. Fleeman, Eugene L. *Tatical Missile Design.* Reston, Virginia: American Institute of Aeronautics and Astronautics, Inc., 2001

3. North Atlantic Treaty Organization. *Missile Aerodynamics.* Nov 1998

4. Washington, William D, "Grid-Fins-A New Concept for Missile Stability and Control," AIAA 93-0035, 31st Aerospace Sciences Meeting and Exhibit, Reno, NV January1993

5. Washington, William D and Miller, Mark S, "Curvature and Leading Edge Sweep Back Effects on Grid Fin Aerodynamic Characteristics," AIAA 93-3480, Applied Aerodynamics Conference, Monterey, CA, August 1993

6. Miller, Mark S and Washington, William D, "An experimental Investigation of Grid Fin Drag Reduction Techniques," AIAA 94-1914-CP, WL Technical Library

7. Fournier, E.Y., "Wind Tunnel Investigation of Grid Fin and Conventional Planar Control Surfaces," AIAA 2001-0256, 39th Aerospace Sciences Meeting and Exhibit, Reno, NV January 2001

8. DeSpirito, James; Edge, Harris L; Weinacht, Paul; Sahu, Jubaraj; Dinavahi Surya P.G.; "CFD Analysis of Grid Fins for Maneuvering Missiles," AIAA 2000-0391

9. DeSpirito, James and Sahu, Jubaraj, "Viscous CFD Calculations of Grid Fin Missile Aerodynamics in the Supersonic Flow Regime," AIAA 2001-0257, 39th Aerospace Sciences Meeting and Exhibit, Reno, NV January 2001

10. Despirito, James; Vaughn Milton E.; Washington, William D.; "CFD Investigation of Canard-Controlled Missile With Planar and Grid Fins in Supersonic Flow," AIAA 2002-4509, AIAA Atmospheric Flight Mechanics Conference and Exhibit, Monterey CA, August 2002

11. Despirito, James; Vaughn Milton E.; Washington, William D.; "Subsonic Flow CFD Investigation of Canard-Controlled Missile With Planar and Grid Fins," AIAA 2003-0027, 41th Aerospace Sciences Meeting and Exhibit, Reno, NV January 2003

12. Chen, Suzhen; Khalid, Mahood; Xu, Hongyi; Lesage, Francois; "A Comprehensive CFD Investigation of Grid Fins as Efficient Control Surface Devices," AIAA 2000-0987, 38th Aerospace Sciences Meeting and Exhibit, Reno, NV January 2000

13. Abate, Gregg L., Duckerschein, Ralf P., and Wayne Hathaway, "Free-Flight Tests of a Generic Missile with Grid Fins," 50th Aeroballistic Range Association Meeting, Pleasanton, CA, November 1999.

14. Abate, Gregg L., Duckerschein, Ralf P., and Wayne Hathaway, "Subsonic/Transonic Free-Flight Tests of a Generic Missile with Grid Fins," AIAA 2000-0937, 38th Aerospace Sciences Meeting and Exhibit, Reno, NV, January 2000.

15. Burnett, C.H. and et al, "PRODAS Version 5.4 Technical Manual," ArrowTech Associated, South Burlington, VT, November 1991

16. Abate, Gregg L., Duckerschein, Ralf P., and Wayne Hathaway, "Transonic Aerodynamic and Scaling Issues for Lattice Fin Projectiles Tested in a Ballistic Range," 19th International Symposium on Ballistics, Interlaken, Switzerland, May 2001.

17. Zucrow, Maurice J. and Hoffman, Joe D., *Gas Dynamic,s Volume I*. NY: John Wiley and Sons, 1976

18. Hill, Philip and Peterson, Carl, *Mechanics and Thermodynamics of Propulsion, Second Edition*. Reading, Massachusetts, 1992

19. Anderson, John, *Modern Compressible Flow with Historical Perspective, Second Edition.* Boston, Massachusetts: McGraw-Hill 1990

20. "Gridgen Overview," Excerpt from unpublished article. http://www.gridgen.com/gridgen/. Pointwise Inc, 2004

21. Hoerner, Sighard F., *Fluid-Dynamic Drag*, Hoerner Fluid Dynamics, 1965

22. "FLUENT Description," Excerpt from unpublished article. http://www.fluent.com/software/index.htm. 2004

23. White, Frank M, *Viscous Fluid Flow 2nd Edition*. New York: McGraw-Hill, 1991

Appendix A: Grid Generation

Three grids were generated on *Gridgen* by the user for this grid convergence study: coarse, fine, refined. All these grids had the same dimensions. First, the grid was modeled only on one fourth of the GTCM. This could be done because of the cruciform geometry the missile had. The reason for doing this was simple; to reduce the number of cells; therefore decreasing the runtime. The connectors were then made; the forward connector was two missile lengths in front of the missile, the rear connectors extended ten missile lengths back, and the top connector was made to be two missile lengths as well. This provided for more than enough space to enclose the shock.

For the coarse grid, the number of points per connector was picked based on the importance of flow characteristics in the region. Therefore, there are many more points located on the surfaces (missile, fin, and sting) than the farfield condition. Once the number of points was assigned, a boundary decay factor of 0.95 was made on each farfield domain. A close up of the empty coarse fin with connector numbers shows that the mesh is very dense, but the number of points on the connectors was needed to ensure that the flow characteristics can be seen on the side faces of the lattice grid fin. The number of cells generated were around 600,000.

Once a coarse grid was made, a much finer grid had to be made. The points were increased from the coarse grid by almost a factor of two. The Farfield connectors and the sting connectors were kept the same because more points would be unnecessary. Because of the increase of connectors points, there were more than 2,000,000 cells.

The refined grid was then made to take into account more information generated during the runs. First of all, the farfield connectors could have fewer points; therefore,

they were decreased up to a factor of two. But, the number of points on the fin and missile was kept the same amount as the coarse grid. But the major difference in the refined grid was the addition of points on the estimated shock wave. The estimation of the shock angle was made using the σ-θ-M relationship for a cone. When assuming 10 degrees as the incidence angle of the nose, the shock angle came to nearly 60 degrees. Therefore, a connector was made at the angle in order to gain more information about the shock. The refinement of the course grid led to more grid cells, but nearly as much as the fine grid. The number came to around 750,000 cells.

Appendix B: Baseline Data Tables

M=0.7

Angle of Attack (degrees)	Coefficient of Moment
5	-2.3210681
0	0.038397503
-5	2.2693094

M=0.77

Angle of Attack (degrees)	Coefficient of Moment
-5	2.5505495
-4	2.1548611
-3	1.6162327
-2	1.0839584
-1	0.50412482
2	-0.9524489
3	-1.486452
4	-2.0448371
5	-2.5682825

M=0.86

Angle of Attack (degrees)	Coefficient of Moment
5	-2.4811495
1	-0.70815159
0	-0.046253006
-1	0.65447383
-5	2.4495571

M=0.875

Angle of Attack (degrees)	Coefficient of Moment
-5	2.2751655
-2	1.0394209
-1	0.45771433
0	-0.031462922
1	-0.56135942
2	-1.0999618
5	-2.3477026

M=0.925

Angle of Attack (degrees)	Coefficient of Moment
5	-2.0134862
1	-0.38116978
0	-0.02788676
-1	0.34605258
-5	1.9340103

M=0.97

Angle of Attack (degrees)	Coefficient of Moment
5	-1.862504
1	-0.36000869
0	-0.023623114
-1	0.30390648
-5	1.7752044

M=1.045

Angle of Attack (degrees)	Coefficient of Moment
-5	1.6250418
-4	1.275921
-3	0.90129364
-2	0.54967884
-1	0.22358048
0	-0.085925582
1	-0.40625005
2	-0.70728312
3	-1.0374235
4	-1.4256348
5	-1.7751357

M=1.19

Angle of Attack (degrees)	Coefficient of Moment
5	-1.4414771
4	-1.1031345
3	-0.76533317
2	-0.45180061
1	-0.19797366
0	0.04522776
-1	0.28762465
-2	0.54440659
-3	0.82837015
-4	1.1703528
-5	1.4736611

Drag Calculation

Mach Number	Drag	Drag w/correction
0.7	0.5783356	0.698724
0.77	0.5983025	0.719329
0.86	0.64680729	0.764984
0.875	0.6631409	0.780873
0.925	0.7051409	0.821343
0.97	0.72795052	0.842901
1.045	0.83439075	0.947379
1.19	0.79862394	0.908845

Moment Derivatives

Mach Number	Moment Derivative
0.7	-28.0966
0.77	-29.5625
0.86	-28.6657
0.875	-27.1316
0.925	-22.5489
0.97	-20.7724
1.045	-19.1509
1.19	-16.1099

Appendix C: Coarse Data Tables

M=0.7

Angle of Attack (degrees)	Coefficient of Moment
-5	1.9920355
-1	0.4611626
0	0.021790269
1	-0.31381311
5	-1.9126278

M=0.8

Angle of Attack (degrees)	Coefficient of Moment
-5	2.2658921
-1	0.48282052
0	0.031318274
1	-0.41227816
5	-2.457113

M=0.85

Angle of Attack (degrees)	Coefficient of Moment
-5	2.07075634
-1	0.66881717
0	-0.013051971
1	-0.7158785
5	-2.6996953

M=0.925

Angle of Attack (degrees)	Coefficient of Moment
-5	2.2419824
-1	0.35003987
0	-0.063923988
1	-0.48065268
5	-2.2535146

M=1.045

Angle of Attack (degrees)	Coefficient of Moment
-5	1.9493957
-2	0.72799457
-1	0.36896943
0	0.02995308
1	-0.29722513
2	-0.66797761
5	-1.8425651

M=1.19

Angle of Attack (degrees)	Coefficient of Moment
-5	1.7763281
-2	0.61998489
-1	0.28079933
0	-0.028079933
1	-0.32897523
2	-0.64803715
5	-1.7142833

Drag Calculations

Mach Number	Drag	Drag w/ correction
0.7	0.43701658	0.559886
0.8	0.45864917	0.577649
0.85	0.4788262	0.587557
0.925	0.52017717	0.635178
1.045	0.64388154	0.756751
1.19	0.62089587	0.730998

Moment Derivatives

Mach Number	Moment Derivative
0.7	-22.3655
0.8	-27.0063
0.85	-27.8071
0.925	-25.6819
1.045	-21.4076
1.19	-19.6705

Appendix D: AFIT Data Tables

M=0.7

Angle of Attack (degrees)	Coefficient of Moment
5	-2.3350294
1	-0.580513
0	-0.10313173
-1	0.35835007
-5	2.0876383

M=0.8

Angle of Attack (degrees)	Coefficient of Moment
5	-3.199073
1	-0.6617547
0	-0.09367755
-1	0.46811299
-5	2.8737735

M=0.85

Angle of Attack (degrees)	Coefficient of Moment
5	-3.1760672
1	-0.89331162
0	-0.095393983
-1	0.69394972
-5	2.9508271

M=0.925

Angle of Attack (degrees)	Coefficient of Moment
5	-2.5943214
1	-0.5247589
0	-0.057696746
-1	0.39267054
-5	2.4169825

M=1.045

Angle of Attack (degrees)	Coefficient of Moment
5	-2.2416513
1	-0.46495113
0	-0.086320531
-1	0.29391382
-5	2.0525341

M=1.19

Angle of Attack (degrees)	Coefficient of Moment
5	-1.9415049
1	-0.34254937
0	0.01350557
-1	0.35219764
-5	1.9095655

Drag Calculations

Mach Number	Drag	Drag w/correction
0.7	0.47513198	0.596001
0.8	0.490994	0.60891
0.85	0.50822956	0.62343
0.925	0.5599825	0.672983
1.045	0.70465767	0.815517
1.19	0.70152958	0.809632

Moment Derivatives

Mach Number	Moment Derivative
0.7	-25.3999
0.8	-34.7015
0.85	-35.5033
0.925	-28.6192
1.045	-24.4937
1.19	-21.9819

Vita

Ensign Karl S. Orthner graduated from The Chesterfield County Mathematics and Science High School at Clover Hill in Midlothian, Virginia. He entered undergraduate studies at North Carolina State University in Raleigh, North Carolina where he graduated Magna Cum Laude with a Bachelor of Science degree in Aerospace Engineering in May 2003 with a minor in Military Studies. He was commissioned through the NROTC North Carolina Piedmont Region Detachment located at North Carolina State University where he was nominated for a Commission as an aviation student.

His first assignment was to enter the Graduate School of Engineering and Management at the Air Force Institute of Technology. Here he will obtain a Masters of Science degree in Aeronautical Engineering. Upon graduation, he will be assigned to Pensacola, Florida in order to begin flight training.

REPORT DOCUMENTATION PAGE

Form Approved
OMB No. 074-0188

1. REPORT DATE *(DD-MM-YYYY)*	**2. REPORT TYPE**	**3. DATES COVERED** *(From – To)*
04 JUN 04	**Master's Thesis**	22 JUN 03 – 04 MAR 04

4. TITLE AND SUBTITLE

AERODYNAMIC ANALYSIS OF LATTICE GRID FINS IN TRANSONIC FLOW

5a. CONTRACT NUMBER

5b. GRANT NUMBER

5c. PROGRAM ELEMENT NUMBER

6. AUTHOR(S)

ORTHNER, KARL S, Ensign, USNR

5d. PROJECT NUMBER

5e. TASK NUMBER

5f. WORK UNIT NUMBER

7. PERFORMING ORGANIZATION NAMES(S) AND ADDRESS(S)
Air Force Institute of Technology
Graduate School of Engineering and Management (AFIT/EN)
2950 Hobson Way
WPAFB OH 45433-7765

8. PERFORMING ORGANIZATION REPORT NUMBER

AFIT/GAE/ENY/04-J09

9. SPONSORING/MONITORING AGENCY NAME(S) AND ADDRESS(ES)
Air Force Research Laboratory
Munitions Directorate
Eglin AFB, FL 32542

10. SPONSOR/MONITOR'S ACRONYM(S)

11. SPONSOR/MONITOR'S REPORT NUMBER(S)

12. DISTRIBUTION/AVAILABILITY STATEMENT
APPROVED FOR PUBLIC RELEASE; DISTRIBUTION UNLIMITED.

13. SUPPLEMENTARY NOTES

14. ABSTRACT. Lattice grid fins have been studied for missile tail control for several years. A lattice grid fin can be described as an unconventional missile control surface comprised of an outer frame supported by an inner lattice grid of lifting surfaces. This unconventional fin design offers favorable lift characteristics at high angle of attack as well as almost zero hinge moments allowing the use of small and light actuators. In addition, they promise good storability for potential tube-launched and internal carriage dispenser-launched applications. The drawback for the lattice grid fins is the high drag and potentially poor radar cross section performance produced by this unconventional control surface configuration.

Current research at the United State Air Force's Aeroballistic Research Facility (ARF) at Eglin Air Force Base in Florida has indicated there is a critical transonic Mach number where normal shock waves are believed to be present within some of the grid cells. At this particular Mach number, there is a dynamic instability with severe variations of the pitch moment coefficient. A computational fluid dynamics (CFD) study was conducted to investigate these findings. The missile model was numerically modeled in *Gridgen* and computational tests were run in *Fluent*. These were inviscid tests that of course ignored viscous effects. Therefore, a correction factor was applied to the drag coefficients in order to develop results closer to that of the experimental data. No correction factor was found for the pitching moment coefficients, but the trend line results showed the same characteristics of the experimental data. Finally, another fin configuration was developed that produced less drag and similar dynamic stability that the other lattice grid fin configurations tested.

15. SUBJECT TERMS

16. SECURITY CLASSIFICATION OF:			**17. LIMITATION OF ABSTRACT**	**18. NUMBER OF PAGES**	**19a. NAME OF RESPONSIBLE PERSON**
REPORT	**ABSTRACT**	**c. THIS PAGE**			LtCol Raymond C. Maple
U	**U**	**U**	**UU**	106	**19b. TELEPHONE NUMBER** *(Include area code)* (937) 255-3636, ext 4577

Standard Form 298 (Rev: 8-98)
Prescribed by ANSI Std. Z39-18